The Impact of Energy Routers on the Planning of Transmission and Electric Vehicle Charging Stations

by

Yousef Alali

A Thesis Presented in Partial Fulfillment
of the Requirements for the Degree
Master of Science

Approved July 2020 by the
Graduate Supervisory Committee:

Yang Weng, Chair
Qiushi Cui
Keith Holbert

ARIZONA STATE UNIVERSITY

August 2020

ABSTRACT

Transmission line capacity is an obstacle for the utilities because there is a load increment annually, and new power plants are being connected, which requires an update. Energy router (ER) is a device that provides an additional degree of freedom to the utilities by controlling the reactive power. The ER reactive power injection is demonstrated by changing the line's reactance value to increase its capacity and give the utility a deferral time for the project upgrade date. Changing the reactance manually and attaching Smart Wire's device to the branches have effectively solved the overload in three locations of a local utility in Arizona (LUA) system.

Furthermore, electric vehicle charging stations (EVCSs) have been increasing to meet EV needs, which calls for an optimal planning model to maximize the profits. The model must consider both the transportation and power systems to avoid damages and costly operation. Instead of coupling the transportation and power systems, EVCS records have been analyzed to fill the gap of EV demand. For example, by accessing charging station records, the moment knowledge of EV demand, especially in the lower order, can be found. Theoretically, the obtained low order moment knowledge of EV demand is equivalent to a second order cone constraint, which is proved. Based on such characteristics, a chance-constrained (CC) stochastic integer program for the planning problem is formulated. For planning EV charging stations with ER, this method develops a simple ER model to investigate the interaction between the mobile placement of power flow controller and the daily pattern of EV power demand.

ACKNOWLEDGMENTS

First of all, I would like to thank professor Yang Weng for always being available to help, his unconditional support, and guidance throughout my thesis. His comments, feedback, and suggestions improved me a lot. I will always honor the chance he gave me to lead the utility project. I really appreciate his time and dedication with me. I'm so thankful for professor Weng and his team, who supported me.

Moreover, I'm so grateful for the presence of Dr. Quishi Cui in this work, I've learned a lot from him, he has been sharing his knowledge with me since May 2019 and always willing to give me more of valuable information, I am much beholden for trusting me and share with me his valuable time. Also, for his talented assistance that developed every single section in this thesis.

I would like to thank professor Keith Holbert for sharing with me worthy information that helped a lot to understand the power system, especially nuclear power plants. Also, to thank him for sharing his time by accepting my request to be a member of my thesis.

I am blessed with my mother, who always encourages and wishes me the best. I would like to thank her for her patience and the great love that pushed me a lot to do this thesis. Also, I would like to thank my father, the main supporter for me who has been asking and caring about every single thing in my study years especially this thesis since the first day I decided to do it, I would like to thank him for always making the worse sound simple.

Finally, I am blessed with all of my friends and family members who supported and kept asking about me that's meant a lot, thank you all for being there for me none of this would happen without your encouragements.

TABLE OF CONTENTS

CHAPTER Page

CHAPTER Page

LIST OF TABLES

Table Page

LIST OF FIGURES

Figure Page

Figure Page

Figure Page

Figure Page

Chapter 1

INTRODUCTION

The method for transmitting power through a line has been improving since the debate started in the late $19th$ century between Thomas Edison and Nikola Tesla about the type of current to be used [8]. To provide electricity for wide areas with different requirements, the type of line is divided into two categories, which are the transmission lines and distribution lines. Transmission line has been upgrading and additional components being attached to it aiming to maintain stabilized power flow. Transmission lines are being designed to be more controllable, reliable, and secured to protect the system from outages and blackouts, which requires controlling devices to achieve these features. Flexible alternating current transmission systems (FACTS) is one of the enhancement devices that can be attached to the transmission line. The FACTS devices will assist in reaching the utility goals with less economical cost and high reliability. Especially, with the increment in power rating that utilities provide to the consumers annually.

Furthermore, not only the power system is improving, the transportation system has been as well. The new generation of transportation systems relies on the power system because it operates using electricity instead of gas. The main reasons behind the switch are to reduce the emission, and the fuel cost. The average annual cost of driving gasoline vehicles is $1,117 and for electric vehicles (EVs) is $485 in the U.S. depending on the prices in each state [9]. However, to charge EVs, it requires more attention than fueling gas vehicles because of the influence on the power grid. The EV can be charged in either the owner's house or electric vehicle charging station (EVCS). So, to plan an EVCS optimal placement requires considering the effects on

the power system and meeting consumer needs.

In this chapter, the literature review of energy router, EV, and EV charging records are discussed. Then, the problem definition states the issues and how this thesis is solving them. The thesis outline describes each chapter's content.

1.1 Background

1.1.1 Flexible Alternating Current Transmission Systems

Electronic power controllers were used to ensure power flow stability by controlling the voltage and angle of HVDC transmission only. Then, Dr. Narain G. Hingorani presented flexible alternating current transmission systems (FACTS) in 1988 to apply electronic power controllers for AC transmission line. FACTS is a group of devices aiming to increase the line's capacity while reaching the same security and voltage regulation when an additional line is added. So, instead of adding a line to the system, a FACTS device can be placed such as voltage source converter (VSC), static phase shifting transformer (SPST), static var compensator (SVC), static synchronous series compensator (SSSC), etc. SSSC will be discussed and tested by applying it to different case studies, which proved the device's effectiveness.

AC transmission line power flow relies on the reactance value in the system. Equation 1.1 represents the power flow with assuming there is no losses in the line. It shows that the real power P is in an inverse proportion relation with the reactance X. On the other hand, the reactance has a direct proportion relation with the line's length, which has been making series capacitors necessary to maintain the power flow.

$$P_{max} = \frac{V_1 V_2}{X} sin(\theta_1 - \theta_2) \tag{1.1}$$

Equation 1.1 represents the power flow on transmission line, but the main concern is to control the reactive power on the line. Controlling the reactive power on the

line can be represented in Equation 1.2, where Q_C is the injected reactive power. Magnitude and phase angle of the voltage are defined as $V_1\angle\theta_1$ at the sending node and $V_2\angle\theta_2$ at the receiving node.

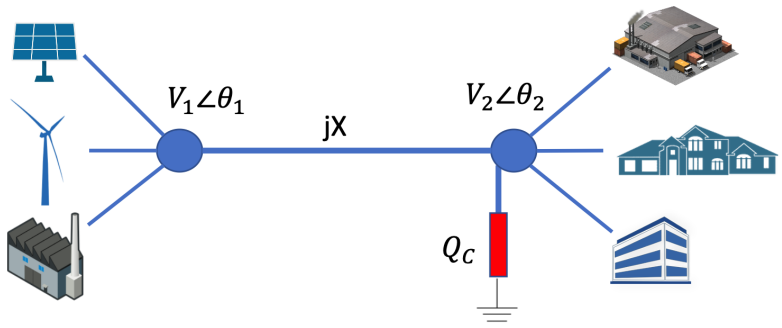

Figure 1.1: Reactive Power Control

$$Q_C = \frac{V_2^2 - V_1 V_2 cos(\theta_1 - \theta_2)}{X} \tag{1.2}$$

Applying a controlling device at the receiving node as shown in Figure 1.1 that is designed following Equation 1.2, can double the maximum power being transferred. FACTS devices have been divided into two classes, which are variable impedance type and VSC based. VSC device is more compact and considered to be better than a variable impedance type. Thus, SSSC that is one of the VSC devices, is studied and used to solve the issue of overload and maintain stability of the system [10].

1. Different Applications Compering to Energy Router

   Different devices were invented to control stability and increase line capacity. Capacitors are used to increase the transmitted power, but they could not decreases it. In [11], it shows that the SSSC can increase and decrease the transmitted power. In addition, capacitor banks, VAR compensators, and synchronous condensers are used to ensure stability and compensation. However,

they have an issue, which is the lag in terms of fast response due to the mechanical operation [12]. Some devices have close operation principles to the SSSC's, but there are differences between them. For instance, back-to-back (BTB) converters are being used to control phase shifting and frequency (timescale) of voltage, so what is the need for SSSC and it's more expensive? SSSC can control power flow of transmission lines, and change set point with the ability to avoid the lag in time. So, it's more flexible to be used in the transmission system that operates at high voltage as shown in [2].

Multiple FACTS devices are designed for different operational uses like unified power flow controller (UPFC), thyristor controlled series compensator (TCSC), SSSC, static synchronous compensator (STATCOM), etc. [13]. The FACTS can be divided into two main categories, which are FACTS and distributed FACTS (D-FACTS). D-FACTS are cheaper than the SSSC, but it's only allowed to be used withing max voltage of 10 kVA [14]. In term of better application than the SSSC, in [15], it compares the SSSC with SMES. Super-conduction magnetic energy storage (SMES) is more expensive than the SSSC. The paper showed that SMES has better critical clearing time than the SSSC does, which means better line transfer capacity. In [10], it showed that STATCOM is better than the SSSC at low voltage levels, but STATCOM best location to be placed is the midpoint. On the other hand, the SSSC is directly proportional to the reactive voltage injected, which makes it better than the STATCOM in increasing the power transfer.

2. Energy Router

The remaining of the thesis will introduce the SSSC as energy router (ER) since it was the name used with the local utility in Arizona (LUA) and in the

case studies. ER is designed to provide the utility an option of controlling the reactance in transmission lines [4]. The ER will be attached to the transmission line in series, with additional circuit connections, and it could require additional tower or an update for the used tower due to the heavy weight of the ER [4]. To understand how the ER attached and its operation principle three VSC devices will be discussed. STATCOM is connecting in a shunt with the line to inject the reactive current, which can be done by regulating the bus voltage. ER is connecting in series with the line as shown in Figure 1.2, to inject the reactive voltage. Unified power flow controller (UPFC) is connecting in both ways because it controls both the real and reactive power by injecting both the voltage and current [10].

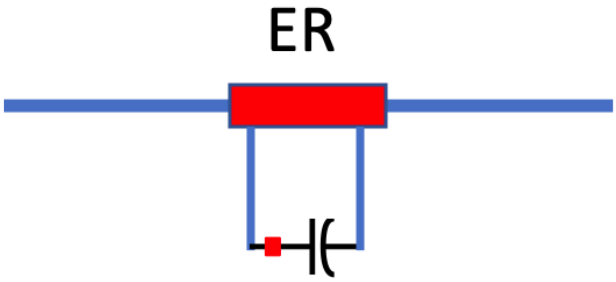

Figure 1.2: ER Connected in Series to the Line

Figure 1.2 is showing the capacitor, which is a part of the ER that provides energy from the DC terminal [10]. The capacitor will be charged by pulling some power from the line [12]. The capacitor is better to be connected to an energy source because an issue can occur at low line current stages, which is necessary to be mentioned. The ER series insertion will inject the line voltage in series with the current. The voltage will be injected in quadrature comparing

to the line current [12], [10]. The following bullet points will be used to explain the ER's operation methodology and benefits.

- Energy Router Principles

  The operating principles of the ER can be discussed in three major things. First, is to control the reactance on the transmission line, which will happen by using either inductive or capacitive mode or lagging and leading position. Second, ER determines if there is a fault that occurred and stops the flow to the device by isolating the frequency and magnitude flowing from the line, which is known as bypass mode [4]. Third, is to increase the stability of the system when contingency condition occurs [10].

- Energy Router Affects and Impact

  The effect of using the ER is to provide the utility more freedom of controlling the reactance in the system. It will help to solve the issue of overload on the grid. The solution will also help the utility to stop damages caused by fault of other lines on the system and get ready for the new generation of renewable power plants [2].

  (a) ER Impact on Harmonics

  ER will reduce the harmonics on the system, which can happen due to different reasons like, the inverters [1]. Also, switching is causing losses on the system, which makes the power electronic devices limited to one off-on, and one on-off per cycle. However, ER uses complex multi-pulse inverters method, which cancels harmonic voltage by applying basic six-pulse inverters that are coupling the AC terminals [1]. Figure 1.3 shows ER with 24 pulses represented by the Voltage

Source Inverter (VSI). Note, the previous reference discussed ER using VSI, which is rarely used in the new generation of ER research. Most of the modern researches and companies discussed ER with Voltage Source Converter (VSC). Both VSI and VSC will reduce harmonic, but converters are more helpful in increasing the speed simulation and improve the convergence [16].

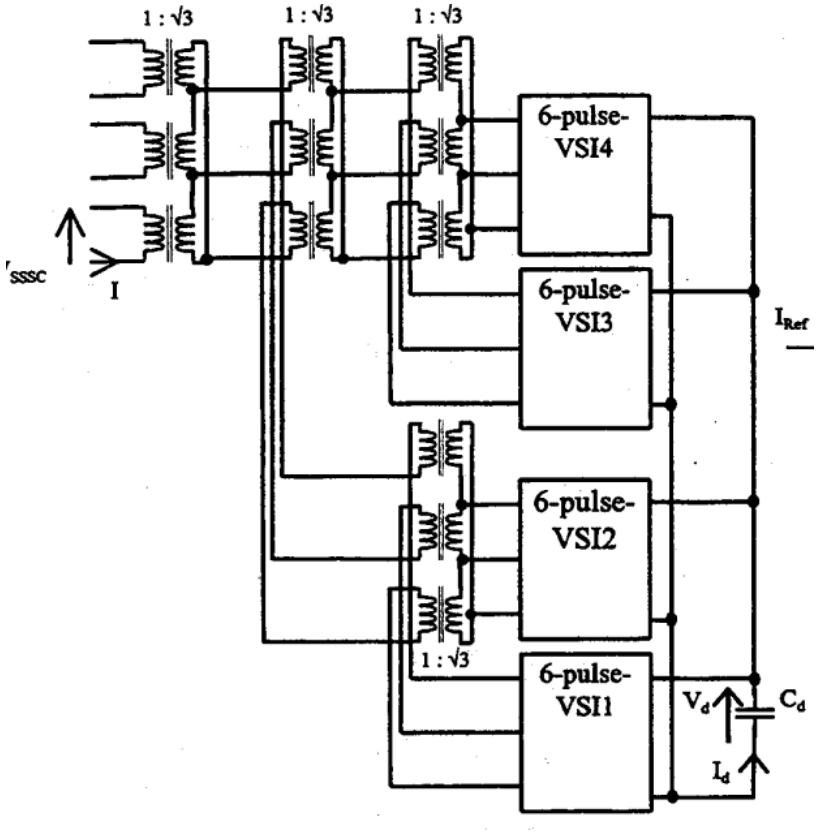

Figure 1.3: ER 24-pules to Deal with Harmonics [1]

In [17], ER assists in dealing with the harmonics on the system, and it shows how ER reduced the harmonics that effected in maintaining the steady state condition of the power flow. It used a 48 gate turn off voltage source converter (GTO-VSC) that was attached to ER, which assisted in reducing the harmonic more than the 6 or 24 pulse. So,

as a conclusion from the previous references, increasing the number of pulses will decrease the harmonics, which means ER will assist in reducing harmonic in the system.

(b) ER Influence when Short Circuit Occurs

To explain the short circuit clearly, check Figure 1.4. The ER is located on line $1-4$, so when the fault happens in the same line $1-4$, then the ER will have no impact on the system since it will bypass the power flow. However, if the fault occurred in any other line on the system the ER will fix the issue by changing the reactance.

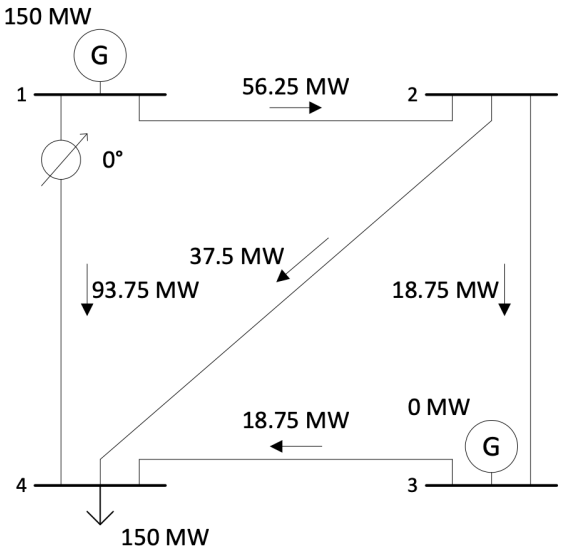

Figure 1.4: ER Connected in Series to Line 1-4 [2]

Further investigation regarding the ER impact when a short circuit occurs will be shown in Chapter 2. Three case studies will clearly explain ER's influence on the LUA system. ER's model is provided by Smart Wires, which is named Smart Valve in their company.

(c) ER and Power Flow

Controlling the reactive power on the system means the losses can

be decreased [18]. When a fault occurs in one line, the relay will stop the power flow into that line, which will create an overload on the system. To control the problem, the line with ER attached to it will change the voltage phase angle to specific values that will keep it at the required level.

Multiple devices can be used to assist in the phase-shifting for instance, the ER and IGBT are applied in [19]. So, ER will control the post-contingency on the system to reduce losses [2], which will assist in maintaining secured power flow.

To understand how the ER will impact the power flow Figure 1.5 shows the phase angle injection of ER. In [10], the complex power formula found, which is driven to find the ER characteristics on the power flow by presenting the complex power of the receiving end shown in Eq. 1.3.

$$S_2 = \frac{S_0 Z^*}{Z^* + jA} = \frac{S_0 Z^*}{R + j(A - X)} \tag{1.3}$$

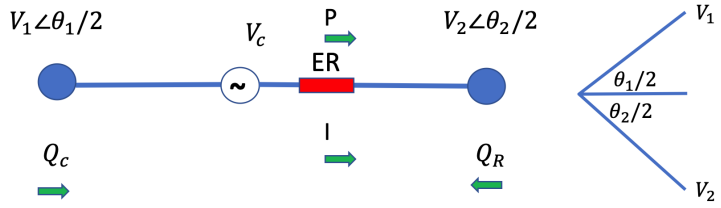

Figure 1.5: ER Attached on a Single Line and Phasor Diagrams

Where S_2 is the receiving end, and A can be between $-\infty$ to $+\infty$. So, to find the ER impact on the system, Eq. 1.3 can be applied to

find the complex power values at the receiving end.

- How the ER Operates?

  The reactance is important in the system because it can change the angle between voltage and current. There are two types of reactance modes, which are the capacitive X_c and inductive reactance X_l. The two types are used to manage the angle between V and I. X_c, or positive mode is to have the voltage lagging the current, which is used to improve the line's current. However, X_l or negative mode is to have the voltage leading the current of the line. So, by controlling the reactance it means the angle can be in phase, or out of phase depending on the grid load [20]. The focus on voltage and current in this section will be in term of phase angle, not magnitude. The reason behind that is the ER affects the angle of the line more than the magnitude. The phase angle in the transmission line can be different within, $30, 60,$ or 90 degrees between V and I. The ER will make the difference in angle depending on the readings the control unit is receiving from the line. The inductive and capacitive can affect reactance in the system by making the system lagging or leading. To have a better understanding, the capacitive and inductive will cause a 90° difference between the current and voltage. Figure 1.6 shows the relationship between current and voltage with angle differences due to leading once, and lagging for the other. In other words, reactance assists to have the current in a different phase compering to the voltage and by doing this, the system can be controlled, which is the basic concept of the ER to control reactance on the system.

- ER Control Methodology

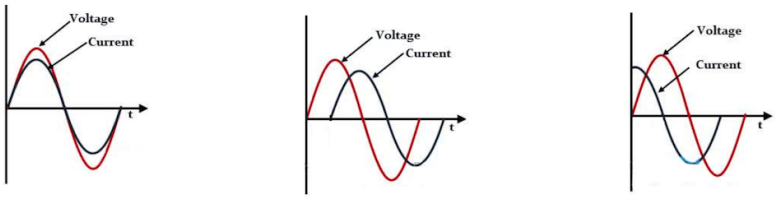

Figure 1.6: Inductive and Capacitive Modes [3]

The control in ER is divided into three types, initially how it controls the line and receives data. Then, the devices that are used to control in the ER will do the calculation. Lastly, sending orders to operate for a certain mission. To explain each type in order, the H-bridge, IGBT, and current transformer devices are used because they operate as sensors, but for high voltage uses. These devices are controlled or programmed to collect a specific type of data, and what to do if it receives an order from the main control room. Second, after receiving the data, the ER will make the calculation to maintain stability by avoiding reaching the overload on the grid. The last type of control is to send orders to the ER location to set the reactance at a specific value, or to use the H-bridge that will bypass the fault occurred to protect the device itself.

To connect the three types of control, there must be communication and an optimal location found for the ER placement [4]. To clarify the three controlling parts, first is the phase locked loop, which is used for synchronization, second is the measurement of voltages inputting to the voltage regulator, and third is the measurement of $axis$ for the converter's voltage. For the communication between the ER and the utility's control unit it will focus on operating with different grids. ER will receive data from the main control unit, and send it using communication and control

system or end to end ($E2E$) system, which is shown in Figure 1.7 [4], [19].

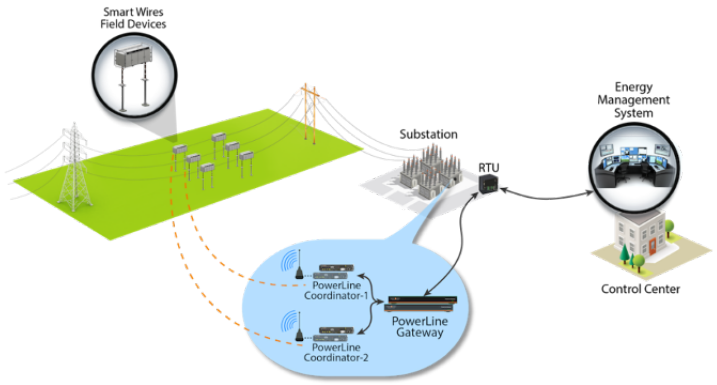

Figure 1.7: ER Communication with the Control Center to Make the Accurate Changes in Reactance [4]

Furthermore, the ER is designed to control the reactance of the power flow on the transmission line. When a short circuit occurs, the ER is programmed to a default stage to avoid the need of communicating with the main control unit, which is named as bypassing as shown in [4]. Before describing the ER's control methodology in mathematical form, the explanation of the ER's communication method will be classified first in 2a.

(a) ER Communication Method

The communication in ER will receive data from the main control unit and this data will be sent using the internet, because of the high speed, accuracy of data exchange it has. To have a better vision of how the communication in the ER is operation there are three components to be explained, which are shown in Figure 1.8.

First is the Cellular Enabled PowerLine Guardian that is used to receive and send the data to the control unit and responsible for the

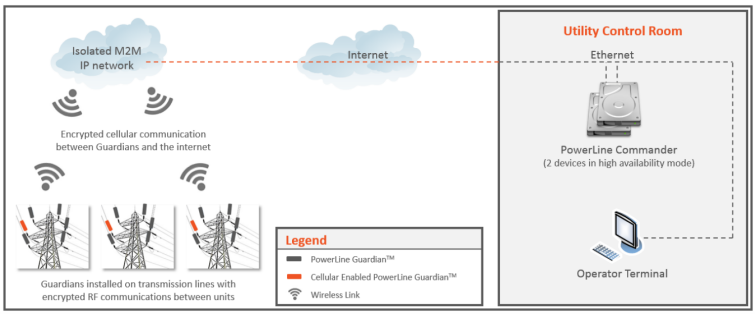

Figure 1.8: The Three Components in the ER for Communication [5]

communication. Second, is PowerLine Commander, which is the Energy Management System (EMS). Third, is the power Guardian that is designed to inject the impedance of the line after receiving the data [5].

(b) ER Deployment

The deployment of ER will go over three main parts, the transportation, towers, and ground-based. This section will assist in understanding the time for transportation, and an estimation of the additional cost due to the new parts required.

i. Tower Base

The ER has a heavy weight, so it requires an upgrade to the tower, where it can handle the additional weight and carry it. Figure 1.9 shows the design that Smart Wires made for attaching the ER. There is a second option, which is to replace the tower with the one designed by Smart Wires [6].

ii. Ground Base

Ground base is to carry the device at close locations to the substations or inside it. Figure 1.10 shows the ground base of

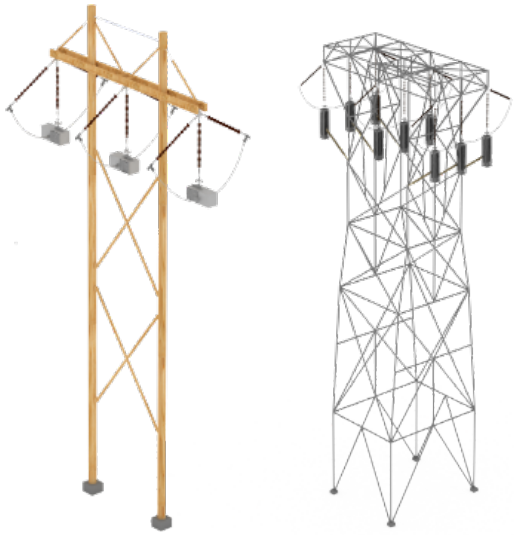

Figure 1.9: ER Tower Base [6]

Smart Wires design [6].

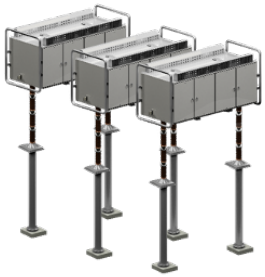

Figure 1.10: ER Ground Base [6]

iii. Mobile ER

The mobile container can be ready to ship within short time. Installation can be done within different periods depending on the location and can take from a few hours (eight) to two days. Figure 1.11 shows the container provided by Smart Wires [6].

- Different Applications Leveraged by ER

The ER has been used with different devices to find the best power flow

Figure 1.11: Mobile ER [6]

on the system. For instance in [21] it was used with STATCOM to control the power flow during contingencies and faults. Since the ER is capable of controlling the reactance on the system, it was studied to solve different issues caused by different reasons. In this section, some applications will be discussed to clarify the ER importance.

(a) Energy Management for Power Plants

Energy management in the ER is to reduce losses on the grid, with better controlling opportunities. As mentioned earlier, the ER focuses on controlling the impedance on the line. To control it, it will assist in having the flexibility to add new generator sources with fewer changes on the power system and to solve the damping power oscillation. In [22], it explains how the ER is efficient in controlling the damping oscillations.

The power system is being built with specific requirements, which are being changed due to the new needs. For instance, the generator plants are being built depending on the location. The location must be safe and can be reached to different states or cities depending on the MW rating for it. The renewable energy depends on the natural source location to be sunny, windy, etc. [23]. And due to the increment of renewable energy being used and the unstable amount of power it

provides, a FACTS device will assist in solving these issues. In [24], it shows the ER is being used for applying wind turbines to the system and provides the ability to have better power damping.

The ER will provide the flexibility of energy management by shifting from leading to lagging position or the opposite depending on the condition. In [25], it discusses how the ER will assist in connecting a wind plant to the grid located in Indiana. The ER will solve the voltage collapse issue due to the lack of reactive power on the system and maintain stability and efficiency. The result of using the ER to combine wind power plant with a diesel generator on the system shows that the reactive power and active was controlled, which solves the problem.

(b) ER Impact on Power Swing

In [26] it studied the impedance that is shown in distance relay when a power swing occurs. The ER is used to shift the angle on the line when a power swing occurs in the system. It shows the difference between the inductive mode and capacitive mode, by using a relay that has a smaller radius on capacitive mode. Also, it proved how effective it was in terms of power flow stability.

(c) ER Impact on Transient Damping

From [27, 28, 29], it's clear that the ER can solve the transient damp on the system. In [27], the paper solved the second dip in dynamic response that occurs on induction motor when the output is adjusted. The ER solves the issue by phase-shifting to avoid the different dynamics that happened in the line and keep the power flow in between the required limits. Also, it was used to increase active

power in the transmission line. In addition, the ER has fast operation principles to maintain the steady-state condition. In [30], it tested the ER to fix the transient damping in the system, which was fixed within 2 cycles.

The ER's definition and usage are explained in terms of its principles, effects, and impact, applications that are leveraged by it, operation, and control methodologies. The impact on the grid and operation when different conditions occurs showed that the ER will assist in increasing the transmission line security. The control method in term of mathematical and communication forms are presented to provide a clear vision of the ER's is modeled. In addition, different applications of ER are explained like applying it to solve renewable generation issues. Chapter 2 will apply the ER on a utility grid, and its model is formulated in Chapter 4 for EVCS planning method.

1.1.2 Electric Vehicle and Electric Vehicle Charging Records

EV number is increasing because of two main reasons, which are pollution and energy prices. In [31], it considered the same two reasons and it was published in 1964. To understand why the EV market is increasing recently, a brief introduction of the EV is discussed. Also, the charging records are introduced due to their importance in finding the EV impact on the power grid.

- Electric Vehicles

  EV is a method of transportation that is first found in the $19th$ century with a top speed of 14 miles/hr. Different studies found how the EV will assist in economical term. In [32], it demonstrates the savings by comparing an electric wagon with a horse. The EV began to grab more attention, which made 60 electric taxis drove in New York roads. While EVs were being welcomed by

the society and more researches were found, Ferdinand Porsche built the first hybrid vehicle in 1898 [33].

In addition, the early method to charge the EV used to be complicated, and an expert is required to do such a job. In [34], it introduces electric automobile operating using a rotary motor, compounded gear that reduces the motor's weight and size while providing enough torque, and a battery. The battery provides power for $1 - 2$ hours, which stores the power using compressed air. The method to charge a battery required an expert with a differential watt-meter, and periodic inspection using a hydrometer.

However, the gas vehicle industry has ended up the EV's because of their limited speed, and they used to cost more than double the price of the gas vehicle [33]. In 1922 the gas vehicles were used to drive with high speed for long distances while the EVs were still being introduced to replace the horses. The main reason is the battery storage that had issues, in [35] it compares the lead cell with the Nickel-iron cell, and both had their disadvantages where one of them had a short lifetime and the other one was costly.

Although the EVs industry almost disappeared, scientists were still digging into the topic to enhance the technology. In [36] it discussed different designs of EVs, and one of them used two motors that are operating with the battery in pairs. Maximizing the gear-ratio can be reached by using a double-reduction drive from a single motor [37]. Generation rubber tire to charge the EV is also modeled, which had two methods of induction and conduction the charges from and to the tires. Once the vehicle is charged the current will flow to the street instead of the car. The method was not preferred because the vehicles had enough electric charge to shock a person even when it's no longer moving [38].

Furthermore, the pollution from the gas emission and lack of oil made the EV concept introduced again [31]. In [39], it finds that using a DC motor is better than an AC because it's lighter, requires 60% additional current to reach maximum torque, and operates at larger gear induction. Converters were being applied to the circuit, which provides the ability to increase the motor's performance while the lead-acid battery capacity reaches to 108 V. To charge the EV, a $115V$ with a 60 Hz source is required [40]. At the same time duration computers were also well designed to function different applications, which made the study in [41] demonstrates a model that had the ability of controlling the EV. An electric van is designed in [42], which had a maximum speed of 90 km/h, using a three-phase squirrel cage induction motor rated for 27 kW. The van battery ran out fast, which recommended applying a battery interchange or attaching on-board charger to have a longer driving range. Yet the EV couldn't take place in the market because it created more pollution than the gas vehicles since it impacted the demand, which increased the power plant emissions [43]. So, the main reasons behind the delay of the EV industry are three:

1. EV used to cost more than double the price of gas vehicles.
2. The battery storage was limited.
3. The power plants had large emission rates, which will be increased to meet EV needs. In such a condition, the EV will not assist in decrease the pollution comparing to gas vehicles.

The problems that affected the EVs market are solved due to the integration of renewable power plants, battery improvement in range and life, and the lower operational cost. Therefore, the EVs have been popular worldwide and the number of EVs will skyrocket especially with the governments' subsidies. For

instance, the number of EVs in the U.S. will reach 18.7 million in 2030, which will require 9.6 million charging ports [44]. In addition, China is planning to reach five million EVs in 2020 [45] and the Indian government is aiming for a huge switch from a gas vehicle to EV in 2030 [46].

There are benefits of adapting the EV, which are economical profit, and pollution reduction. EV impact on pollution is analyzed in terms of direct and life cycle emissions, which found the EV will reduce both. The direct term emissions for gasoline vehicle produces during fueling and from the exhaust, which decreases to zero for an EV. The life cycle emission is emitted from power generator and petroleum extraction, which is less for the EV and can reach zero if a renewable source is used [47].

In [48], it compares three Tesla models fast charging prices with gasoline vehicle fueling costs, which estimates the supercharger cost as 0.26 kWh and the Gasoline cost as 2.85 per gallon. For the driving distance of $1,500$ miles, the costs of three models are shown in Table 1.1.

Table 1.1: Supercharger and Gasoline Costs of Three Tesla Models

Model	Supercharger cost	Gasoline cost
S	\$116	204
X	\$132	204
3	\$100	153

The EV operational cost have been increasing its market shares. The growth number in 2018 comparing to 2017 reached 64% globally, 34% in Europe, 79% in the U.S., and 78% in China. Figure 1.12 shows the EV growth number in the U.S., which reached 1.18×10^6 vehicles [7].

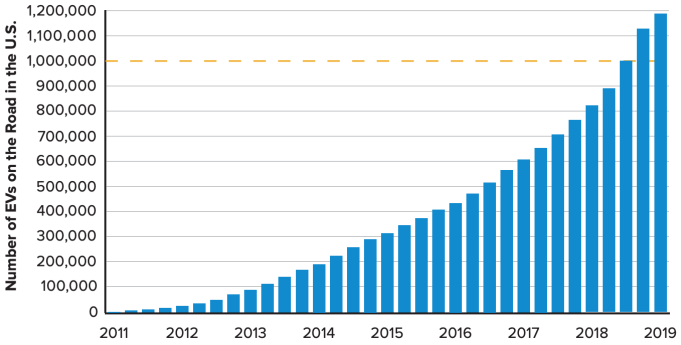

Figure 1.12: EVs Number in the U.S. [7]

Moreover, the driving range of the EV has been increasing because the battery improvements. In [49] it shows two electric Nissan vehicles, which are LEAF S PLUS with battery capacity of 62 kWh and LEAF with 40 kWh battery. LEAF model can drive up to 149 miles on a single charge, where the LEAF S PLUS drives up to 226 miles. Chevrolet also designed an EV and called it Bolt EV, which has driving range of 259 miles and 66 kWh battery [50]. Audi e-trone integrates a 95 kWh battery with driving range of 204 miles in a charge [51]. The ranges and types of the battery are different from one EV to another, which is the same for the charging time.

- Electric Vehicle Charging Records

  To charge an EV there are rules and regulations that must be followed because it can result to a big damage on the power system if not. For instance, the U.S. Department of Energy lists three levels of charging. First, 120 V AC plug that can be named as slow charging, which can be located at houses. Second, 240 V AC that can be placed in public charging station. Lastly, is the DC fast charging, which is rated for 480 V AC [52, 53]. The charging time for each level is different and it depends on the battery type. For instance, applying the

fast charging level to the Audio e-trone for 10 minutes will provide a range of 54 miles, Chevrolet Bolt for 30 minutes will drive it for 100 miles, and Nissan LEAF for 40 minutes will charge 80% of the battery, which is equivalent to 119.2 miles [49, 50, 51].

EVCSs have been recording the charging transactions to reach maximum profit. EVCS records are discussed to understand the provided information and based on them study their behavior.

– Colorado Data

The city of Boulder, Colorado provided a data set for EVCSs in five zip codes. The data set represents useful information, but not all of the features are used. Table 1.2 shows the first three rows of Colorado's EVCS.

Table 1.2: Boulder, CO EVCS Data Set

Station Name	City	State/Province	Postal Code	Transaction Date	Transaction Start Time	Energy (kWh)	Gasoline Savings (gallons)	Port Type
BOULDER / ATRIUM ST1	Boulder	Colorado	80302	2/26/20	12 : 47	3.833	0.481	Level 2
BOULDER / N BOULDER REC 1	Boulder	Colorado	80304	2/29/20	20 : 19	18.64	2.339	Level 2
COMM VITALITY / 1104 SPRUCE1	Boulder	Colorado	80302	2/29/20	18 : 14	5.196	0.652	Level 2

The data set is analyzed in a useful way when it's applied in filling the transportation system in Chapter 4, by providing the EVCS demand at different day periods. For this chapter, the data set is separated depending on each zip code. Then, for each transaction year, every month, and per hour, the sum of energy consumption in kWh is found. The dataset is provided from January 2018 to February 2020. Figure 1.13, shows the five plots for each zip code presented in hour vs sum of kWh.

Figures 1.13a, and 1.13e, are showing energy consumption for 2018, and 2019. Figure 1.13d, is showing kWh consumption for 2019 and 2020, but

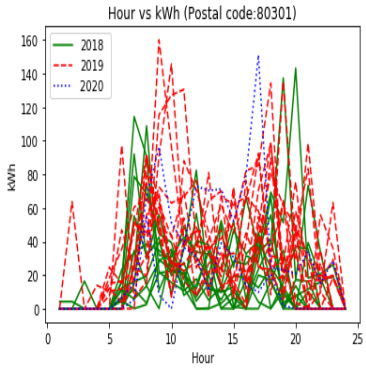

(a) Sum of EVCS Energy for Zip Code: 80301

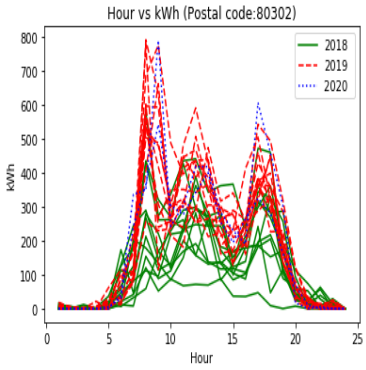

(b) Sum of EVCS Energy for Zip Code: 80302

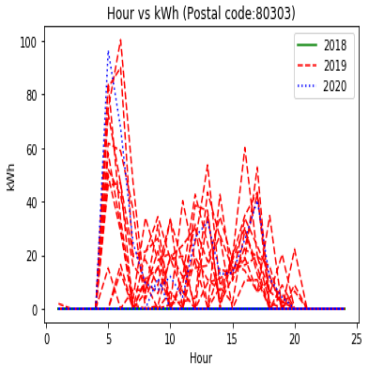

(c) Sum of EVCS Energy for Zip code: 80303

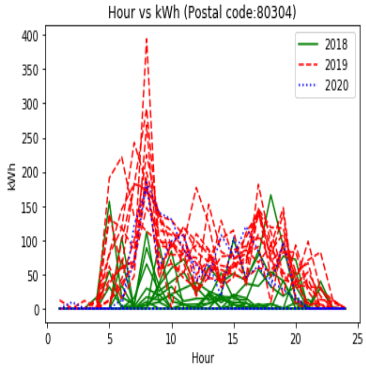

(d) Sum of EVCS energy for zip code: 80304

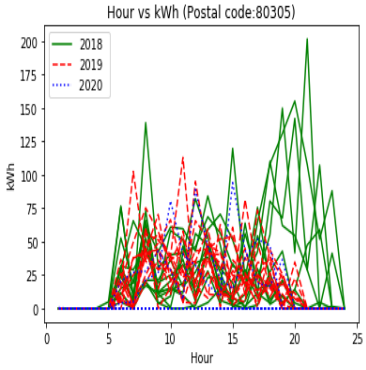

(e) Sum of EVCS energy for zip code: 80305

Figure 1.13: Colorado EVCS Energy Consumption for 26 Months. Each Line Shows the Sum of kWh Consumption in $y - axis$ for Each Month in 24 Hours as Shown in the x-axis.

few for 2018. Figure 1.13c, is showing for 2019 with couple ones in 2020, but not 2018. Figure 1.13b, is showing the consumption for the three years and it has the most amount number of transactions, which give it the advantage to be further investigated because the more data is available the better analysis and more efficient prediction can be found. Table 1.3, is

showing the number of transactions (NT) for each zip code, which verifies the plot shapes.

Table 1.3: Number of Transactions in Five Zip Codes for the City of Boulder

Zip Code	80301	80302	80303	80304	80305	Total
NT	1766	12382	561	2936	1666	19311

The data set description and observations are discussed by showing a sample from the table and separate the data depending on the zip code.

– California Data

Palo Alto, California data set is provided in [54], which shows the information for EVCS during 72 months from 2011 to 2017. The data will be studied first in term of the zip code and the one with largest records of charging will be investigated. The kWh consumption will described and observed for the 24 hours during the 72 months. To have a look on the studied data, Table 1.4 shows the first three rows with some important features. The number of columns is 39, but and not all of the features are shown in the table.

Table 1.4: Palo Alto, CA EVCS Data Set

Station Name	Transaction Date (Pacific Time)	Charging Time (hh:mm:ss)	Energy (kWh)	City	Postal Code	Year	Month	Hour
PALO ALTO CA / HAMILTON #1	29/07/2011 23 : 20	01 : 54 : 03	6.250	Palo Alto	94301	2011	7	20
PALO ALTO CA / HAMILTON #1	30/07/2011 00 : 02	00 : 01 : 54	0.107	Palo Alto	94301	2011	7	0
PALO ALTO CA / HAMILTON #1	30/07/2011 12 : 34	04 : 17 : 28	14.952	Palo Alto	94301	2011	7	8

The data set will be separated following Boulder's method, which is depending on each zip code. After grouping the data, the sum of energy presented in kWh will be found for each transaction at every year, month, and hour. The data set is given for 72 months, which are from July 2011

to July 2017. To find how the load consumption is diverging at each zip code, Figure 1.14 plots it for the 72 months.

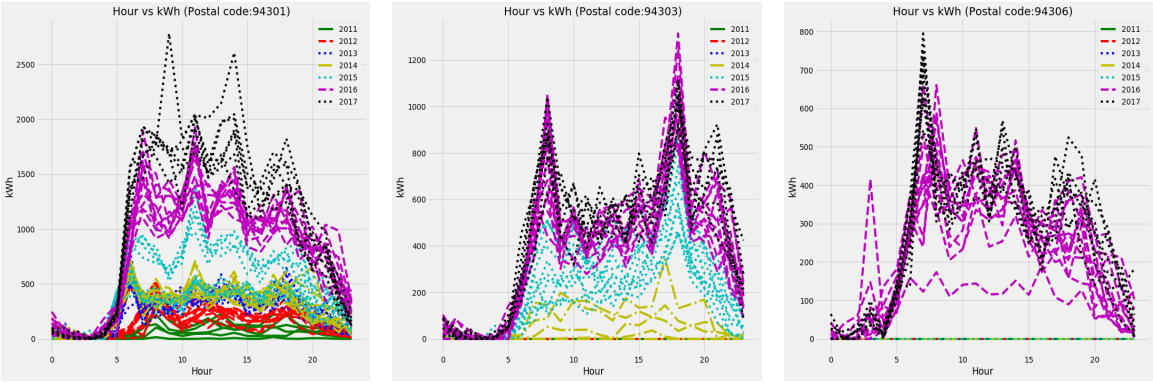

(a) Sum of kWh consumption for zip code: 94301

(b) Sum of kWh consumption for zip code: 94303

(c) Sum of kWh consumption for zip code: 94306

Figure 1.14: California EVCS Energy Consumption for 72 Months. Each Line Shows the Sum of kWh Consumption in y-axis for Each Month in 24 Hours as Shown in the x-axis.

From Figure 1.14, the load at different areas shows an increment between the hours 05 : 00 to 20 : 00 while at early hours from 00 : 00 to 04 : 00 the load is almost zero. Note that the data set is provided from Jul 2011 so the first seven months are not plotted since they are not given. Figure 1.14b shows the transactions are recorded starting from 2014, which means the EVCS is built in this year. Figure 1.14c is providing the data starting from 2016. In addition, The number of transaction for each zip code is given in Table 1.5.

From Table 1.5, the three zip codes for EVCSs in Palo Alto are 94301, 94303, and 94306. The data represents 133, 559 charging records, where each zip code varies with the number of records. Zip code 94301 shows

Table 1.5: Number of Transactions in Three Zip Codes for the City of Palo Alto

Zip Code	94301	94303	94306	Total
NT	90,022	29,049	14,488	133,559

90,022 records, 94303 lists 29,049 records, and 94306 presents 14,488 records. So, the decision has been made to analyze the zip code with the highest number of charging occurred between July 2011 to July 2017, which is 94301. Furthermore, to compare the time of charging to discussed models, Figure 1.15 shows the charging duration for all 72 months.

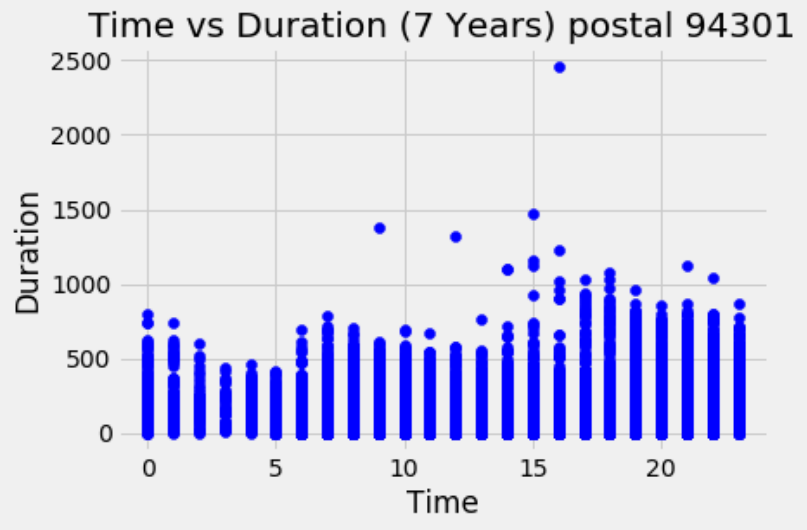

Figure 1.15: Palo Alto 94301 Charging Duration From 2011 to 2017

EV charging records for two data sets are discussed, which shows that different features are recorded. The data sets for the two cities showed useful information such as the transaction time, energy used, and the charging duration. The three features are separated depending on their largest transactions record and in Chapter 3 they will be observed and studied.

1.2 Problem Definition

While new power plants are establishing and the load is increasing, maintaining a secured power flow has been a hard task. The new power plants are mostly renewable since the governments worldwide are encouraging it because it fights the pollution and has a lower operational cost. For instance, the wind turbine is located depending on multiple factors and one of them is how windy the place is. When the wind turbine plant is connected to the power grid, the transmission line in the system is designed for a limited current rate. So, to overcome this problem utilities upgrade their transmission line capacity, but building new line is costly and might lead to delaying the project timeline. Although upgrading the line sounds like the only solution, but the ER will also solve the problem. The ER will inject the reactance with a specified value that will provide the controlling over the reactive power in the line. When the reactive power is controlled, the line limits can be increased, which will solve the overload problem with lower cost and faster time. In addition, when the ER is purchased and the reactive power is no longer assisting in solving the overload, it can be attached to another location and still assist the stability of the system.

The items operating on electricity are variant, but the most noticed one is the EV. The EV has an impact on the power system especially the distribution area in the current time, but it will significantly impact the transmission in the near future due to the EVs growing numbers.

EV charging duration varies, which affects the power flow stability if enough load is used. The problems can be voltage oscillation, transient damping, overload, etc. If any of these problems occur without fast action, then major damage will happen in the system. So, to avoid the issues EVCS impact on the grid can be clearly found if the transactions at each time are recorded. When this is the case, the time series

analysis method can be applied to understand the behavior of the data. Also, to estimate if an issue will occur in the future, the trend and seasonality of the historical data are studied using an exponential smoothing method. The EVCS behavior can be represented numerically or by plotting it, which means to plan a new one can consider the findings to avoid any problem occurring in the system.

EVCS planning models considered both distribution and transmission system. The references [55, 56] studied EVCS planning method with coupling the transportation system, which can be influenced by different random factors such as an accident. However, the presented model will consider the EVCS data set that represents the EV demand to fit the planning method. EVCS planning with considering transmission grid has been already studied in [56, 57, 58], but none has considered to apply the ER to provide an ability of controlling the power flow to the system.

Since the ER can enhance the operation of the transmission system, and EVCS is impacting the grid; An optimal EVCS planning method is formulated while considering the ER to control the power flow depending on real EVCS data set. The model will assist both sides, the utility, and EV owners because it will maintain low prices and stability of the power flow.

1.2.1 Thesis Statement

This thesis will explain the effect of using an energy router on the transmission line and EVCS planning. The ER placement on LUA transmission lines using Smart Wires model is to solve the overload and provide a deferral time to upgrade the projects. ER impact on EVCS planning is formulated with an objective function that considers the estimation of EVCS historical records. This thesis finds how effective the ER is to enhance the power flow stability in the electrical system.

1.3 Claims of Originality

The work of this dissertation enhances transmission system and EVCS planning following the original contributions:

- Rigorous validation of ER impact to enhance the transmission system stability by applying the device and its mathematical model on a local utility in Arizona grid. ER model is presented by Smart Wires company.
- Development of forecasting method using exponential smoothing model that is applied on Boulder, CO and Palo Alto, CA EVCS data sets. The method analyzed the charging behavior to understand its impact on the power grid.
- Novel formulation of EVCS placement using knowledge moment, which is enhanced by ER, based on chance constraint is generated. The impact of ER and its mobile using mobility matrix are investigated in terms of EVCS planning.

1.4 Thesis Outline

Chapter 2: ER placement on LUA transmission line is studied for three case studies each represents a different project. First, since the ER injects the reactance of the line, it was changed manually by multiplying X value with a specified range. Although the results solved the problem, the same projects are tested with real ER model provided by Smart Wires. The outcome of placing an ER on the system is positive, where it solves the overload with faster time and lower cost.

Chapter 3: EVCS data sets for two cities, which are Boulder, CO, and Palo Alto, CA are analyzed. First, the kWh is studied and observed depending on a specified time period. Then, mean and standard deviation values are found to understand EVCS behavior. Also, forecasting methods are applied to predict future energy con-

sumption, but one of them successfully had the good fitting to the historical data set.

Chapter 4**:** EVCS optimal planning model is formulated while the power flow is controlled by ER and EV demand presented by the EVCS demand. The ER is modeled to be tested for $30-bus$ IEEE system, which has 41 branches and 30 buses. Three scenarios are tested, which are distributing the load in different location to find the ER.

Chapter 5**:** The conclusion of the thesis provides a summary and discusses every chapter's content, findings, and future work.

Chapter 2

ENHANCING THE OPERATIONAL RELIABILITY AND EFFICIENCY OF TRANSMISSION GRIDS WITH ENERGY ROUTERS

2.1 Introduction

Energy router (ER) is a FACTS device that is known in power system with the name of SSSC. The ER controls the voltage, current, or reactance through injecting the impedance of the transmission line, which is studied in [12, 59, 60]. Reference [59], considers ER to control the line's voltage to increase the system stability. In [12], injecting the voltage of the transmission line using ER is found, which damped out the oscillation in the system and ensured its stability. ER is also applied to damp the oscillation by injecting the voltage phase in series with the line current [60]. Although the previous cited publications have good findings, the ER is not tested on real power system, which considers more factors.

In this chapter, the ER will be tested by attaching it to a system of local utility in Arizona (LUA). First, since the ER is able to shift reactance, current, or voltage to inject the reactive and real powers to maintain stability on the system. The reactance is shifted by multiplying it with different values between $0 - 100$, which is an estimation average for the ER's ability to change X value. Then, a real model of the ER is applied on LUA grid to test it and compare the results of the multiplication method. Each method is applied to three case studies, which represent three different locations, and years. The results will show the deferral time the ER will provide instead of upgrading the system. In other words, when the ER is attached, an annual load increment of 1.8% will be applied to the previous year's load value; Then the

current value I will be checked to find if an overload solved or not.

2.2 Data Analytics for Utility Transmission Planning

LUA is considered under the WECC region, which combines more than a state. Every utility faces different problems, for instance, outages, overload, static and dynamic security, etc. For LUA case this section will find what are their needs from the provided data. LUA data was provided in (*.sav*) format, which requires PSLF software to read the information. In addition, there are files in (*.p*) format, which shows LUA's projects plan from $2019 - 2025$. So, (*.p*) files provided the upgrades LUA planning to work on for six years. Also, the information provided by Smart Wires is explained to assist in understanding how the ER will be attached to LUA system.

The main files are provided in a format that can be opened using PSLF for both LUA and Smart Wires. So, an introduction to PSLF, LUA files, and Smart Wires information is introduced.

2.2.1 Simulation Tool: PSLF

PSLF is a power system program that simulates the electrical system for many utilities because of its ability in connecting wide areas together. There are many parameters provided in each sheet in PSLF and there is one way to understand them, which is by going to PSLF's manual. Some parameters are described to give a picture of how PSLF operates.

- Bus parameters

  The Bus information has the name in PSLF as Busd. It started with bus numbers, their names and kV base. Then, the type of bus from (-2) to (2),

scheduled voltage, bus voltage magnitude (pu) are defined.

- Branch parameters

  The branch data is called SECDD in PSLF. The sheet started with From bus number, bus name, base voltage, To bus number, bus name, base kV voltage.

- Transmission parameters

  The transmission information is named Tran in PSLF. The sheet started with from bus number, name, from bus base voltage, to bus number.

These are some of the sheets information in PSLF, but not all of the parameters are explained because explaining the simulator is beyond this chapter goal, and the information is not allowed to be shared. So, the format of the provided files (*.p*) and (*.sav*) will be explained in terms of their operation principles.

- (*.p*) File

  (*.p*) files are being used by PSLF as a coding page, which defines the parameters and information will be represented on the (*.sav*) files. In addition, PSLF manual showed (*.p*) definition as store directly under working directory. Also, it showed that (*.bat*, *.p*) files are used to execute the program.

- (*.sav*) File

  (*.sav*) files are being used in PSLF to represent the power flow in binary format. So, (*.sav*) file shows the LUA power flow for six different time periods. It was clear the same states, cities were defined in all six (*.sav*) files, but when the power flow was running using PSLF the reactive and real power losses were different, which clearly shows that the provided data represents different time periods with the load increment of 1.8%.

From the previous items, it's clear that the ($.p$) file is used to apply and upgrade the system's power flow file ($.sav$), which is the case to apply the ER model from Smart Wires to LUA grid. More information can be discussed regarding the data mining and description of PSLF, LUA, and Smart Wires files, but due to their sensitivity, the case studies of solving the overload in LUA system using will be discussed. All of the buses, lines, and branches names used in this chapter are given names. The names of alphabet letters are used to represents the buses. However, the numerical results, parentage, current, and reactance values are based on the real information of LUA. .

2.3 Energy Router Implementation on LUA Grid to Reach Maximum Deferral Time by Reactance Multiplication

The ER will control the power flow of the line by controlling its reactance, which will impact the current rating in the line. The mathematical form for the ER to inject the reactive power is found in Eq. 2.2, which is found after expressing the reactive power on the receiving end Q_R as Eq. 2.1 shows;

$$-Q_R = VIsin(\frac{\delta}{2} - \phi) \tag{2.1}$$

$$-Q_R = \frac{V^2}{X_L}(1 - cos\delta) - \frac{VV_p}{X_L}cos(\frac{\delta}{2} - \phi) + \frac{VV_r}{X_L}sin(\frac{\delta}{2} - \phi) \tag{2.2}$$

where X_L is the line's reactance, δ is the phase angle, V_{C_p} is the active magnitude and V_{C_r} is the reactive magnitude of the injected voltages [10]. From Eq. 2.2 it's clear that the ER is injecting the voltages, wherein this chapter the reactance will be controlled by the ER. Controlling the reactance will have an impact on the reactive power that will lead to control the current of the line, which is shown in Eq. 2.1.

This section will change the value of the line's reactance by multiplying it with

a range of $0 - 100$. The range is expected to represent ER's ability of injecting the reactance since there are different types of ER. The ER types will be discussed in section 2.4 because their model is not applied yet. Before moving to the case studies the following enumerators will explain how the problem is formulated and the followed method to solve it, which is based on the flowchart in Figure 2.1. The steps are used for both reactance multiplication and applying the ER model methods, but there are different assumptions for applying ER on the system, which will be discussed in section 2.4.

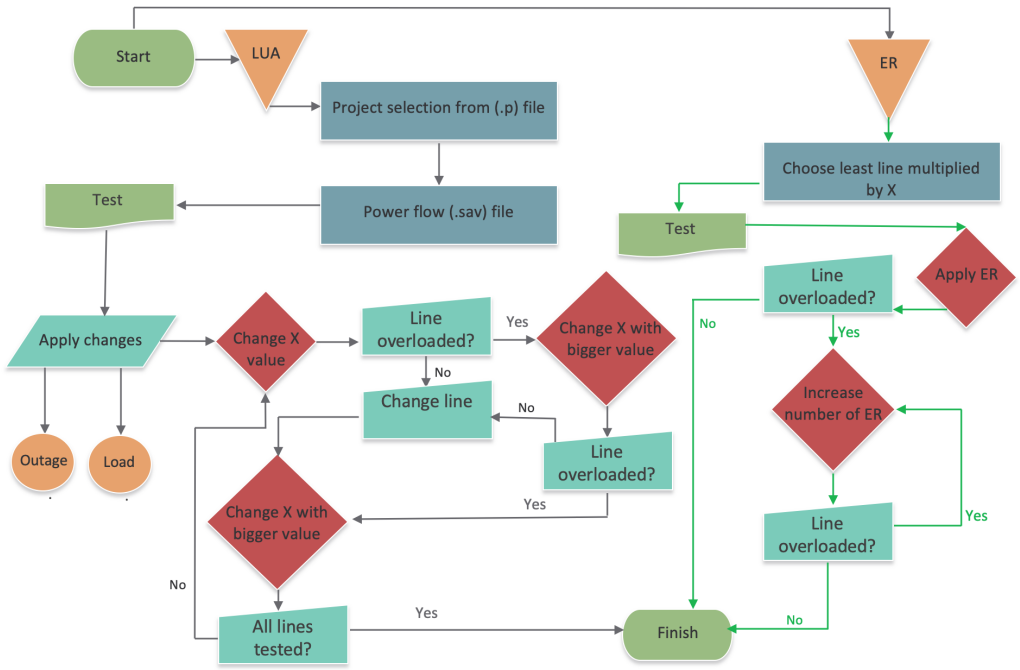

Figure 2.1: Flowchart Describing the Case Studies Solving Methodology

.

1. Project selection

   LUA provided multiple files that showed the projects they are planning to do in term of upgrading their lines or switches due to an overload, which occurs

when an outage happens. The case studies applied the ER to increase the capacity of the line and avoid the upgrade of a switch and line.

2. Excel documentation

   The original data of the overload line or switch and its neighbors are documented with the load of the same year in an excel sheet. Then, the outage is applied to cause the overload and the data are written down in the same excel sheet. The second sheet shows the line with overload and the reactance of the same line and its neighbors are multiplied with the values between $0 - 100$. The third sheet will increase the load and multiply the reactance with the same values for the lines that solved the overload in the first year. The progress is repeated for 10 years. The line or switch that is multiplied with the least value of X and solved the overload for the longest years will be chosen as the best line to apply the ER on it. In a case where two neighbor lines have an overload situation when the outage is applied, the reactance will be multiplied by and for the first year, both lines will be checked if the overload has been solved on the location or not. If yes, the one with higher overload rate will be considered for the rest of the years.

3. ER Placement

   Smart Valve is the ER model provided by Smart Wires company. The ER placement will be depending on the results from the multiplication method, which finds the longest deferral with the least X injection. If one ER solves the issue, then it will be the final result; If not, another ER is added to the system. In some cases the ER that fitted the line's current limits has another model with stronger injection ability, which will be applied instead of using additional ER.

The previous enumerators discussed the followed steps to solve an overload in LUA system using the two methods. The steps are tested in three case studies to find if the ER is able to solve the problem or not. The case studies for multiplication method have three assumptions, and the first is the range of multiplying the reactance is between $0 - 50$, but if the maximum value doesn't solve the overload, the range of multiplication will be increased to 100 just to ensure that this line or switch will not assist in solving the overload. Second, each line's reactance will be changed separately to find the best line that will assist in increasing the capacity. Last, is the reactance of the line and its neighbors will be changed and their values will be checked to avoid solving the problem in one location and starting another issue in another line or switch.

2.3.1 Reactance Multiplication Case Study (City A - City B)

Case study I is to apply the ER instead of upgrading a switch located between two buses (City A - City B). ER will shift the phase angle between the voltage and current, which is the reactance (X) of the line. Thus, the testing focuses on X impact on overload. LUA plan is to increase the line capacity from 1200 A to 2000 A because when there is an outage located between one of four different locations an overload will happen in the switch between City A and City B. Figure 2.2 shows the names of the four locations that will cause the overload and Table 2.1 will provide the parentage rate City A and City B switch will reach.

Each outage gave City A - City B switch different rates, where City F - City D had the worst case-scenario, which makes it applied to further investigate X multiplication influence on the line. Note that the original rate for City A - City B switch is 1200 A. After applying the outage each line of the switch neighbor will have its reactance value being changed. First, Figure 2.3 will visualize how the switch is connected to

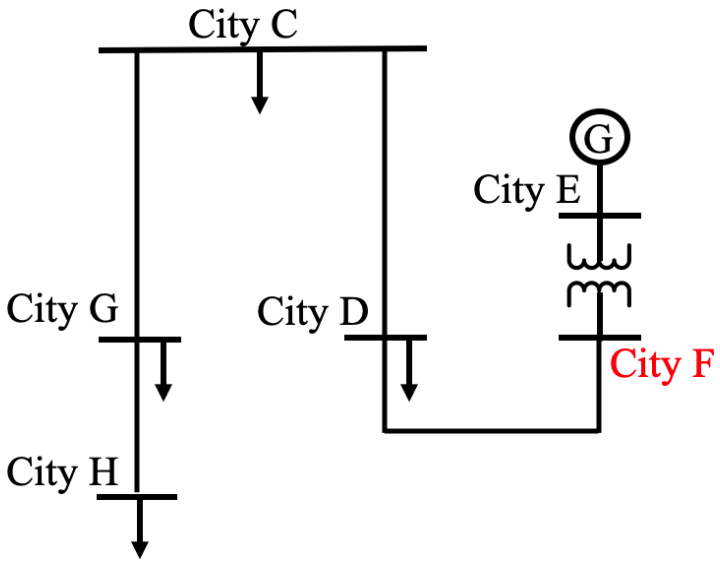

Figure 2.2: Four Outage Locations, when One of them Occurs, an Overload Between City A - City B will Happen

Table 2.1: Four Outages that will Make an Overload in City A - City B

Location	Line Amps	Line percentage
City F - City D	1293.9	107.8%
City C - City D	1258.9	104.9%
City C - City G	1226.5	102.2%
City G - City H	1130	94.2%

the outage location and shows the switch rate of the overload.

So, while the outage between City F - City D is applied, City A - City B will have a rate of 107.8% in 2020. Four locations will have their X value changed, which are the overloaded switch and its neighbors. Figure 2.4 is zooming in to the overload location, which will assist in matching the results shown in Table 2.2. It also shows

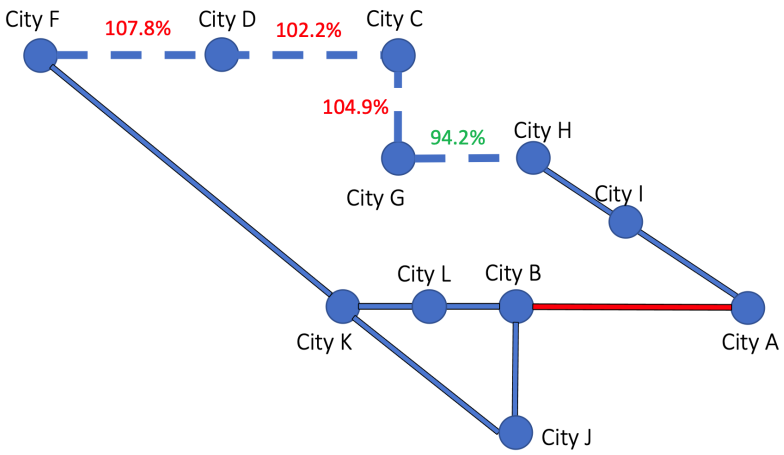

Figure 2.3: Outage Implementation in the Four Locations to Find Higher Overload Rate Between City A - City B

the best location recommend to place the ER since it had the highest deferral with the least reactance multiplication value. The green arrows are used to show that there is an additional connection between the from-bus to the to-bus. Table 2.2 shows the information about the overload switch and the ones connected to it. The reactance values X will be multiplied by the range between $0-100$, which is represented by N. The year of deferral is showing how many years the overload will be solved for the new reactance value. The Amps rate is showing the percentage the line will reach at the specified year of deferral.

Table 2.2: X Multiplication Results of City A - City B

From	To	Original Reactance [pu]	$X \times N$	New Reactance [pu]	Type #	Year of Deferral	Line Amps Rate
City A	City B	0.0006	75	0.045	Switch1	2 Years	100%
City B	City J	0.0006	75	0.045	Switch2	No def.	106.6%
City L	City B	0.0136	50	0.68	Line1	3 Years	100%
City I	City A	0.02848	3	0.0844	Line2	9 Years	100.1%
City I	City A	0.02848	5	0.1424	Line2	10+ Years	92.7%
City I	City A	0.02848	10	0.2848	Line2	10+ Years	77.7%

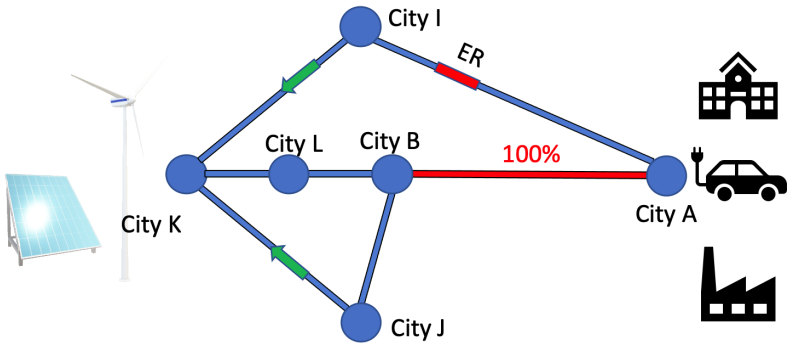

Figure 2.4: Overload Between City A - City B when City F - City D Outage is Applied

The range is assigned to be between $0 - 50$, but for some cases, the values are increased up to 100, which is to verify that this location will not assist in solving the overload. From Table 2.2 Changing X in the same location of the overload City A - City B is not effective because the current rate is still not in the limits range. To solve the issue, X of the other three lines on the system is changed and the power flow was tested again. However, changing the reactance for the second switch City B - City J will not decrease the overload percentage. The third location is named line1 for City L - City B and it solved the overload, but for 3 years with having it reactance multiplied in a large number 50. Line2 City I - City A changed the current values with a larger difference, which can solve the overload issue for 9 years when multiplied by 3 and for more than 10 years when $N = 5$. The results found the best line to apply the ER on, which will be line2 (City I - City A) because it reached the maximum deferral project time assigned in this project, which is 10 years, with changing the reactance with a small value.

2.3.2 Reactance Multiplication Case Study (City C - City D)

Case study II presents LUA plan to update an overload location in 2020 from 1200 A to 2000 A. The 2019 upgrades are applied in this project, which focuses on

230 kV lines in the grid, but it didn't affect the overload locations. In this case study, the annual load increment for two years is 2.198% instead of 1.8% for one year. The reactance multiplication range is between $0 - 40$. There are two overload locations where the outage is applied to either of the other two locations. The overload lines are located between City C - City D, and City C - City G, which are shown as Line1 and Line 3 in Figure 2.5. Table 2.3 shows the percentage when each outage is applied for the two lines, where the higher percentage of the outage and of overload locations are considered to check the reactance changing impact.

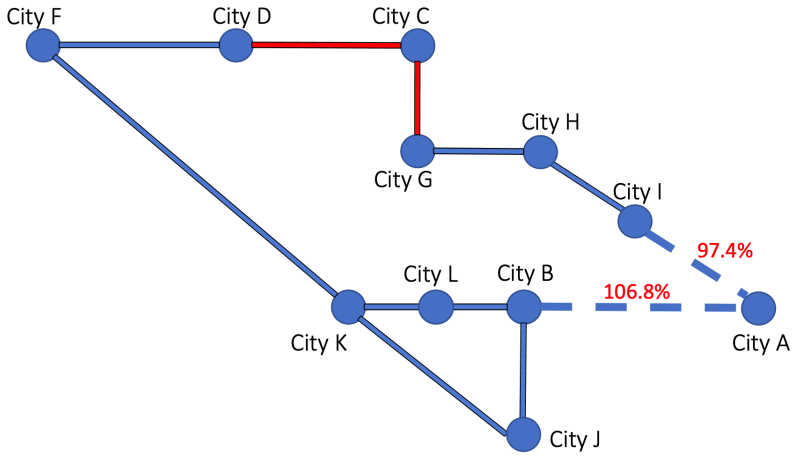

Figure 2.5: Applying Outage in the Two Locations to Find Higher Overload Rate Between Both City C - City D and City C - City G

Table 2.3: Two Outages that will Make an Overload in City C - City D and City C - City G

Location	Line1 Amps	Line1 percentage	Line3 percentage
City A - City B	1282.5	106.8%	103.7%
City I - City A	1169.1	97.4%	94.3%

It is clear from Figure 2.5 that the outage between City A - City B will create the

worst-case scenario because it has a larger percentage 106.8%. The other outage does not cause an overload in the same year, but with load increment percentage it will. From Table 2.3 it is clear that City C - City D has a larger overload percentage than City C - City G. So, City C - City D line current values are further investigated to explain the results, and the other line was always checked during simulation to ensure that both locations have been solved when X is changed. Figure 2.6 and Table 2.4 are showing the values of City C - City D line when the outage applied between City A - City B.

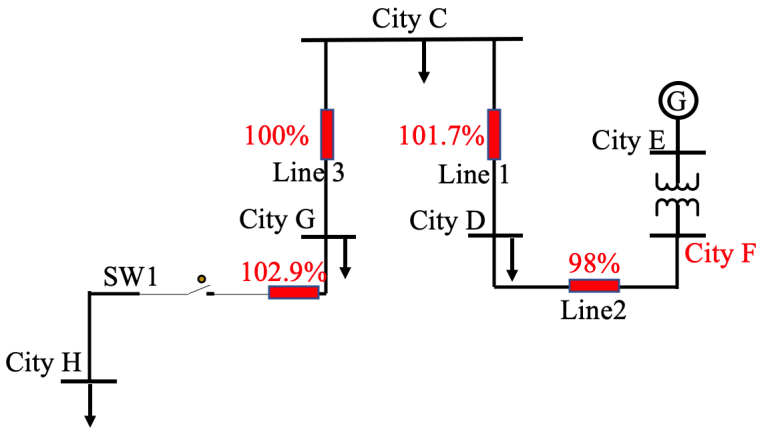

Figure 2.6: Overload Between City C - City D when City A - City B Outage is Applied

Table 2.4: X Multiplication Results of City C - City D

From	To	Original Reactance [pu]	$X \times N$	New Reactance [pu]	Type #	Year of Deferral	Line Amps Rate
City C	City D	0.00197	24	0.04728	Line1	2 Years	101.7%
City D	City F	0.003542	4	0.142	Line2	10+	98%
City D	City F	0.003542	10	0.354	Line2	10+	74.9%
City C	City G	0.03307	4	0.132	Line3	5 Years	100%
City C	City G	0.03307	10	0.331	Line3	10+	78.2%
City G	City H	0.0006	40	0.024	Switch1	No def.	102.9%

Figure 2.6 showed the overload location with it's neighbors and the red boxes finds the percentage Line1 will have when X is shiffted in the box's placement. Table 2.4 showed that switch1 will not assist in solving the problem, Line1, which is the same location of the overload will fix the problem for 2 years with X being multiplied by 24. Line2 maintain the current limits for more than 10 years with changing the reactance to $(X \times 4)$. Line3, which is the second overload line with less rate, showed good results by having the deferral for 5 years by multiplying it by 4 and more than 10 yeas when $X \times 10$. So, the robust placement of ER will be on Line2 City D - City F, when there is an outage between City A - City B.

2.3.3 Reactance Multiplication Case Study (City M - City N)

Case study III considers LUA plan to update two overload locations, which are City M – City N and City L – City N in 2025 from $1200A$ to $2000A$. The overload will occur when either an outage between City F – City D or City C – City D happens. The assumptions for this case study are the annual load increment for every year is 1.8% and changing the line's reactance to a certain value between the range $X \times (2 - 32)$. Figure 2.7 shows the overload and its neighbor's reactance values. Table 2.5 is finding the overload worst-case scenario by applying the two loads.

Table 2.5: Two Outages that will Make an Overload in City M – City N and City L – City N

Location	Line1 Amps	Line1 percentage	Line2 percentage
City F – City D	1221.5	101.8%	100.9%
City C – City D	1206.7	100.6%	99.3%

Table 2.5 shows the worst case scenario for the overload in Line1 and Line2 will

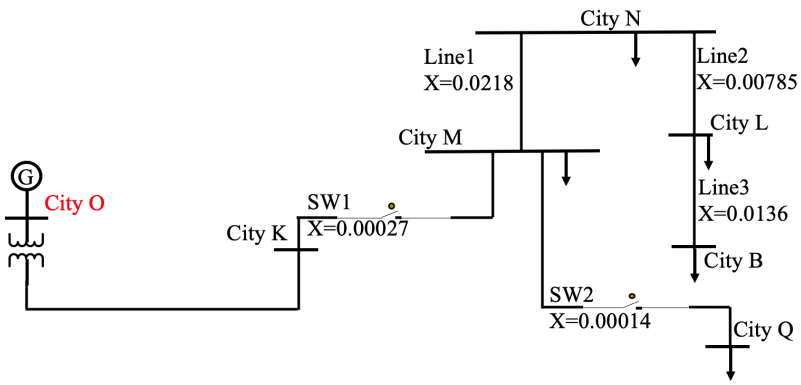

Figure 2.7: Applying Outage in the Two Locations to Find Higher Overload Rate Between Both City M – City N and City L – City N

occur when the outage between City F - City D with values of 101.8%. The outage will give larger overload percentage to Line1 comparing to Line2. So, Line1 values are explained in the results Table 2.6 and Figure 2.8 while during simulation both locations were being watched carefully.

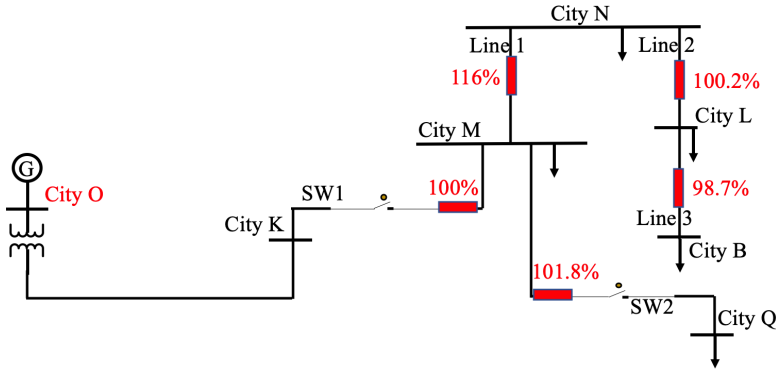

Figure 2.8: Overload Between City M – City N when City F – City D Outage is Applied

Figure 2.8 showed the reactance being changed in five locations instead of four because bus City C is connected to two lines and a switch, which all considered

Table 2.6: X Multiplication Results of City M – City N

From	To	Original Reactance [pu]	$X \times N$	New Reactance [pu]	Type #	Year of Deferral	Line Amps Rate
City M	City K	0.00027	12	0.00324	Switch1	2 Years	100%
City M	City K	0.00027	16	0.00432	Switch1	5 Years	100.2%
City M	City Q	0.00014	32	0.00448	Switch2	No def.	101.8%
City M	City N	0.02183	16	0.3493	Line1	No def.	116%
City L	City N	0.00785	2	0.0157	Line2	7 Years	100.2%
City L	City N	0.00785	4	0.0314	Line2	9 Years	100.1%
City L	City B	0.0136	2	0.0272	Line3	10+ Years	98.7%

neighbors the overload locations. Switch1 solved the overload for 2 and 5 years but with a multiplication value of more than 10, which means it will require a big change in the reactance. Switch2 didn't solve the overload, which makes it a bad decision to place the ER on. Line1 also didn't solve the problem and made it worse because it directed more flow into the overload, which is the case of switch between captive mode and inductive mode, but neither solved the overload because a new problem happened in another location. Line2 increased the project deferral for 7 years by multiplying the value by 2 and for 9 years when $(X \times 4)$. Although Line2 showed a good result, Line3 has better because it reaches the maximum deferral with only multiplying the reactance value by 2. Line3 is the best location to place the ER since it solved the overload for more than 10 years with the least multiplication value between the three case studies not only for the tested one.

2.3.4 Section Summary

In this section three case studies are discussed, which focuses on solving the overload in LUA transmission line when an outage occurs. The overload is solved by multiplying the reactance values of the line or switch and its neighbors after applying the worst case scenario that will occur when an outage is applied. Each location

values are tested separately and each case study had good results where the overload is solved for the maximum deferral assigned to this project by multiplying X with small values $(2-5)$. From the represented results, it's clear that the ER is able to enhance the stability of the power flow in the system by controlling the reactance value that will affect the line's reactive power. To verify the results, a real model of the ER will also be applied to the system to shift the reactance under the same scenarios for the three case studies in section 2.4. An important observation from the result is that the reactance controlling on a line is better than a switch because the switch has lower reactance values, which decrease its impact and requires large values of multiplication.

2.4 Energy Router Placement on LUA Grid using Smart Wires Model

The ER model is provided by Smart Wires company, which is named Smart Valve and it has been applied and tested on LUA grid. The provided Smart Valve model is intended for steady-state power flow studies only, for both capacitive and inductive ER modes. The model is provided in a single script in $(.p)$ format that contains information for multiple deployments, which means more than one ER can be applied and with different types. The model is provided with three injection modes, which are reactance, voltage, and current. The current mode is applied in the three case studies, which follows the multiplication method results to place the ER. In the multiplication method, the reactance was multiplied within a specified range, wherein the Smart Valve model there is a deployment usage, which is the injection rate that the ER can reached. The ER maximum deployment will be reach when it equals to 100%. Figure 2.9 shows the ER behavior of injecting the reactance and current, which is for the Smart Valve model $10-3600i$.

Figure 2.9 shows the reactance and current injection ranges for ER model $10-$

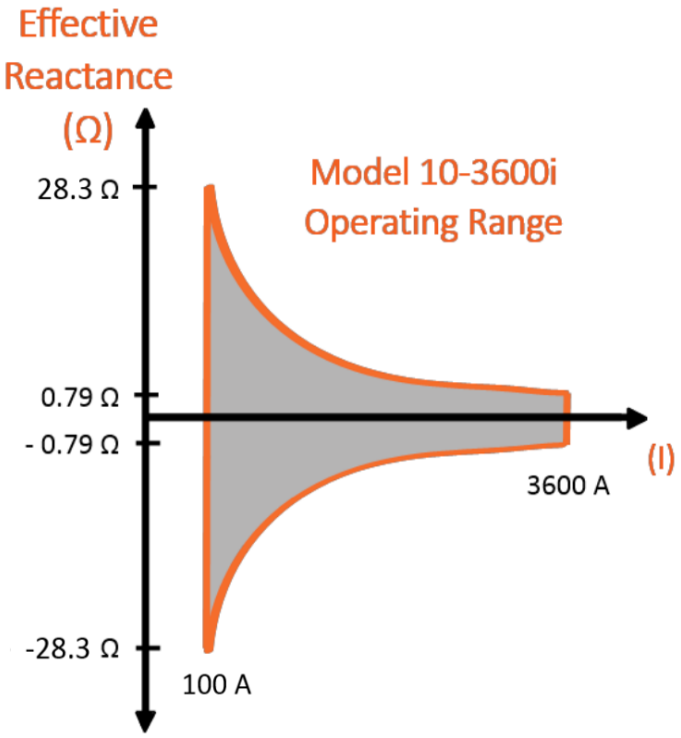

Figure 2.9: ER Injection Behavior [4]

$3600i$, which is from 0.79 Ω to 28.3 Ω and for current is 100 A. To understand the range Smart Wires provide for an ER, the table in Figure 2.10 shows each type and it's operating range.

The table in Figure 2.10 shows each ER type and its parameter, where each has its own rates. The first type is SmartValve $1-900$, which represents its current rate from the name. If the line is rated for 700 A, then the ER with a current rate of 900 A can be applied, but if the line is rated for 1200 A, then the choice will be ER with a rate of 1800 A, which named as SmartValve $5-1800$. The maximum injection voltage rate of the SmartValve $1-900$ is $+/-1132$ V, where the $(+/-)$ represents the inductive and reactive modes. Remember in the multiplication method the reactance is injecting not voltage and in this section, the current is considers. The emergency

Device	Maximum Injection [kVAr]	Max/Min Voltage Injection [Volts]	Continuous Current Rating [Amps]	2-Hour Emergency Rating [Amps]
SmartValve 1-900	1000	+/- 1132	900	1080
SmartValve 1-1800	1000	+/- 566	1800	2160
SmartValve 2-3600	2000	+/- 566	3600	4320
SmartValve 5-900i	5000	+/- 5660	900	1080
SmartValve 5-1800i	5000	+/- 2830	1800	2160
SmartValve 7.5-2700i	7500	+/- 2830	2700	3240
SmartValve 10-3600i	10000	+/- 2830	3600	4320

Figure 2.10: Smart Wires ER Parameters [4]

rating is when there is an outage or an overload in the line. The ER will know the difference between an outage and overload by this rating. If the line is designed with rating of 900 A and the current in the line reaches a value between $900 - 1080$ A, then the ER will try to control the reactive power for two hours and then bypass. However, if the same line has a rating for more than 1080 A, then the ER will immediately bypass the power flow for protection reasons. The ER model is clearly explained and to apply it there are three assumptions considered, which are the least line reactance multiplication that solved the overload is assumed to be the best location to place ER on, deployment rate must maintain to be $< 100\%$, and a current injection mode is applied.

2.4.1 ER Attachment Case Study (City A - City B)

In this case study, the same locations considered the first case study for the multiplication method is used. So, the outage is applied in City D - City F line, and the overload is located in City A - City B. The results in Table 2.2 showed that Line2 (City I - City A) is the best location to place the ER on because it had the deferral for

9 with the lowest multiplier value. Line2 has a current rate of 1935 A, which makes ER type $7.5 - 2700i$ applied because it has a current rate of 2700 A as shown in the table in Figure 2.10. Figure 2.11 shows the ER being placed on the line and Table 2.7 find the results.

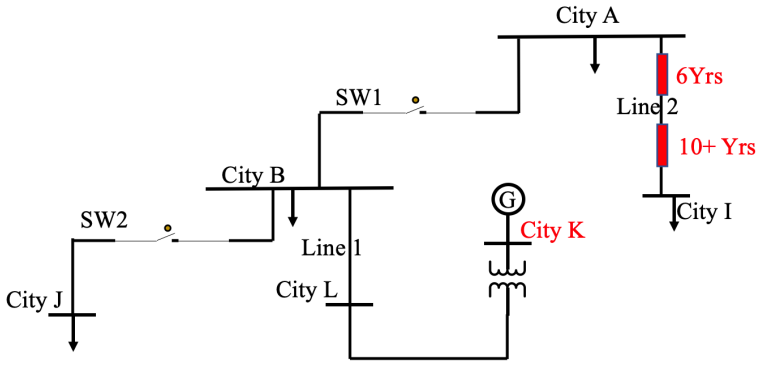

Figure 2.11: ER Placement on Line2

Table 2.7: ER Applied on City A - City I (Line2)

# of ER	1 ER	2 ER	2 ER Max injection
Year of deferral	6 Years	10+ Years	10+ Years
Amps	1202.5	1155.2	1103.5
Year	2025	2030	2030
Deployment Usage	98.18%	74.54%	98.53%

Table 2.7 shows the result of injecting the voltage from the recommended location by the multiplication method for case study I. Attaching one ER solved the overload for six years and when two ER were applied the deferral increase to more than 10 years. Also, the maximum injection rate for two ERs is tested, which decreased more than 100 A and reached the maximum deferral year assigned in this project. Furthermore, the deployment usage is found when the model is running, which can

be seen in Figure 2.12 from the PSLF results.

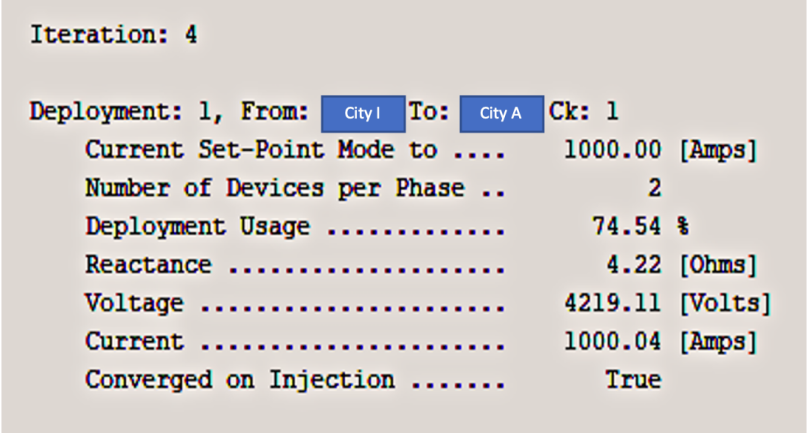

Figure 2.12: Two ERs Applied on City I – City A, Results From PSLF

The ER model has successfully solved the overload for more than 10 years using two devices and 6 years when one device is applied.

2.4.2 ER Attachment Case Study (City C - City D)

Case study II is applying the ER on the recommended line from the multiplication method, which is Line2 (City D - City F). The overload is on two lines, but the one a with larger overload rate is considered, which is Line1 (City C - City D). The overload occurs when the outage between City A - City B is applied. The ER model is also $7.5 - 2700i$ because Line2 current rate is 1935 A. Figure 2.13 shows the ER placement on Line2 and Table 2.8 finds the results.

Table 2.8 showed the result of applying the ER on Line2, where one ER solve the overload for 2 years, 2 ERs have 5 years of deferral, and 3 ERs have reached the maximum deferral time in this projects. So, in this case, LUA can apply one ER, and after two years the second ER, which will give them 5 extra years to extend the project's upgrade time.

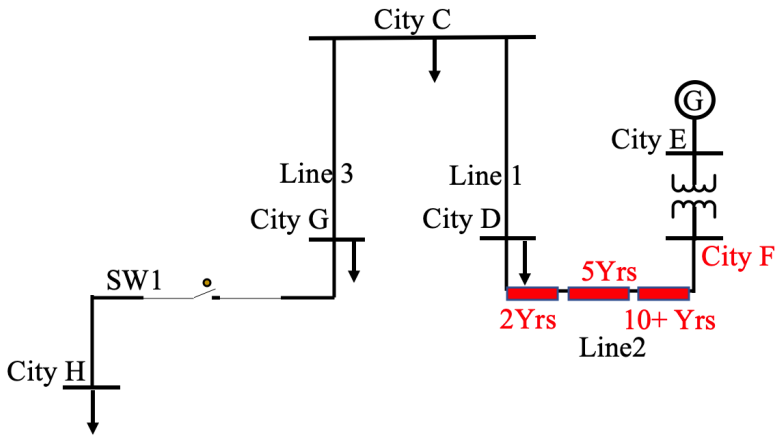

Figure 2.13: ER Placement on Line2

Table 2.8: ER Applied on City D - City F (Line2)

# of ER	1 ER	2 ER	3 ER
Year of deferral	2 Years	5 Years	10+ Years
Amps	1214	1209.7	1109
Year	2022	2025	2030
Deployment Usage	84.58%	56.2%	98.19%

2.4.3 ER Attachment Case Study (City M - City N)

The multiplication method suggested to attach the ER on Line3 (City L - City B), when the overload is located in City M – City N due to, the outage in City F – City D. Figure 2.14 shows the ER placement on Line3 and Table 2.9 provide the results.

Table 2.9 shows the results for applying two types of ER, where the first type is $1-1800$ and the second is $5-1800i$. ER $1-1800$ has a voltage injection rate $+/-566$ V, which solved the overload for 6 years. ER $5-1800i$ has a larger injection rate of $+/-2830$ V, which reached the maximum deferral years assigned to this project

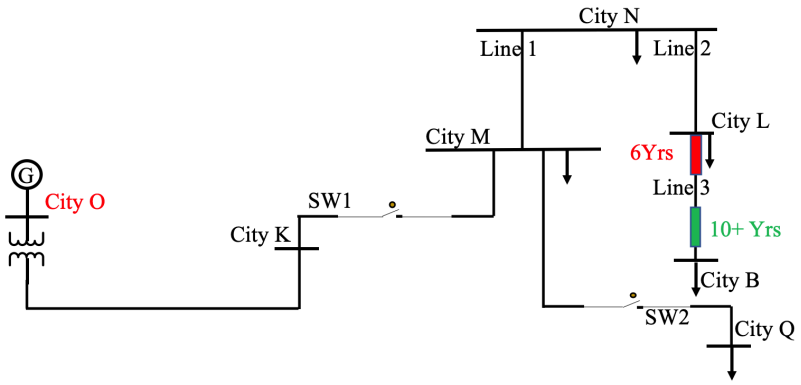

Figure 2.14: ER Placement on Line3

Table 2.9: ER Applied on City L - City B (Line3)

# of ER	1 ER	2 ER
Year of deferral	6 Years	10+ Years
Amps	1200.8	1068.7
Year	2031	2036
Deployment Usage	72.48%	49.51%

(10+) years. Note that both ER has the same continuous current rating, but their injection rate is different, which means the one starts with 5 is more enhanced.

2.5 Conclusion

In this chapter, the ER is introduced, and following its mathematical form for controlling the reactive power by injecting the reactance in three case studies are discussed. The first method is to multiply the line's reactance value within a specified range. The overload location and its neighbors use the same method and the one which solves the overload for the longest time with least multiplication values is considered the best location to place an ER. The second method is to apply the real

ER model provided by Smart Wires on LUA transmission lines and test different deployment rates in case study I, more than one ER on the same line in case study II, and two ER types in case study III, which has the same continues current ratings. Lastly, the ER guarantees to increase the stability of power flow on the transmission line by controlling its reactive power, which is proved using two methods and six case studies in this chapter.

Chapter 3

ELECTRIC VEHICLE CHARGING STATION DATA ANALYTICS

Time series analysis (TSA) methods are presented in different publications to predict the future using exponential smoothing, ARMA, and polynomial curve fitting models [61, 62, 63]. In [61] ARMA and exponential smoothing predicting the future disease rating and then compares, where ARMA had better accuracy in fitting the data. Short term traffic flow is predicted using ARMA with exponential smoothing to assist in controlling the real-time flow [62]. Transmission line transient stability is forecasted using polynomial curve fitting to assist the relay in protecting the system from power swings [63].

In this chapter, TSA will be studied to show how the EVCS will impact the power grid, and then predict the future. Two EVCS data sets are studied, which are located in Boulder, Colorado, and Palo Alto, California. The first rows of the data set will be shown to provide more understanding. So, the energy will be studied for each year during the provided years. The charging duration is also studied for each month to provide more observation from the EVCS impact on the electrical system. Then, the standard deviation and mean of the energy summation during 24 hours is found. The data sets will first be divided depending on each zip code and the one with more records is considered because the more data that is provided, the better prediction will be found. For the data prediction, different forecasting TSA methods are applied, which are polynomial curve fitting, autoregressive moving-average, and exponential smoothing. Knowing the future will assist in planning the EVCS and avoid any issues like the overload. So, the aim of this chapter is to find the EVCS impact on the power grid by studying different features and forecasting them.

3.1 Electric Vehicle Charging Station for the City of Boulder, Colorado

The EVCS data for the city of Boulder, Colorado [64], is studied to find the energy consumption at every hour during the day. From Table 1.3 the TSA will be applied for the zip code of 80302 to find EVs behaviour during 26 months. Then, the mean and standard deviation are found for the 24 hours.

3.1.1 Boulder Data Set Description and Observations

Colorado records are analyzed in Figure 3.1, which shows the sum of energy consumption for each month at a certain hour.

The energy usage at early hours of the day ($00:00 - 04:00$) is almost 0 kWh, but between the months 10 to 15 there is an increment between 5 kWh - 25 kWh as shown in Figures 3.1a, and 3.1b. This usage is rarely considered for charging EV since the charging station might be closed and there are few people who are awake at these hours. So, the reason could be that the EVCS operation consumption in the winter season increases for the first year. As mentioned the data is given from Jan 2018 to Feb 2020, which means between October 2018 to March 2019 the EVCS was using energy while the charging station is closed. However, it seems the EVCS owners fixed the problem in the next year, which can be noticed in the second year the problem might be solved where Figures 3.1a, and 3.1b are showing 0 kWh for the same season at the following year, which can be seen in the months 22 to 26 that represents the date of October 2019 to Feb 2020. At $05:00$, the energy starts to increase up to 50 kWh, which seems like the starting time of charging the EVs, but with few vehicles being charged. Figures 3.1c, and 3.1d, are showing increment from $06:00$ to $20:00$ in the consumption for more than 100 kWh. Figure 3.1h, represents the hours from $21:00$ to $23:00$ and the usage is decreasing to below 50 kWh, which

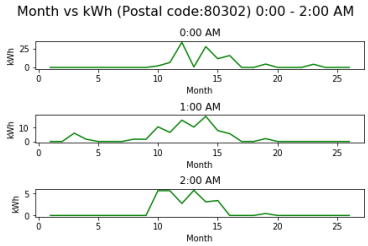

(a) Sum of EVCS Energy for the Zip Code: 80302 Between 00 : 00 - 02 : 00

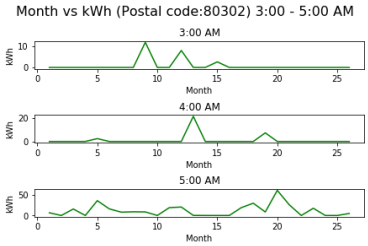

(b) Sum of EVCS Energy for the Zip Code: 80302 Between 03 : 00 - 05 : 00

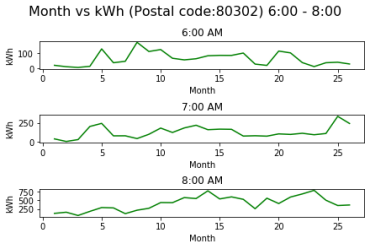

(c) Sum of EVCS Energy for the Zip Code: 80302 Between 06 : 00 - 08 : 00

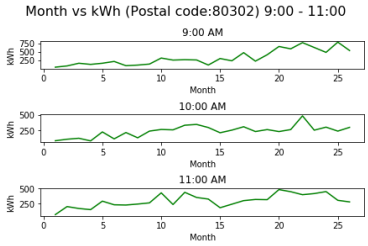

(d) Sum of EVCS Energy for The Zip Code: 80302 Between 09 : 00 - 11 : 00

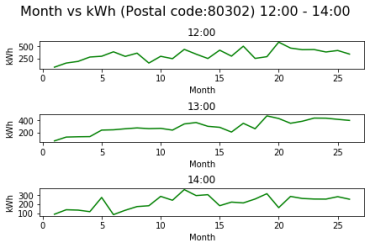

(e) Sum of EVCS Energy for the Zip Code: 80302 Between 12 : 00 - 14 : 00

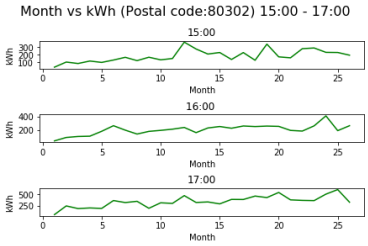

(f) Sum of EVCS Energy for the Zip Code: 80302 Between 15 : 00 - 17 : 00

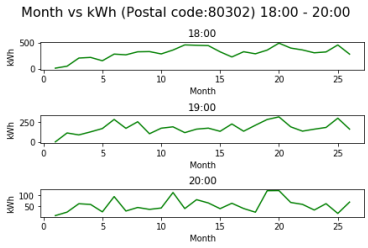

(g) Sum of EVCS Energy for Zip Code: 80302 between 18 : 00 - 20 : 00

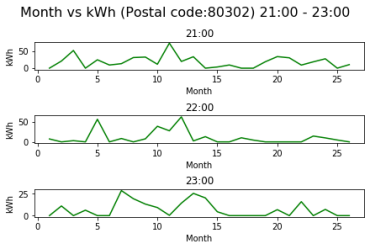

(h) Sum of EVCS Energy for the Zip Code: 80302 Between 21 : 00 - 23 : 00

Figure 3.1: Colorado EVCS Energy Consumption for 24 Hours

seems that few people are charging at these hours that might be the closing hours.

Furthermore, the hours from 7 : 00 to 20 : 00 will be clearly explained in the following items.

- EVCS low load usage $(50 - 200)$ kWh

  Figure 3.1c, at 06 : 00, and Figure 3.1g, at 20 : 00 are showing the EVCS is operating with value of 100 kWh.

- EVCS normal load usage $(250 - 400)$ kWh

  Figures 3.1c, at 07 : 00, 3.1e at 13 : 00, 3.1f at 15 : 00 and 16 : 00, and 3.1g, at 19 : 00 are showing the EVCS station operation have value between 250 kWh to 400 kWh.

- EVCS heavy load usage $(450 - 750)$ kWh

  Figure 3.1c at 08 : 00, Figure 3.1d at 09 : 00 the consumption is rapidly increasing, which reached up to 750 kWh. Figure 3.1d at 10 : 00 and 11 : 00, Figure 3.1e at 12 : 00, Figure 3.1f at 17 : 00, and Figure 3.1g at 18 : 00 are showing that the energy usage goes up to 500 kWh.

After analyzing the data in the plots and explaining them, there are important observations that will be listed as the following.

1. EV owners are increasing and it can be seen obviously in Figure 3.1e by the increment of the curves. So, the number of the EV will increase in the city of Boulder, which will increase the load on the power grid.

2. An overload might occur at the hours 08 : 00 to 09 : 00 because the kWh is higher than any other time.

3. The energy consumption in the winter season is more than the other seasons, which can be clearly seen between the months $10 - 12$, and $22 - 24$.

4. The higher energy consumption value is located at 80302

3.1.2 Mean and Standard Deviation of Boulder's Data

The mean and standard deviation (SD) will be applied Chapter 4, which will use them to find and optimal charging station placement location with ER to reduce the total cost. So, the mean value will present the mean of kWh consumption for the 26 months at a specified hour. The SD will also present 24 values for the 26 months. Both the mean and SD values are shown in Table 3.1, which will show only the values of the zip code of 80302. Figure, 3.2 visualize Table 3.1, which clearly shows that the EV are mostly being charged between the hour 05 : 00 to 20 : 00.

Table 3.1: Mean and Standard Deviation for 24 Hours in 80302

Hour	SD [kWh]	Mean [kWh]	Hour	SD [kWh]	Mean [kWh]
0	8.533	4.074	12	115.929	331.484
1	5.156	3.399	13	104.565	298.324
2	1.946	1.03	14	74.020	221.626
3	2.714	0.864	15	78.884	183.957
4	4.314	1.202	16	73.263	204.982
5	14.30	11.821	17	120.878	338.800
6	43.652	63.327	18	115.775	306.804
7	75.12	130.417	19	70.874	177.087
8	203.337	408.809	20	30.417	55.021
9	217.541	329.351	21	17.503	18.665
10	89.232	240.216	22	16.928	10.506
11	103.229	296.598	23	8.753	7.049

From Table 3.1, the kWh consumption usage can be observed in the following numbers.

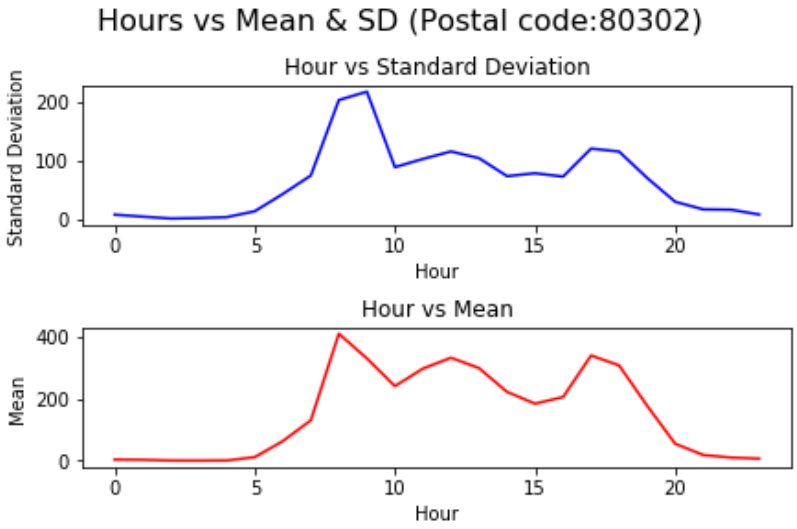

Figure 3.2: Energy Consumption SD and Mean Values of 26 Months for 24 Hours in 80302

1. From the hour 0 to 4, and 23 the SD values are below 10, which shows low kWh consumption. Mean values are also low, which are lower than 5 except the mean of the hour 23. So, during the hours 0 to 4 the load will not have a big impact on the power grid.

2. The hours from 5 to 7 the energy consumption is increasing.

3. The hours 8, 9, 11, 12, 17, and 18 presents the highest values for both SD and mean, which must be noticed because it will be a reason for overload.

4. The hours 10 to 13, 14, and 16 are also showing high kWh, but not as large as the previous hours. These hours can be a reason for overload in the long term, which must be considered.

5. The hours 15 to and 19 are the in same range of hour 7, which can be considered as low or medium load.

6. The hours from 20 to 22 are showing that the kWh values are decreasing, which is a low energy consumption usage.

The observation clearly described how charging the EV is impacting the grid during different hours of the day. The mean and SD will be used and further analyzed in Chapter 4 for planning the EVCS.

3.1.3 Section Summary

In this section, Boulder's data set for EVCS has been analyzed to find how the EV owners are impacting the power grid. First, the zip code with the highest number of transactions has been explained in detail by showing their plots and provide important observations such as the overload that might occur between the hours $08:00-09:00$. Then, the SD and mean were found for the data set and observed following the table and figure provided in the same section. So, the TSA is applied to find how the EVCSs are influencing the electric system and from visualizing the plots the tables it is clearly seen when the load will be large or small. To forecast the data set, the more information is provided the better prediction will result because it will have a bigger number of data to train on. Thus, the next section represents a new data set with more records to apply TSA for present analyses, and future prediction.

3.2 Electric Vehicle Charging Station for the City of Palo Alto, California

The EVCS data for the city of Palo Alto, California [54] is studied following the area with largest transactions, which is 94301 as shown in Table 1.5. For each month the energy consumption and charging duration is observed by plotting them and describe each one. The SD and mean values will be found by summing the 72 months energy consumption. After observing the data, it will be forecasted using polynomial, autoregressive moving-average, and exponential smoothing.

3.2.1 Palo Alto Data Set Description and Observations

Palo Alto EVCS records are studied considering two features, which are energy and charging duration. From the curve shape, mean, and SD values, the EVCS impact of the power grid will be observed.

EVCS Energy Consumption for Each Hour in the 72 Months

The area with a zip code of 94301 will be studied in detail for the 24 hours. The data is separated to present each hour's consumption of kWh on a duration of 72 months. To explore the kWh consumption, Figures 3.3 and 3.4 is showing each hour usage.

Figures 3.3 and 3.4 shows 79 months versus the the sum of kWh consumption for the 24 hours, which showed that the peak usage is between hour 09 : 00 to 14 : 00 and 07 : 00. Also, the kWh is rapidly increasing starting at the hour 06 : 00. Then, from the hour 20 : 00 it starts to decrease and goes almost to zero starting from the hour 00 : 00 to 04 : 00 since there is no hour 24 : 00 when the data started recording at hour 00 : 00. The provided bullet points in the bottom are used to explain the plots.

- Low consumption $(0 - 800)$ kWh

  From hour 00 : 00 to 05 : 00 and 23 : 00 the energy usage is low where there are few people charging their cars at this time.

- Medium consumption $(900 - 1800)$ kWh

  The hours 06 : 00, 08 : 00, 10 : 00, and $15 : 00 - 22 : 00$ have the medium load usage, which can be considered for the long term to avoid any issues.

- High consumption $1900 - 3800$ kWh

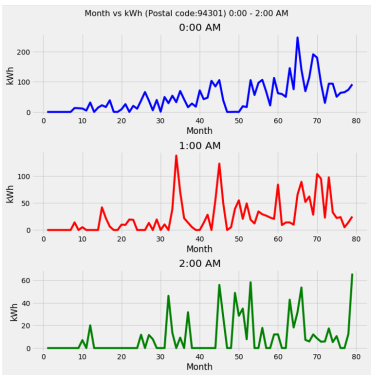

(a) Sum of Energy Consumption Between $00:00-02:00$

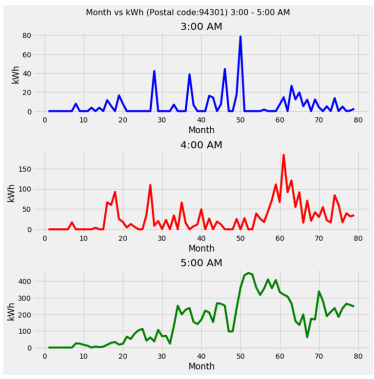

(b) Sum of Energy Consumption Between $03:00-05:00$

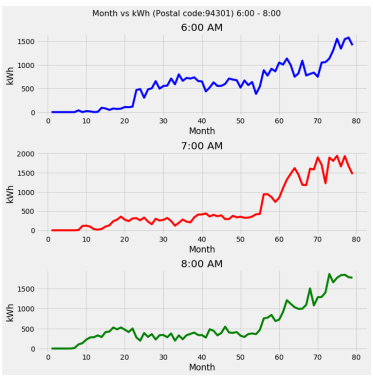

(c) Sum of Energy Consumption Between $06:00-08:00$

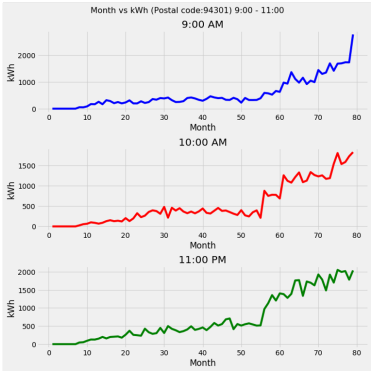

(d) Sum of Energy Consumption Between $09:00-11:00$

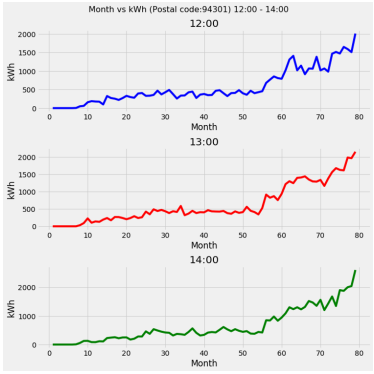

(e) Sum of Energy Consumption Between $12:00-14:00$

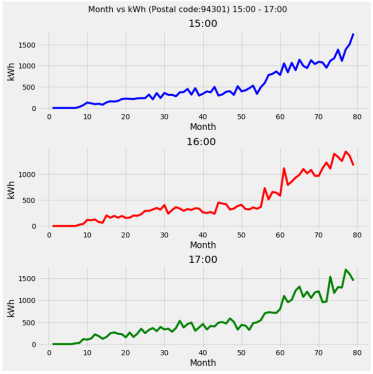

(f) Sum of Energy Consumption Between $15:00-17:00$

Figure 3.3: California EVCS Energy Consumption for 72 Months in the Area with Zip Code of 94301 From Hour $00:00$ to $17:00$.

The hours $07:00$, $09:00$, and $11:00-14:00$ have high energy consumption, which must be considered to protect the system from damages.

After explaining each hour and how the EVCSs are operating, the following numbers points will discuss the observations for the figures.

1. From Figures 3.3 and 3.4 it is clearly shown that the number of EV is increasing annually or even monthly by looking at the kWh consumption increment slope

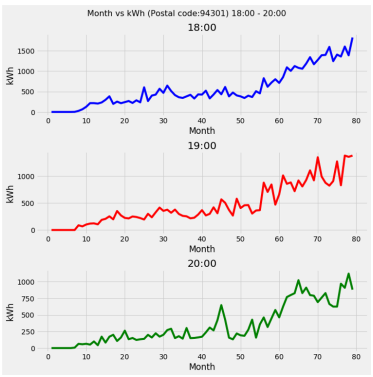

(a) Sum of Energy Consumption Between $18:00-20:00$

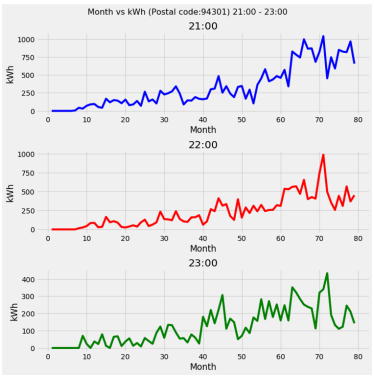

(b) Sum of Energy Consumption Between $21:00-23:00$

Figure 3.4: California EVCS Energy Consumption for 72 Months in the Zip Code 94301 From Hour $18:00$ to $23:00$.

on all hours.

2. The EVCS have the lowest energy consumption from $01:00$ to $04:00$ where few people are charging as shown in Figures 3.3a and 3.3b.

3. The energy consumption is separated into low, medium, and high. The low type will not have a big impact on the power grid. The medium type does have an impact, but will not be the reason for issues in the short term. However, the high type needs to be considered because it might cause an overload in the system.

4. From $06:00$ to hour $18:00$ the number of EVs being charged is increasing for more than 1500 kWh, which can be a reason for problems on the grid especially in the winter season. Note that hour $16:00$ is about $1,000$ kWh, which shows fewer owners are charging at this time.

5. The higher NT is located in 94301, which means it's the largest load between

the three.

After observing the data set by explaining the kWh usage, the EV charging can be studied more to list more findings. Thus, the charging duration of the EVCS at each year, month, and hour is found.

Analyzing EV Charging Duration for Each Month of the 72

The EV is being charged for different times, which makes studying the charging duration assistant in providing better pictures of how the EVCSs are affecting the power grid. Palo Alto's data set analysis for the charging duration will be discussed in the following figures. So, every month is plotted separately and the changes have been observed, but only the first and last years are presented to avoid repetition.

- Charging Duration from 2011 to 2014

  Starting with Figure 3.5, which shows every month in the year of 2011 except January to July because the information is not provided, which might means this EVCS opened in 2011. In addition, each month is plotted separately in 3.6 to zoom in into the time of charging duration.

  The following items are used to explain the plots and list the important observations for the years $2012 - 2014$.

  - July's plot has few charging records, but it is clearly seen that the time varies from one EV to another as shown in Figure 3.6a.
  - In August the duration has a maximum value of 250 minutes, where most charging is clearly seen between 50 to 150 minutes as shown in Figure 3.6b.
  - The rest of the figures have similar shapes bust not the same, where the most of the durations are between 50 minutes to 250 minutes.

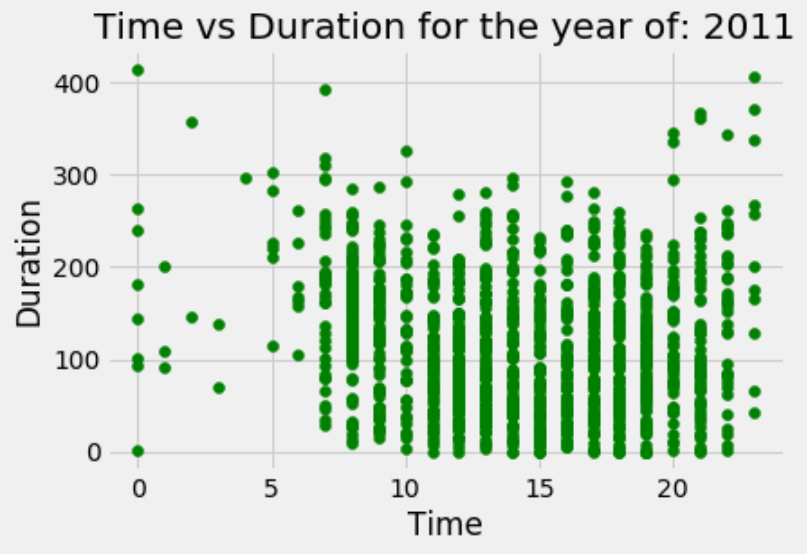

Figure 3.5: Palo Alto 94301 Charging Duration for Year: 2011

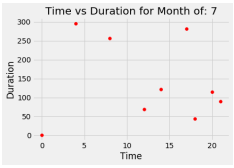

(a) Jul 2011

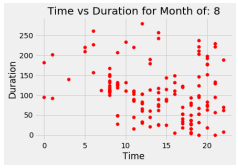

(b) Aug 2011

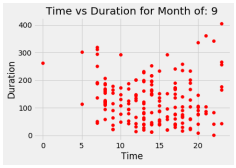

(c) Sep 2011

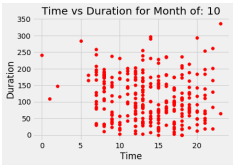

(d) Oct 2011

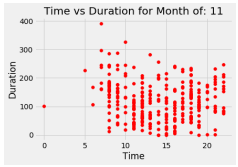

(e) Nov 2011

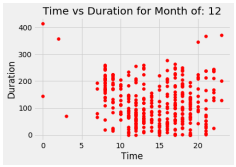

(f) Dec 2011

Figure 3.6: California EVCS Charging Duration for 2011 in the Area with Zip Code of 94301.

- Average the duration for charging the EV has increased in 2012 about 50 minutes, which gives it the range from 50 to 300 minutes.
- The maximum duration recorded in 2014 has jumped to 1200 from 800 minutes in 2013.

– The average of the charging duration is decreasing starting from 2013 to be mostly less than 250 minutes, which can be due to introducing fast-charging machines in the EVCSs.

- Charging Duration from 2015 to 2017

The number of recorded months in 2017 is seven since the data covers the EVCSs information until July 2017. Figure 3.7 shows the charging duration in 2017 and Figure 3.8 shows every month's charging periods.

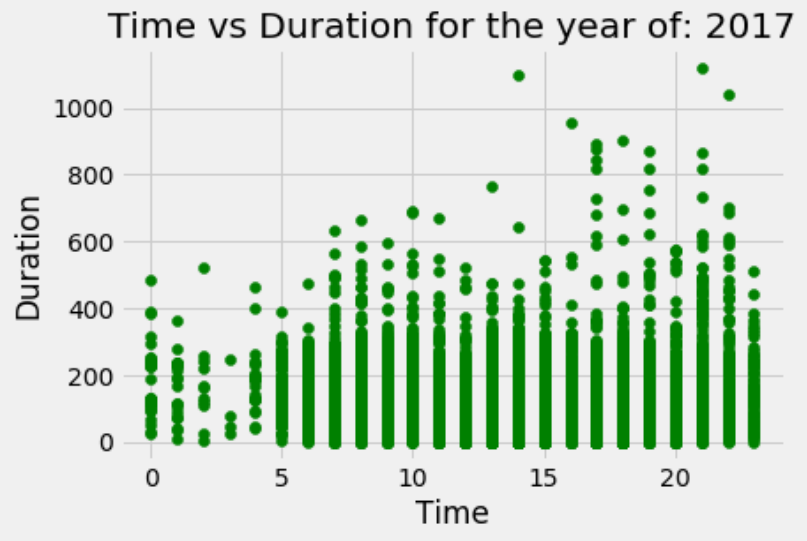

Figure 3.7: Palo Alto 94301 Charging Duration for Year: 2017

To describe the plots in Figure 3.8, the following items are provided.

– The average for all months is mostly limited by 200 minutes, which means it decreased compared to 2014.

– The maximum duration has jumped to 2500 minutes in 2016, which was 1500 minutes in 2015. It can be noticed that both of these long periods charging happened only once in 2015 and 2016 in the same month, which is January.

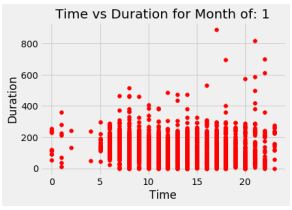

(a) Jan 2017

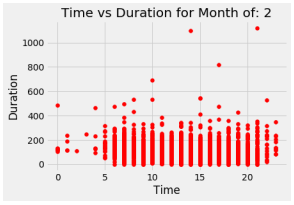

(b) Feb 2017

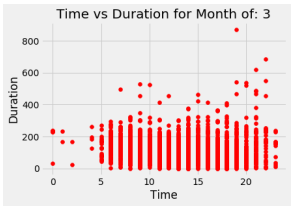

(c) Mar 2017

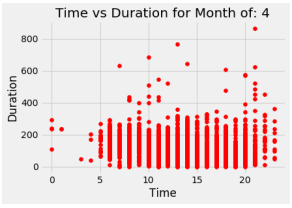

(d) Apr 2017

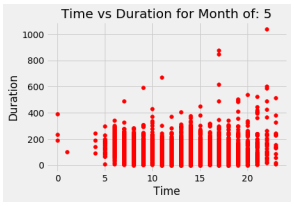

(e) May 2017

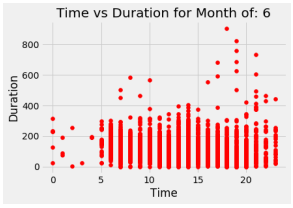

(f) Jun 2017

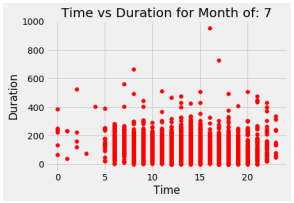

(g) Jul 2017

Figure 3.8: California EVCS Charging Duration for 2017 Months in the Area with Zip Code of 94301.

– The average of charging duration in 2017 is less than 200 minutes for all seven months.

The charging duration in Palo Alto showed that the charging at the hours of the day between 11 : 00 pm to 5 am was the lowest in 2011, the lengthiest charging duration was on January 2016 with a value of 2500 minutes and the average duration of charging reached to less than 200 minutes in 2017. The first year seemed like the charging station might be closed between the 12 : 00 am to 05 : 00 am, but going through each month of the next years it showed that there were only a few EVs being charged at theses hours and the EVCS seems to be open 24 hours a day. The number

of EVs is increasing, which can be clearly seen from the number of charges between the hours 9 : 00 pm to 05 : 00 am. The maximum duration seems that there was testing or an issue behind this long period because it happened once in some years such as 2015 and 2016. The average charging duration has been decreasing, which proves the fast charging is being used more often and the batteries of EVs are being updated to be charged within less duration.

Section Summary

In brief, in this subsection, the energy and charging duration is observed and described by plotting and explaining them. It was clear from both that the EVs are being more purchased, which means a larger load on the grid. The energy represented in kWh found the hours that can be a reason for the overload. For the charging duration, it showed that the fast charging and the upgraded batteries are being used to decrease the required number of minutes; These observations meet what references [65] discussed about the shorter time an EV will require it be charged due to the new generation of batteries. Furthermore, to discover the data and find how the EVCSs will affect the grid from the Palo Alto's data the SD and mean values are discussed next.

3.2.2 Mean and Standard Deviation of Palo Alto's Data

The SD and mean values for the zip code 94301 are studied to find EV's impact on the power system. Figure 3.9 shows the plot of both values during 24 hours. Table 3.2 provides the couple values during a day to clearly understand how the EVCSs are consuming the kWh.

Figure 3.9 shows that the peak usage of kWh is between the hours $10 - 12$. The mean values show more details about the consumption, which can be clearly visualized

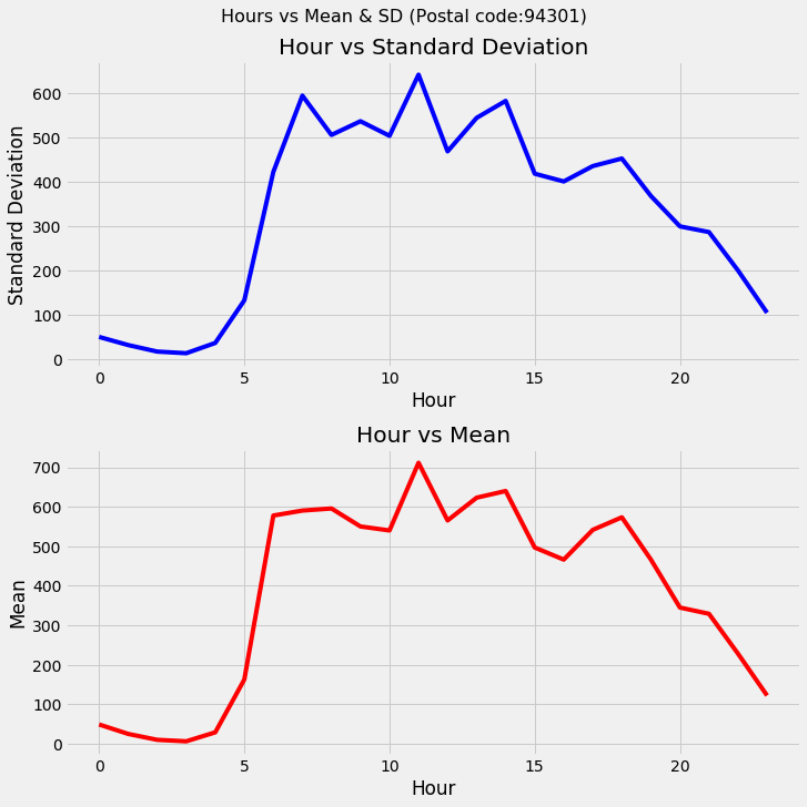

Figure 3.9: Energy Consumption SD and Mean Values of 72 Months for 24 Hours in 94301

by the more details on the mean curve especially between the hours $5 - 10$. Table 3.2 shows the values of mean and SD during 24 hours. The following numeration explains the table.

1. The hours between $0 - 4$ shows the lowest energy consumption for the mean values, which are below 50 kWh. The SD values for the same hours are also lower than 50 kWh.

2. The hours 5, and $22 - 23$ had larger values for both the mean and SD, which will affect the power system, but with a low rate $(100 - 230)$ kWh.

3. The medium consumption can be separated into small, middle, and large groups.

Table 3.2: Mean and Standard Deviation for 24 Hours in 94301

Hour	SD [kWh]	Mean [kWh]	Hour	SD [kWh]	Mean [kWh]
0	49.190	48.569	12	467.652	565.319
1	30.848	24.687	13	543.247	623.011
2	16.107	9.696	14	581.474	639.911
3	12.435	5.957	15	417.300	496.791
4	35.575	28.652	16	399.793	466.161
5	131.598	162.320	17	434.490	541.521
6	421.364	577.775	18	451.530	573.302
7	593.406	590.347	19	367.171	466.348
8	504.702	595.667	20	298.526	344.705
9	535.625	550.075	21	285.613	328.901
10	502.721	539.999	22	199.061	227.885
11	640.636	711.445	23	103.756	121.998

The small medium can be seen during the hours $20-21$, which had the values smaller than 400 kWh for the mean and between $250-300$ kWh for the SD. The middle medium will have mean values between 450 to 500 kWh, which are shown in hours $15-16$, and 19. The large medium values are between $500-600$ kWh that can be found in the hours $6-10$, 12, and $17-18$.

4. The large consumption have mean values between $600-700$ kWh at the hours 11, and $13-14$. Although the previous hours considered large, hour 11 had the largest value, which was 711 kWh.

The SD and mean table showed three consumption types to find how the EVCS will impact the grid. The low usage can be seen in the late and early hours of the day

$0-4$, which will not have a big impact on the gird. The second group is the medium one, which was divided into three types that must be considered in the long term to avoid issues on the grid. Also, the large consumption hours are found, which must be considered due to the big impact it has. The largest consumption occurred at 11 and it can be a reason to have an overload in the system.

3.2.3 Forecasting Palo Alto Data Set using Time Series Analysis Methods

Two data sets have been described and observed in kWh, but one of them will be forecasted because it has a higher number of transactions. The bigger the number of rows provided by the data set, the better training the model will have, which makes the prediction data more robust. Palo Alto data set energy consumption for the zip code 94301 will be forecasted using optimization method represented by polynomial curve fitting. Also, different TSA methods that applied both machine learning and optimization to predict the future kWh ratings. This part will discuss, which method is best to be used for the data by testing them.

Polynomial Curve Fitting for Energy Consumption Data Set

The polynomial curve fitting method is applied to Palo Alto's data set with the zip code of 94301. The polynomial curve fitting will basically match a line to the data and find their coefficients a_m depending on the least square fit [66]. For linear form least-square fit, the function $f(x)$ is represented in equation 3.1.

$$f(x) = a_0 f_0(x) + a_1 f_1(x) + ... + a_m f_m(x) = \sum_{j=0}^{m} a_j f_j(x) \tag{3.1}$$

The basis function is every $f_j(x)$, which is a predetermined function of x as Eq. 3.2.

$$S = \sum_{i=0}^{n} [y_i - \sum_{j=0}^{m} a_j f_j(x_i)]^2 \tag{3.2}$$

From the derivation described in reference [67], the matrix of the notation can be presented as $Aa = b$. The polynomial equation to fit the data is $f(x) = \sum_{j=0}^{m} a_j x^j$, which can be found if the polynomial degree is m that gives the basis as defined in equation 3.3.

$$f_j(x) = x^j \quad (j = 0, 1, ..., m) \tag{3.3}$$

Where $Aa = b$ matrix for the polynomial fitting is shown Eq 3.4.

$$A_{kj} = \sum_{i=0}^{n} x_i^{j+k} \quad b_k = \sum_{i=0}^{n} x_i^k y_i \tag{3.4}$$

It is important to mention that with increasing the number of m the polynomial method will have higher noise, which makes the low m values more helpful to apply the equation [67].

Furthermore, the polynomial curve fitting is applied to 94301 data set to find if the method can be used to predict the future kWh consumption. The degree m of the equitation is tested for the values from $1-6$ to find, which curve fits the data the best.

- Polynomial Curve Fitting to the Power m of $1-6$

  The polynomial curve fitting is tested and plotted for each degree from $1-6$. Every two degrees are plotted in the same figure and the important findings will be listed in the bottom. Since the polynomial curve fitting to the power 1 and 2 didn't match the expectations, it has been increased to be tested with the values of 3 and 4. The polynomial curve fitting to the power of 3 will be represented in yellow and to the power 4 will be in orange. Figures 3.10 and 3.11 shows kWh consumption in 24 plots each shows an hour of the day for the 72 months. It can be seen the number of months is shown as 79 in the plots, but when referring to it the value 72 is used instead. This is because the

data provided from July 2011 and the plots are considering the first six months, which appears always as zero.

From Figures 3.10 and 3.11 the hours 1 to 5 the curve can't be specified in a shape because of the low consumption of of EVCS energy (< 250 kWh). The 6^{th} hour shows many people in 2015 are charging their vehicle, but then it decreases again in the next years. The 7^{th} hour shows an increment wave shape for both powers, but the power to the $4th$ fits the data closer, which is better. From the 8^{th} hour to the 21^{st} hour the shape looks like a bird's body where the energy consumption increases then stay almost at steady state from the 20^{th} month to the 40^{th}. The hour 23^{rd} and 24^{th} takes the increasing wave shape again, where the energy consumption values in kWh are decreasing again. Tables 3.3 and 3.4 show the coefficients for the degree with values of 3 and 4 during the 24 hours.

Table 3.3: Polynomial Coefficient Values for the Degree m of 3 and 4 for the Hours $1 - 12$ in 94301

Hour	$m = 3$	$m = 4$
1	$-0.00053x^3 + 0.06729x^2 - 0.918x + 9.624$	$-5.044 \times 10^{-05}x^4 + 0.007541x^3 - 0.3495x^2 + 6.602x - 22.16$
2	$-0.0003203x^3 + 0.03216x^2 - 0.1202x + 1.807$	$-1.361 \times 10^{-05}x^4 + 0.001858x^3 - 0.08033x^2 + 1.909x - 6.76$
3	$-0.000113x^3 + 0.011x^2 + 0.023x - 0.2563$	$8.786 \times 10^{-06}x^4 - 0.001519x^3 + 0.0836x^2 - 1.287x + 5.279$
4	$-0.0001162x^3 + 0.008524x^2 + 0.05788x + 0.2585$	$2.532 \times 10^{-07}x^4 - 0.0001567x^3 + 0.01062x^2 + 0.02013x + 0.4181$
5	$-0.0002455x^3 + 0.02991x^2 - 0.3217x + 9.136$	$-6.205 \times 10^{-05}x^4 + 0.009683x^3 - 0.4829x^2 + 8.93x - 29.96$
6	$-0.004028x^3 + 0.406x - 5.07x^2 + 13.54$	$6.757 \times 10^{-05}x^4 - 0.01484x^3 + 0.9643x^2 - 15.14x + 56.11$
7	$0.00655x^3 - 0.7536x^2 + 39.71x - 240.9$	$0.0004232x^4 - 0.06117x^3 + 2.744x^2 - 23.39x + 25.77$
8	$0.006257x^3 - 0.2947x^2 + 10.44x + 6.798$	$-0.0004696x^4 + 0.0814x^3 - 4.176x^2 + 80.45x - 289.1$
9	$0.01466x^3 - 1.332x^2 + 41.06x - 76.97$	$-0.0002885x^4 + 0.06082x^3 - 3.716x^2 + 84.07x - 258.7$
10	$0.01603x^3 - 1.467x^2 + 45.08x - 168.6$	$0.0001058x^4 - 0.0008951x^3 - 0.5931x^2 + 29.31x - 101.9$
11	$0.009032x^3 - 0.731x^2 + 26.26x - 102.4$	$-8.566 \times 10^{-05}x^4 + 0.02274x^3 - 1.439x + 39.03x - 156.4$
12	$0.004466x^3 - 0.126x^2 + 10.27x + 3.029$	$-0.0003776x^4 + 0.06488x^3 - 3.246x^2 + 66.57x - 234.9$

From Tables 3.3 and 3.4 the third coefficient x^3 on the equation for the $3rd$

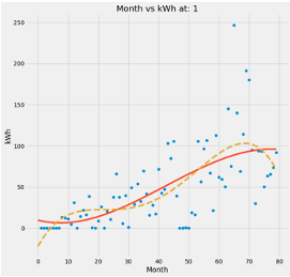

(a) Degree 3&4 hr. 1

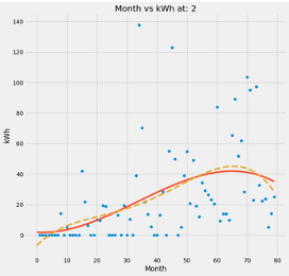

(b) Degree 3&4 hr. 2

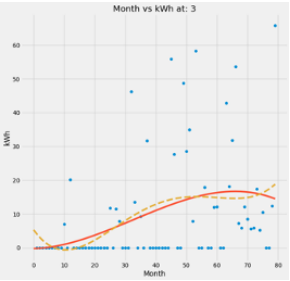

(c) Degree 3&4 hr. 3

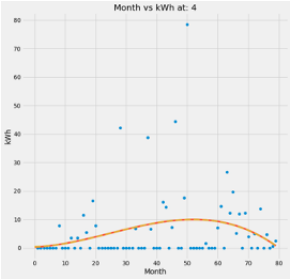

(d) Degree 3&4 hr. 4

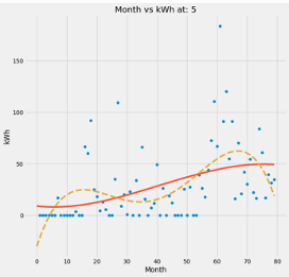

(e) Degree 3&4 hr. 5

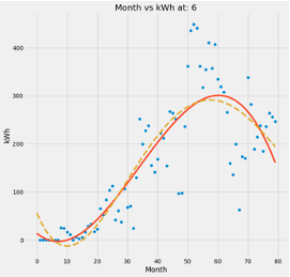

(f) Degree 3&4 hr. 6

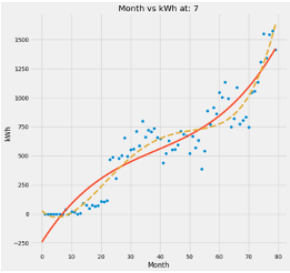

(g) Degree 3&4 hr. 7

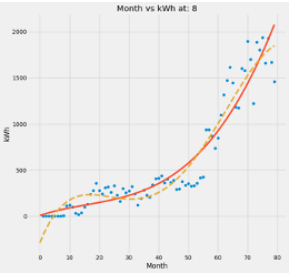

(h) Degree 3&4 hr. 8

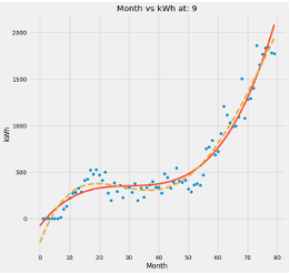

(i) Degree 3&4 hr. 9

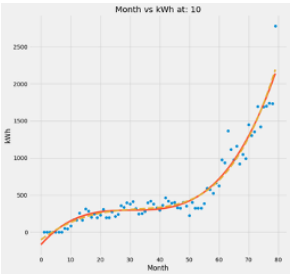

(j) Degree 3&4 hr. 10

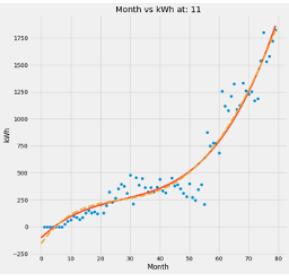

(k) Degree 3&4 hr. 11

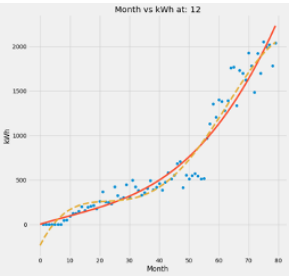

(l) Degree 3&4 hr. 12

Figure 3.10: Polynomial Curve Fitting Based on Energy Consumption Data for the Hours $1-12$ in the Area with Zip Code of 94301. Each Plot Shows the Curve Fitted During an Hour of the Day with m Values of 3 and 4.

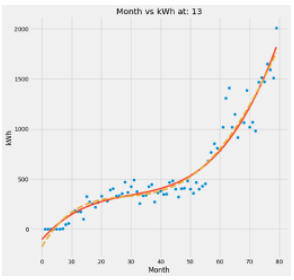

(a) Degree 3&4 hr. 13

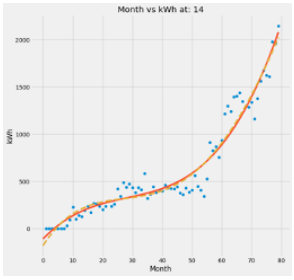

(b) Degree 3&4 hr. 14

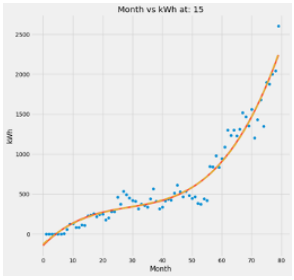

(c) Degree 3&4 hr. 15

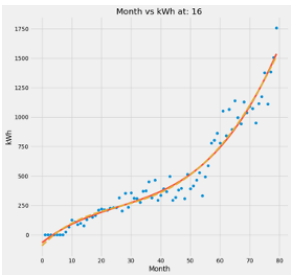

(d) Degree 3&4 hr. 16

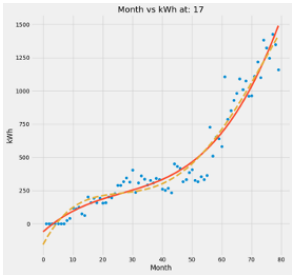

(e) Degree 3&4 hr. 17

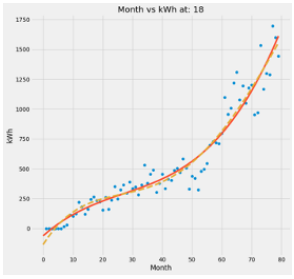

(f) Degree 3&4 hr. 18

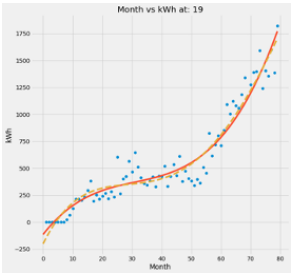

(g) Degree 3&4 hr. 19

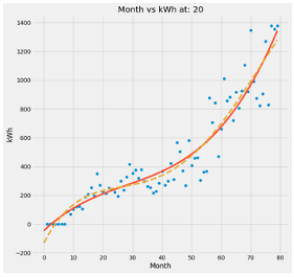

(h) Degree 3&4 hr. 20

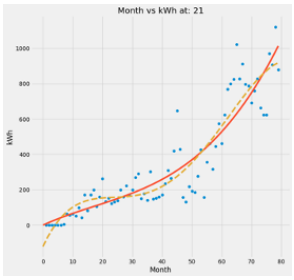

(i) Degree 3&4 hr. 21

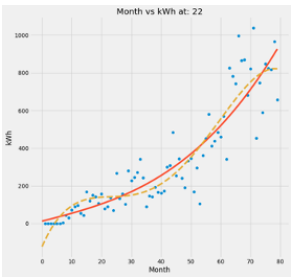

(j) Degree 3&4 hr. 22

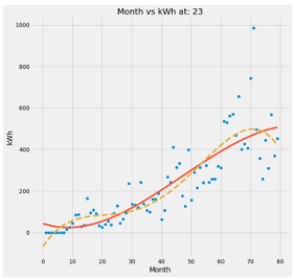

(k) Degree 3&4 hr. 23

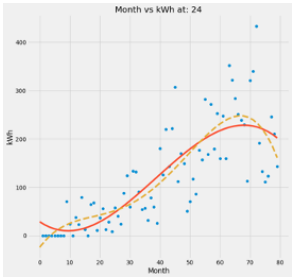

(l) Degree 3&4 hr. 24

Figure 3.11: Polynomial Curve Fitting Based on Energy Consumption Data for the Hours $13-24$ in the Area with Zip Code of 94301. Each Plot Shows the Curve Fitted During an Hour of the Day with m Values of 3 and 4.

Table 3.4: Polynomial Coefficient Values for the Degree m of 3 and 4 for the Hours $13-24$ in 94301

Hour	$m=3$	$m=4$
13	$0.01026x^3 - 0.9243x^2 + 33.26x - 103.1$	$-0.0001139x^4 + 0.02848x^3 - 1.865x^2 + 50.24x - 174.9$
14	$0.01076x^3 - 0.9113x^2 + 32.55x - 106.7$	$-0.0001113x^4 + 0.02856x^3 - 1.831x^2 + 49.14x - 176.8$
15	$0.0127x^3 - 1.098x^2 + 37.68x - 144.1$	$2.614 \times 10^{-05}x^4 + 0.008516x^3 - 0.8823x^2 + 33.79x - 127.7$
16	$0.005803x^3 - 0.4492x^2 + 19.55x - 66.54$	$-4.169 \times 10^{-05}x^4 + 0.01247x^3 - 0.7937x^2 + 25.77x - 92.8$
17	$0.006389x^3 - 0.5091x^2 + 19.99x - 61.72$	$-0.0001527x^4 + 0.03082x^3 - 1.771x^2 + 42.76x - 157.9$
18	$0.006254x^3 - 0.5073x^2 + 22.21x - 61.94$	$-0.0001163x^4 + 0.02486x^3 - 1.468x^2 + 39.55x - 135.2$
19	$0.01013x^3 - 0.9438x^2 + 35.18x - 113.7$	$-0.0001372x^4 + 0.03209x^3 - 2.078x^2 + 55.64x - 200.1$
20	$0.005273x^3 - 0.4406x^2 + 19.48x - 45.33$	$-0.0001345x^4 + 0.0268x^3 - 1.552x^2 + 39.54x - 130.1$
21	$0.002433x^3 - 0.1268x^2 + 7.638x + 0.4095$	$-0.000192x^4 + 0.03316x^3 - 1.714x^2 + 36.27x - 120.6$
22	$0.001141x^3 + 0.005327x^2 + 4.027x + 12.3$	$-0.000214x^4 + 0.03538x^3 - 1.763x^2 + 35.93x - 122.5$
23	$-0.00216x^3 + 0.304x^2 - 4.657x + 42.87$	$-0.0001762x^4 + 0.02603x^3 - 1.152x^2 + 21.61x - 68.15$
24	$-0.002177x^3 + 0.2527x^2 - 4.181x + 28.69$	$-8.374 \times 10^{-05}x^4 + 0.01122x^3 - 0.4393x^2 + 8.304x - 24.07$

degree ($m=3$) has negative values during the low consumption of kWh, which can be clearly seen in the hours $1-6$ and $23-24$. However, for the rest of the hours where the kWh is rated higher the values are positive for third degree's (x^3) coefficients. For the fourth degree ($m=4$) the coefficients of x^4 have lower values ($\times 10^{-5}$) for medium and low kWh ratings. On the other hand, the higher rates of kWh had larger values ($\times 10^{-4}$).

Although there are good findings when $m=3$ and $m=4$ regarding the kWh usage, the main focus for this section is the polynomial curve fitting. Figures 3.10 and 3.11 didn't meet the aim because it's not showing the details of how the kWh is operating during peak, normal hours. However, the curve is going through the points with enough variance values that make the fourth degree's (x^4) curve named as best-fitting. Since the fourth degree had better fitting the

fifth and sixth degrees are tested as well.

The overall observation for $m = 1 - 6$ are the following:

- The linear shape is representing the degree of 1.
- The Nike curve is found from the $m = 2$ and it can simply be observed by that the number of EV was increasing from the year of 2011 to 2013. Then the purchasing for EV stay steady, and from the last months of 2015 to the future it will be increasing, which means more kWh consumption will occur.
- When the degree is 4 the curve is fitting the data better than the power of 3. The curve can still be specified with one shape for different hours for both degrees, which is fitting the data and can use additional method such as ridge regression to predict the future. There are many curves such as, 3.11c, 3.10l, and 3.11i are heading to $+y - axis$ for, which shows the accurate behaviour of the the data set values. So, the $m = 4$ looks like the perfect fit for the data, but addition methods are needed to predict by training and testing the curve, which can't be done by the polynomial curve fitting itself from the provided plot in Figures 3.10 and 3.11.
- The curves for the 5^{th} and 6^{th} are fitting the data in almost the same shape for most of the hours. Since the curve is started to over-fit the data set, then the larger degree will not assist any more in fitting the data. This observation matches what the earlier mentioned reference [67] that the larger value of m, the less useful the polynomial curve fitting is. When the degree m used with a value of 5 and 6 it was obviously seen that increasing the value of m leads to finding neither the best curve fit nor the coefficient values. The values are getting smaller when the degree's values

are increasing, which makes a larger error percentage to fit the data. So, applying the polynomial with a larger degree will no be further applied.

Polynomial curve fitting has been tested on Palo Alto's data set for the zip code of 94301. The mathematical forms are described first to clearly explain how the line will fit the points. Then, the number of variables for the equations is changed to find a robust fit. Each degree represented in m is plotted for 72 months for 24 hours. In addition, the coefficients are shown in tables for each equation with its variables. The tables and figures are observed and described in terms of both how kWh consumption and curve fitting. The polynomial curve fitting is tested from the degree $1 - 6$, but none of them fitted the points enough to predict the future and show the details such as the peak hours. However, the best polynomial fit to the data can be seen in Figures 3.10 and 3.11 for the yellow curves, which represents the fourth degree $m = 4$. The polynomial curve fitting will be a perfect fit for the data, but it needs additional methods to assist it in forecasting. So, the method will be tested to find the future, but with the assistance of different TSA methods that are applied to the data in the next section.

Forecasting Energy Consumption Using TSA Methods

There are a variety of TSA methods for different applications to reach one goal, which is to predict the future. In this section, two methods are applied, which are autoregressive moving-average (ARMA) and exponentiation smoothing (ES). Both are applied on the zip code 94301 and tested first only on one hour, which is the $236rd$. After testing each model and find how fit it would be the rest of the hours will be tested upon it.

- ARMA

The ARMA is based on the polynomial curve fitting, which can be clearly seen by its first and second term. The terms in $ARMA_{p,q}$ are corresponding to the autoregressive polynomial (p) and moving average polynomial(q). Eq. 3.5 represents the relation of the integers [68, 69].

$$Y_t = \mu + \sum_{j=1}^{p} \phi_j (Y_{t-j} - \mu) + \sum_{j=1}^{q} \psi_j \epsilon_{t-j} + \epsilon_t \tag{3.5}$$

Where ϵ_t is the error or the Gaussian white noise, μ is assumed to be zero, $\phi_1 ..., \phi_p$ is autoregressive parameters, and $\psi_1, ..., \psi_q$ is moving average parameters.

ARMA is applied to the data for the hour 23 for 72 months. The data is representing from July 2011 to July 2017. Different time series analysis functions were applied to the system to decrease the error to fit the data. First, the autocorrelation of the data and the partial correlation are found without applying the ARMA model as shown in Figure 3.12a. Before finding the correlation after ARMA is applied, the fitting line to the data is found in Figure 3.12b, which looks the same as polynomial curve fitting using the first degree $m = 1$. Figure 3.12c shows the correlation with applying the ARMA model.

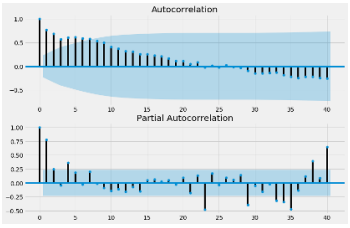

(a) Correlation without Applying ARMA

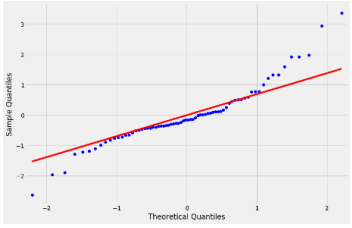

(b) Curve Fitting Depending on the Correlations

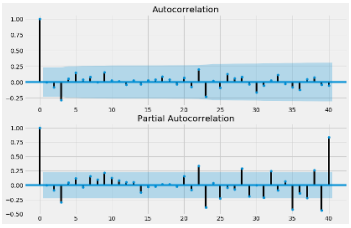

(c) Correlation with Applying ARMA

Figure 3.12: Finding the Data Correlations with and without ARMA at the Hour 23 for 72 Months in the Zip Code 94301

Comparing the plots before and after applying ARMA, it is clear in Figure 3.12a the correlation is out of the shaded area especially on the months $0-5$. On the other hand, when ARMA is applied the shaded area covered almost all of the points. So, it is clear that ARMA will improve the curve fitting. The forecasting using ARMA is found in Figure 3.13.

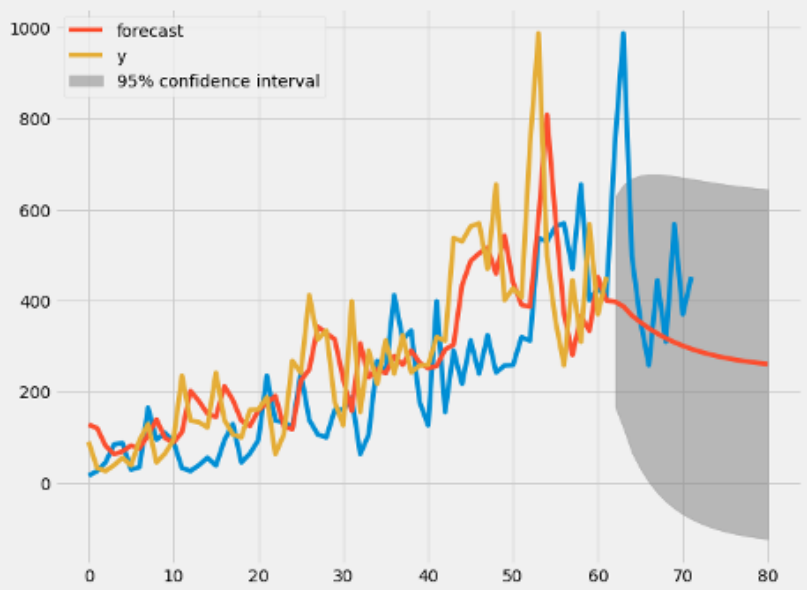

Figure 3.13: ARMA Model Forecasting Energy Consumption for the Hour 23

From Figure 3.13 the forecasting is not fitting the shape it followed while training. The yellow curve is the chosen data for training, which is 60 months and the blue carve is the original data for 72. The orange is the curve forecasting form 72 until the month 79, which was designed to test the predictions by comparing the blue curve from the month 60 to 72. It's clear that on the training months $0-60$, the ARMA curve is learning, but when it was forecasting it didn't follow the training behavior. The blue curve and orange don't have similarities, which makes the testing of the ARMA method fails to predict the future. There are many reasons for failure and in this case, it can be the number

of training data is not enough for the module to train, or the degree of ARMA for polynomial fitting is small, which gives almost a linear behavior. So, more features for the ARMA model is required to reach better prediction.

- Exponential smoothing

  TSA is to use a mathematical model that will study some data, which depends on time and then predict the future data, find when the sales will increase, etc. The exponential smoothing is one method used in TSA, which considers the trend, seasonality, and residuals. The trend can be visualized by a slope to represents the increment and decrement of the data for the long term from historical data. The seasonality can be represented with a fixed frequency of seasonal changes such as hours, days, years. The residual is an additional type that describes the data in the short term. To find the observed data of the ES there are different methods to assist it such as Holt Winter's that can be represented in additive and multiplicative. The additive method represents the linear trend and the multiplicative shows the exponential trend [70].

  ES Mathematical Formulation: Before moving to Holt Winter's model, the ES mathematical form is represented in Eq. 3.6 that represents the naive method, which equals the predicted values to the last observed one [71].

$$\hat{y}_{T+h|T} = y_T, \quad \text{for} \quad h = 1, 2, ..., \tag{3.6}$$

  However, using only one value will not give good forecasting, which makes the observations average weight is applied as Eq. 3.7 shows.

$$\hat{y}_{T+h|T} = \frac{1}{T} \sum_{t=1}^{T} y_t, \tag{3.7}$$

Although, Eq. 3.7 depends on different weights, but it gives all observations the values of 1 to predict the future that means all observations will have the same importance on forecasting. The ES will solve the issue by giving different importance values depending on their time. The observations found at an earlier time will have lower weights and the recent ones will have a larger impact, which makes the prediction more efficient following a series. Eq. 3.8 shows the ES in mathematical form to give each observation different weight [71, 72].

$$\hat{y}_{T+h|T} = \alpha y_T + \alpha(1-\alpha)y_{T-1} + \alpha(1-\alpha)^2 y_{T-2} + ..., \tag{3.8}$$

where $0 \leq \alpha \leq 1$. So, α will control the importance of each observation, which means the higher α the more importance the observation is. The ES model with the level γ_t period included will be shown in Eq. 3.9 for forecasting and Eq. 3.10 is showing the smoothing formula.

$$\hat{y}_{t+h|t} = \gamma_t \tag{3.9}$$

$$\gamma_t = \alpha y_t + (1-\alpha)\gamma_{t-1}, \tag{3.10}$$

Eq. 3.10 includes the level to predict the future, but as mentioned earlier the ES can consider the seasonal and trend components, which are investigated in mathematical form in [71].

Furthermore, Holt Winter will assist in forecasting the data by using the periods with ES. Eq. 3.11 shows the additive and Eq. 3.12 is used for the multiplicative models of Holt winter. [71].

$$\hat{y}_{t+h|t} = \gamma_t + hb_t + s_{t+h-m(k+1)} \tag{3.11}$$

$$\hat{y}_{t+h|t} = (\gamma_t + hb_t)s_{t+h-m(k+1)} \tag{3.12}$$

where b_t is the weighted average and s_t is the seasonal components at time t.

Data set Separation and Description: First, before applying any ES method, the data must be divided into training and testing sets. The model will be applied to Palo Alto's Energy consumption with the zip code 94301 for 72 months in the hour 23. Since the percentage for training is suggested to be more than 60% of the data, then the data is divided into 43 months training set and 29 months testing set. The overall number being used is 72 months, which represents the data from July 2011 to July 2017. Figure 3.14 represents the training and testing data set.

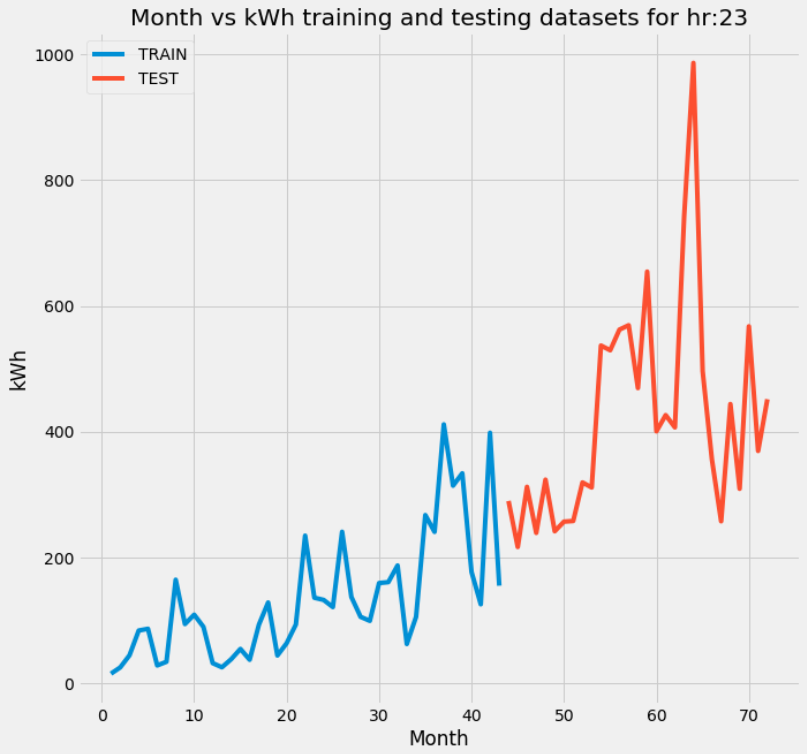

Figure 3.14: Training and Testing Separation for the Hour 23 of the Energy Consumption

After having the training and testing sets ready, the next step will be to visualize the ES period type of training data. Figure 3.15a shows the additive method that can be represented as a trend, where the slope of seasonal and

residual is zero when the a frequency = 1. Figure 3.15b shows the multiplicative method with frequency of 1. The curves of the multiplicative method for the residual and seasonal have the values of 1, which is not having any behavior by the data.

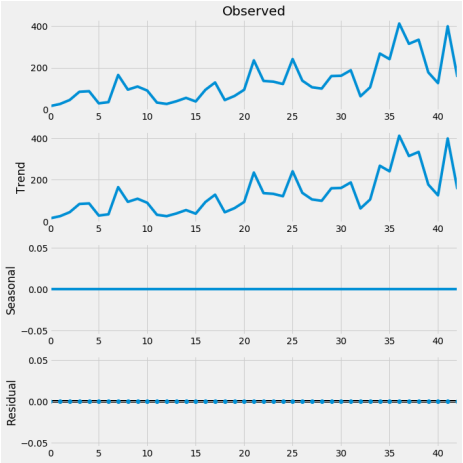

(a) Periods for Additive Method for $f = 1$

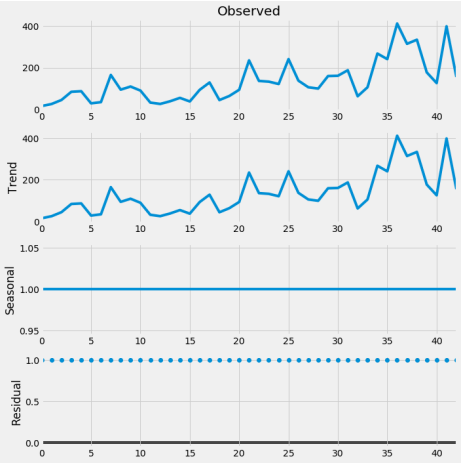

(b) Periods for Multiplicative Method for $f = 1$

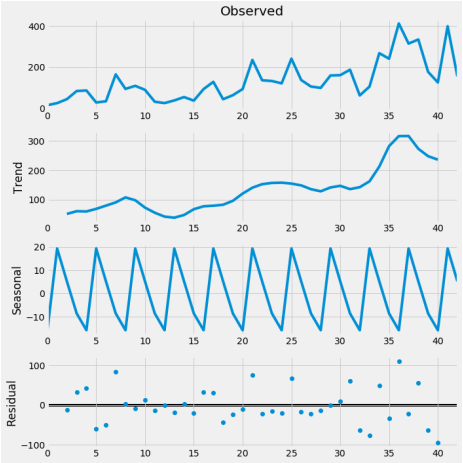

(c) Periods for Additive Method for $f = 4$

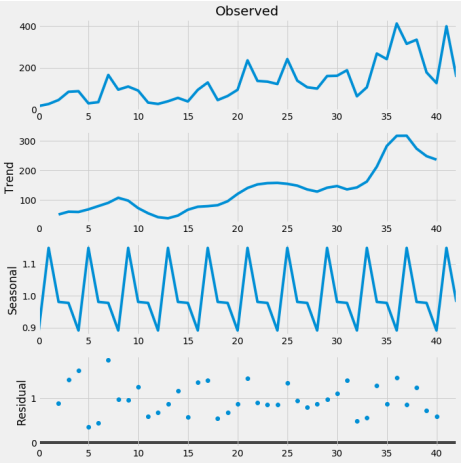

(d) Periods for Multiplicative Method for $f = 4$

Figure 3.15: Finding the Data Periods with Different Frequencies at the Hour 23 for 72 Months in the Zip Code 94301

The frequency is the period of series and because the data plots will be presented for each month and the given data is also in months, then 1 is the number to be used. If the data is given for every 1 month, which is 30 days and the prediction for the seasonal will be every one week (7) days, then it can be calculated as $f = \frac{30\text{days}}{7\text{days}} \times 1\text{week} = 4\text{weeks}$. To ensure that the frequency is meeting ES aim, Figures 3.15c and 3.15d shows the plot with frequencies of 1 month and 4 weeks, which represents the series for in the additive and multiplicative method.

ES Testing Including Different Components: The ES method is applied to the training and testing data to compare the results and then predict the future. The simple smoothing that is shown in 3.8 is applied with different alpha values, which are the smoothing level values. Figure 3.16a shows the simple smoothing with three levels that are represented in two alpha values, which found bad predictions.

Figure 3.16a showed almost the same shape for the predicted slopes, but with different heights and they didn't follow the kWh curve's series. So, Holt winter method will be applied using the additive and multiplicative model to find better predictions. Figure 3.16b applied Holt's model with different methods, which improved the results slightly.

The predicted curve of Holt winter with the exponential has an increment curve instead of a linear shape, which is shown by the damped method in Figure 3.16b and for alpha's Figure in 3.16a, but both are still far from fitting the testing data. So, Holt's and damped methods had linear curves, Holt's with exponential increased to large values because it's not following the limitations, which can be fixed by studying the level and slope of the training data and

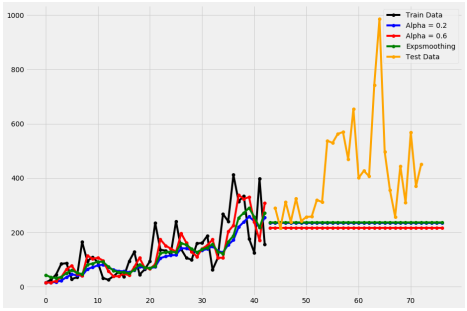

(a) Simple Smoothing with $\alpha = 0.2$ and 0.6

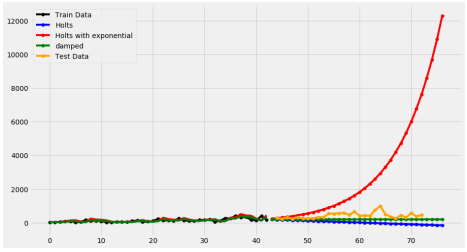

(b) Holt's Model Implementation with Different Methods

Figure 3.16: Data Periods Analysis with Different Frequencies at the Hour 23 for 72 Months in the Zip Code 94301

apply them to predict the testing data. Following equations 3.11 and 3.12 the slope and level of components are found using Holt's linear trend and additive damped method as showing in Figure 3.17a. Figure 3.17b shows the level and slope when applying Holt's and ES together without including the damping.

Figure 3.17a shows that the damping will not assist in predicting the values since into not following the behavior of the data, which clearly affected Figure 3.16b for the Holt's and ES method represented in the red line. Figure 3.17b showed the Holt and ES without applying the damped, which clearly fitted the data in better shape. Figure 3.17c showed Holt's and ES methods that include

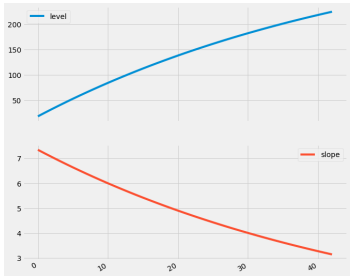

(a) Slope and Level of Holt Damped Method

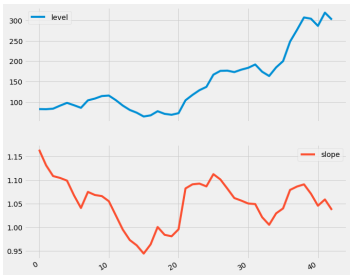

(b) Slope and Level of Holt and ES Methods Combined

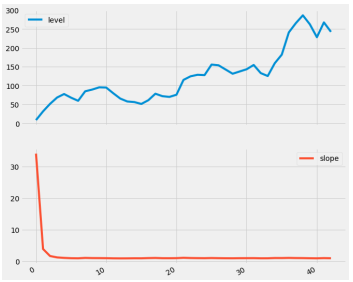

(c) Slope and Level of Holt and ES Including Damping

Figure 3.17: ES and Holt Winter Including Different Methods at the Hour 23 for 72 Months in the Zip Code 94301

damping. The slope shape is not providing the details because of the large value it started at $y - axis = 30$. The damping is not recommended to be further applied because it's affecting the prediction on a negative side.

Since the slope and level are found, let's apply Holt's prediction with the same methods shown in Figure 3.16b. Figure 3.18 provide Holt's prediction values with different methods while applying the level and slope.

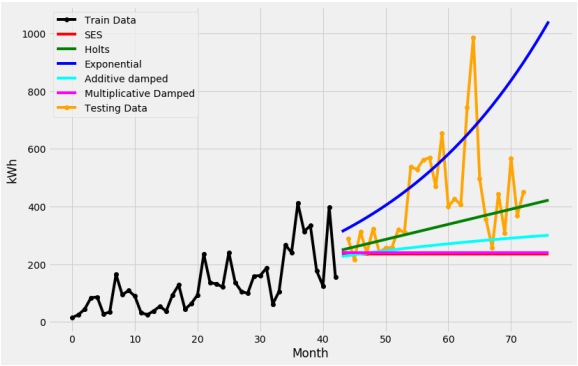

Figure 3.18: Holt with Different Methods Including Slope and Level at the Hour 23 for 72 Months in the Zip Code 94301

Figure 3.18 showed closer fitting to the testing data, where the additive and

multiplicative damped curves are located by the bottom area of the training data. Holt's is shown in the green curve, which is located in a better area than the previous ones. The blue curve is Holt's with ES combined including the slope and plot, which fits the upper area of the testing data.

From the previous figures, Holt with ES showed an improvement in fitting the testing, but it was only using the slope and level from the training data. Holt's can also find the prediction depending on the seasonality and trend to improve the fitting. Figures 3.19 and 3.20 shows for plots for the trend additive and multiplicative, and seasonal additive and multiplicative withe periods of 2.

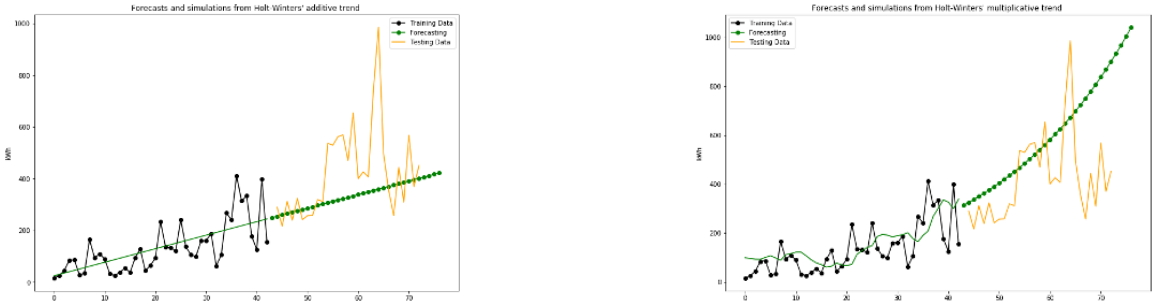

(a) Additive Trend

(b) Multiplicative Trend

Figure 3.19: Additive and Multiplicative Trend and Seasonal with Period of 2 at the Hour 23 for 72 Months in the Zip Code 94301

Figure 3.19 showed two plots using the multiplicative and additive trend methods of ES and Holt's. Figure 3.19a showed the additive trend, which follows the testing increment rate. This matches the trend's definition earlier that is focuses on long term behavior. For the multiplicative method, it had a wider increment rate as shown in Figure 3.19b.

Figure 3.20 shows the additive and multiplicative seasonal methods for the period of 2, which means for every 15 day. Figure 3.20a provide the additive

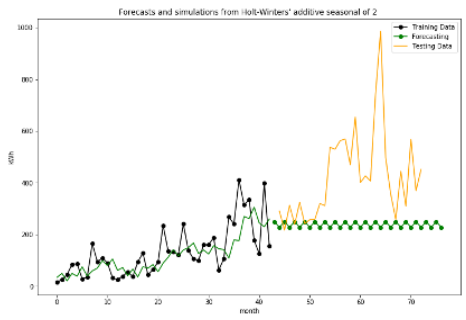

(a) Additive Seasonal with Period of 2

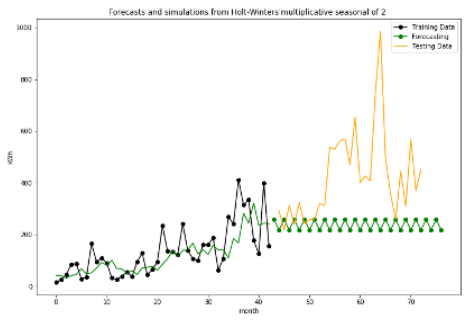

(b) Multiplicative Seasonal with Period of 2

Figure 3.20: Additive and Multiplicative Trend and Seasonal with Period of 2 at the Hour 23 for 72 Months in the Zip Code 94301

seasonal plot with period of 2. For the multiplicative seasonal it's tested in Figure 3.20b. Both of them are filling a part of prediction the testing data, where the additive had smaller periods between one prediction to the other comparing the multiplicative model.

Figures 3.19 and 3.20 shows that the trend is applying the long term shape and the seasonal focus on the short term. So, combining the trend with seasonal (TWS) will be checked to find if the prediction curve will fit the testing data. In Figure 3.21 the TWS additive and multiplicative are plotted for the same period, which is 2. The plots will use (ATWS) for the additive and (MTWS) for the multiplicative TWS.

The ATWS fitted the testing curve from the middle without caring about the changes that occurred in the middle of testing data, which can be seen between the months $55 - 65$ in Figure 3.21a. MTWS in Figure 3.21a is increasing to a point beyond where the testing data is found. The TWS can be still investigated before changing the period to different values, by having the multiplicative

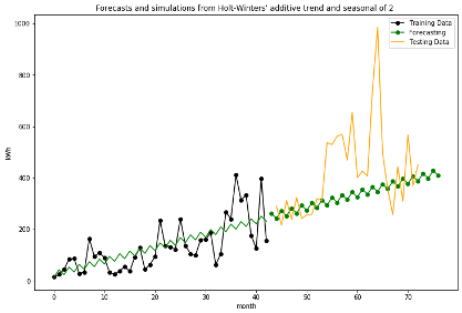

(a) ATWS for Period of 2

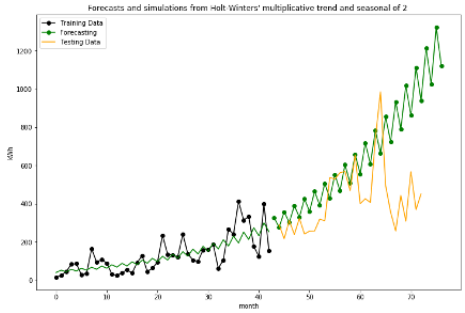

(b) MTWS for Period of 2

Figure 3.21: Additive and Multiplicative TWS for Period of 2 at the Hour 23 for 72 Months in the Zip Code 94301

trend (MT) and the additive seasonal (AS) methods to predict the values. The opposite will also be tested for additive trend (AT) and multiplicative seasonal (MS) models. Figure 3.22 shows the couple plots, the first shows the AT and MS, and the second tests the MT and AS with a period of 2.

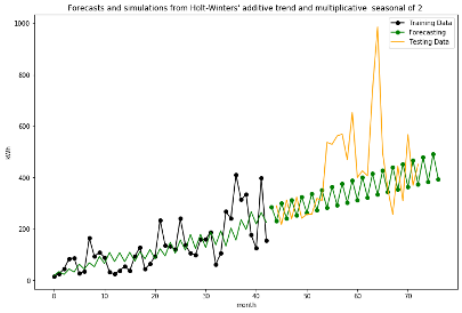

(a) AT and MS with Period of 2

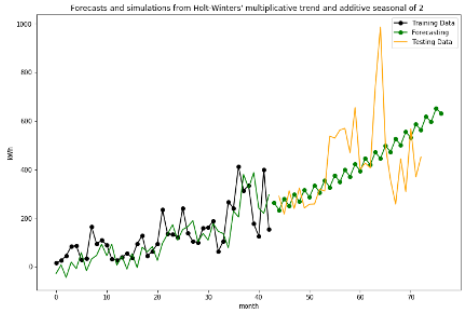

(b) MT and AS with Period of 2

Figure 3.22: (MT - AS) and (AT - MS) Testing for Periods of 2 at the Hour 23 for 72 Months in the Zip Code 94301

Figure 3.22 has the best prediction comparing to the previous methods used in this section. From looking at Figure 3.22a the predicted curve in green is fitting the data with better shape than the MT and AS method in Figure 3.22b.

The number of simulation periods will be tested for the value of 3 to have a clear decision. In Figure 3.23 the (AT - MS), and (MT - AS) methods are plotted.

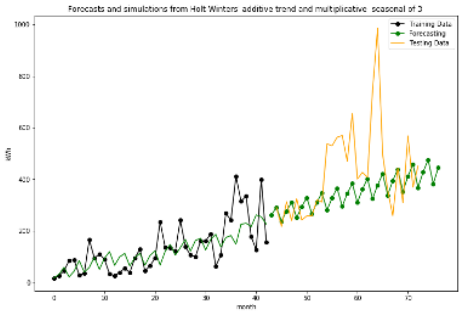

(a) AT and MS with Period of 3

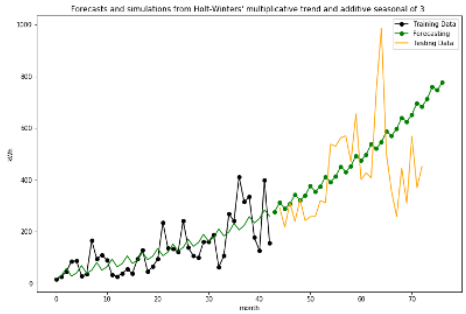

(b) MT and AS with Period of 3

Figure 3.23: (MT - AS) and (AT - MS) Testing for Periods of 3 at the Hour 23 for 72 Months in the Zip Code 94301

Figure 3.23b looks better, but still, the decision must be ensured to take off one of the methods. The simulation period will be assigned to 4 and then one of the methods will be removed. Figure 3.24 will find whether (AT - MS) is better than (MT - AS) method, or not.

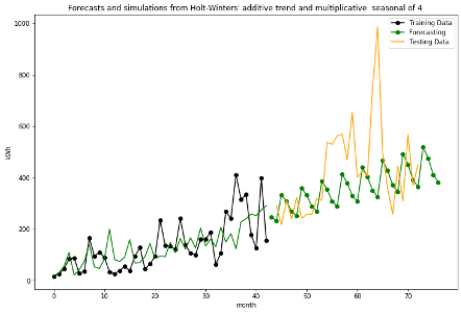

(a) AT and MS with Period of 4

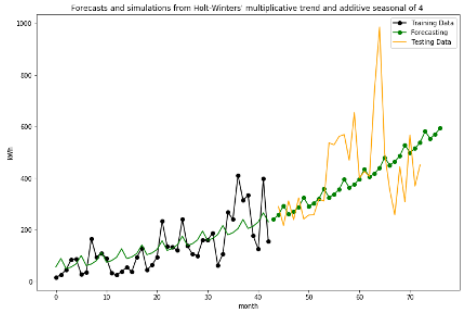

(b) MT and AS with Period of 4

Figure 3.24: (MT - AS) and (AT - MS) Testing for Periods of 4 at the Hour 23 for 72 Months in the Zip Code 94301

Figure 3.24a looks better for forecasting and fitting the data, which can be

seen by the additional movement in the curve. So, AT and MS will be tested for the Holt Winter ES method. The values of the simulation period will be tested for $8, 9, 10, 20$, which will find different slopes to fit the testing curve. The period with the most robustness fit will be later used to predict the other hours of the day from the zip code 94301.

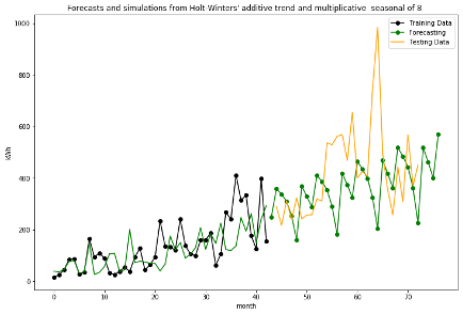

(a) AT and MS with Period of 8

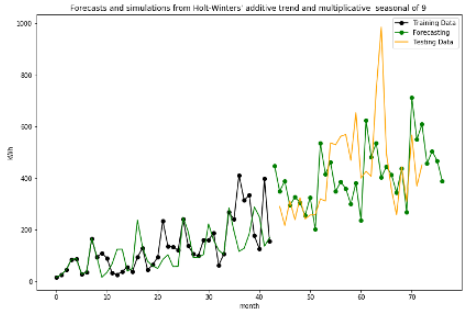

(b) MT and AS with Period of 9

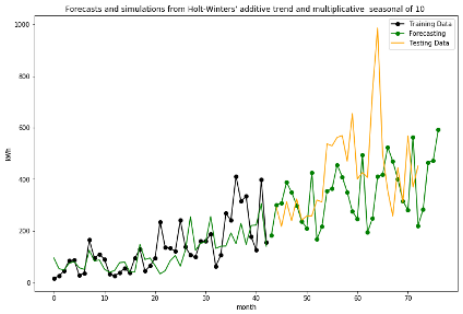

(c) AT and MS with Period of 10

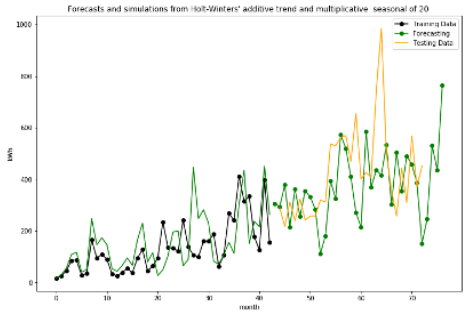

(d) MT and AS with Period of 20

Figure 3.25: MT and AS Testing for Periods of $8, 9, 10, 20$ at the Hour 23 for 72 Months in the Zip Code 94301

Figure 3.25 showed four periods and all of them found good seasonality prediction, which can be obviously seen by the repetition of the curve's behavior. The positive point for the predicted curve is that the curve has ignored the peak values between the month $62 - 64$; It can be considered more advanced than the testing data itself, which represents the historical data. Figure 3.25a shows

the curve with a period of 8, which is close to the testing data, but there is a sharp decrement repeated every eight months. So, AT and MS with a period of 8 is has a good fit with a disadvantage that drives the curve far from the testing. Figure 3.25b is fitting the testing data even for the small details that can be seen between the months of $43 - 50$. Also, on month 70 the predicted data fitted almost exactly the testing points. So, AT and MS with a period of 9 shows a robust fit to predict the data set. Figure 3.25c is plotting AT and MS with a period of 10, which shows a good fit, but it misses the details due to the bigger seasonality it considers. Figure 3.25d can be considered the perfect fit for the testing data, but it has sharp decrement and increment points that it can be seen in the months $53, 57, 60, 71$. So, the decision to forecast will be found with a period of 9 because it had the best prediction comparing to the others. MT and AS with a period of 9 is tested in this section and it predicted the best fit to the testing curve. The same period of 9 can be applied for the rest of the hours from $1 - 24$ to predict their future behavior. However, the prediction for the rest of the hours might require different period values to have better forecasting.

Forecasting kWh for the city Palo Alto in the zip code 94301 required different methods to reach a robust fit that is compared with the testing data. First, the ARMA model is applied to the data and it found bad forecasting. ARMA's prediction can be improved by increasing the degree of the polynomial and applying additional features to follow the behavior of the data. Then, the ES is explained in mathematical form and introduced Holt Winter method to improve the fitting. The data set is divided into training and testing sets to compare the prediction to the historical values. The hour 23 has been studied with different periods to find it's seasonality, trend, level, slope, residuals, and then observe them. The ES is tested with additional methods

such as Holt's, ES by themself, adding the damping, combine them both. However, the damping had a negative impact, where the best method to fit the data is to use ES and MS with a period of 9. For future work, the period value can be changed when forecasting the data because as mention the ES prediction method follows the seasonality, which is the short term behavior, and the trend that represents the long term shape.

3.3 Remarks

In this chapter, TSA methods have been applied to forecast the future and study the principles of EVCS. EVCS data sets are studied for two cities Palo Alto, CA, and Boulder, CO. Boulder's data has five zip codes and Palo Alto's data has three, where the one with the highest transactions is further investigated.

The investigation observed the kWh consumption during 24 for each month, which is 26 for Boulder and 72 for Palo Alto. Then, the SD and mean of the kWh summation during the 24 hours are found and represented in a table. Since CA's data has more transactions it was further investigated by including more TSA methods. The charging duration for each month is found for seven years and then found important observations, for instance, attaching the fast charging to the EVCS, which decreases the minutes it required to charge an EV.

After observing and describing the data, forecasting TSA methods are applied to predict the future. The first method is to apply the polynomial curve fitting, but it didn't work because it required additional constraints. So, the ARMA method that depends on the polynomial smoothing level and autoregressive components. Although ARMA improved the prediction, it shows bad fitting to the historical data curve. Furthermore, the ES method is applied to Palo Alto data set and divided the data into training and testing to compare the prediction to the real data. Additional

constraints is added, which is Holt Winter to improve the prediction. The method depends on seasonality that studies the short term shape and the trend that focuses on the long term behavior. The ES method found a perfect prediction for the hour 23 by using the period of 9. For future work, the rest of the hours can be also studied using different periods to fit the historical data.

Chapter 4

IMPACT OF ENERGY ROUTER ON ELECTRIC VEHICLE CHARGING STATION PLACEMENT

There is a large number of publications that studies an optimal placement for EVCS aiming for almost the same goals, which are reducing the cost, ensuring secured power flow in the system, and meeting consumer requirements that effects the power system demand. Planning electric vehicle charging station (EVCS) models consider both the power and transportation system to reach the efficient result. EVCS planning considering network size to be small [73], large [55, 74, 75], and both sizes [76] has been performed to fit the area's requirements. Charging infrastructure-planning problems for small cities associated with the multi-objective considering power grid, random road traffic, EV user's, and economic characteristics is solved in [73] and it ensured minimum harm to the power grid. In [76], it represents a planning capacity framework considering different charging levels that EVCSs will offer, which is formulated by applying a convolution algorithm to evaluate the customer target in small and large cities while ensuring the quality of service. Novel integrated complicated multiple criteria decision making is approached using uncertain linguistic multi-objective optimization by ratio analysis plus full multiplicative module, and decision making trial and evaluation laboratory in [75], to find an optimal site of EVCS in a large city. So, three sizes are presented to plan EVCS, which will assist in finding the site that meets the demand.

Furthermore, ER devices have evolved over the last decade, becoming more economical and deployable than the original FACTS devices. Additionally, new overhead transmission lines have become more challenging to build in some regions, increasing

the demand for ER devices to augment the transmission capability of the existing transmission networks [77]. Given these drivers, the set of viable locations for ERs has expanded and further complicated the process of planning and operating EVCSs. In addition, system planning and operation have become more complex given the emergence of renewable generation and additional stakeholders. These facts motivate us to deploy ERs to enhance EVCS placement with reduced costs. As shown in Fig. 4.1, less EVCSs are installed due to the top line's congestion. After the deployment of ERs, additional power flows in the bottom two lines resulting in the expanded installation of EVCSs, without violating the line limits.

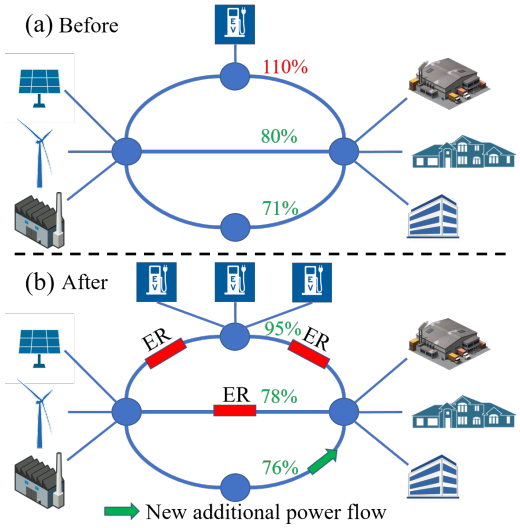

Figure 4.1: Energy Routers' Exemplary Interaction with EVCS Placement. (a) Shows the Overload on the Line and One EVCS is Connected to the Network. (b) Indicates the Overload is Solved and More EVCSs are Applied.

This chapter studies EVCS optimal planning with using ER to reach maximum profit. The system will compare EVCS planning with and without using the ER to show how ER will assist the model.

4.1 Problem Formulation

A well-planned EVCS infrastructure needs to satisfy the EV charging demand at a high probability. Therefore, it is essential to accurately estimate EV demand. Meanwhile, to fill the gap of modeling the interaction between the power flow controller and the EV power demand, a simplified method to model the ERs and its mobility using a mobility matrix is propose. Based on the mentioned two ideas, the EVCS planning into a stochastic integer programming problem is formulated, which is presented at the end of this section.

4.1.1 Chance-constrained EV Demand Estimation

As mentioned in section 1.1.2, a great amount of work has been done to couple transportation modeling into the electrical networks. However, power system operators do not always have access to and the modeling/validating capability of the transport networks. Therefore, trying to address this issue through the data analytics of what is accessible to transmission and distribution planners – the EV charging record data from the EVCSs. The EV charging records are studied in Chapter 3 that contain the individual charging starting and ending time, Zip code, charging power, etc., based on the estimation is made for the EV demand. To satisfy the EV demand at bus i, we have:

$$w_i^T y_i \geq \tilde{D}_i, \ \forall i \in \Phi, \tag{4.1}$$

where w_i is the serviceability coefficient, a deterministic vector such that $w_i := [w_{i1}, \ldots, w_{iJ}]^T$, where J is the order of the serviceability model; and $\tilde{D}_i$ is the EV charging demand, a random vector such that $\tilde{D}_i := [\tilde{D_{i1}}, \ldots, \tilde{D_{iJ}}]^T$ that affects the constraints. It would be a waste of societal resources to require the constraints (4.1) to

hold under any realization of the random demand distribution and a very high probability. Thus, a probabilistic bound, $1-\epsilon$, on the constraint violations is introduce. The charging demand chance constraints are

$$\inf_{\mathbb{P}_{\tilde{D}} \in S_{\tilde{D}}} \mathbb{P}_{\tilde{D}}\{w_i^T y_i \geq \tilde{D}_i\} \geq 1-\epsilon, \ \forall i \in \Phi, \tag{4.2}$$

where $S_{\tilde{D}}$ is an ambiguity set [78] and the chance constraint is satisfied for all distributions within the ambiguity set $S_{\tilde{D}} := \{\mathbb{P}_{\tilde{D}} \in \mathcal{P}' : \mathbb{E}_{\mathbb{P}_{\tilde{D}}}[\tilde{D}] = \mu, \mathbb{E}_{\mathbb{P}_{\tilde{D}}}[\tilde{D}\tilde{D}^T] = \Sigma\}$.

Under many circumstances, only the series of historical data taken from the true (while ambiguous) distribution is known. Here, the historical data can be considered as charging records data from charging stations. Fortunately, power system operators have a continuing collection of historical charging record data that reflects the true EV charging demand. Therefore, having an easily access and predict the lower order moment knowledge from the past data to estimate the EV load demand in the future is possible. In charging record data, the first-order moment directly refers to the mean value of the charging demand at each time slot; meanwhile, the second-order moment can be easily derived from the covariance of the charging demand. For higher-order moments, it is harder to estimate, in the sense that larger samples are required to obtain estimates of similar quality. Therefore, this method focuses only on the first two order moments for EV demand estimation. If the first-order moments of the EV demand data is given, we have:

Theorem 1. *(**Conversion from the Stochastic to Deterministic Integer Program When Given the EV Demand Mean Values**) If $w_i^T \geq 0$, $\tilde{D}_i \geq 0$, $\forall i$ and we are given the first moment knowledge $\mathbb{E}[\tilde{D}_i], \forall i$, then an equivalent formulation for (4.2) is the following deterministic integer program:*

$$\inf_{\mathbb{P}_{\tilde{D}} \in S_{\tilde{D}}} \{w_i^T y_i \geq (1-\epsilon)\mathbb{E}[\tilde{D}_i]\}, \ \forall i \in \Phi. \tag{4.3}$$

Proof. It has be shown in [79] that the standard Markov Inequality is tight; i.e., $\inf_{\mathbb{P}_{\tilde{D}} \in S_{\tilde{D}}} \mathbb{P}_{\tilde{D}}\{w_i^T y_i \geq \tilde{D}_i\} \geq 1-\epsilon = \min(1, w_i^T y_i / \mathbb{E}[\tilde{D}_i])$. Since $0 < \epsilon < 1, \forall i$, applying this equation to (4.2), we get $\inf_{\mathbb{P}_{\tilde{D}} \in S_{\tilde{D}}}\{w_i^T y_i \geq (1-\epsilon)\mathbb{E}[\tilde{D}_i]\},\ \forall i \in \Phi$. □

It is a stochastic integer program problem to guarantee that the planned charging stations are satisfying the EV demand at each bus no matter what the probability distribution of the charging demand is. This is hard to solve. However, Theorem 1 indicates that this stochastic integer program can be converted into a deterministic one as long as we have the mean value of the EV demand in the past.

If we are given both the first and second moments of the charging demand, $\mathbb{E}[\tilde{D_i}^k],\ k = 1, 2$, it is straightforward to calculate the corvariance matrix Σ_i: $\Sigma_i^{jk} = \mathbb{E}[(\tilde{D_{ji}} - \mathbb{E}[\tilde{D_{ji}}])(\tilde{D_{ki}} - \mathbb{E}[\tilde{D_{ki}}])], \forall j, k = 1, \ldots, n$, where Σ_i^{jk} is the value in the jth row and kth column of Σ_i and $\tilde{D_{ji}}$ is the jth element of vector $\tilde{D}_i$.

Theorem 2. ***(Reformulation of the Chance Constraint into a Second-Order Cone Constraint)*** *Assume we have the first two-order knowledge of the charging demand data, denoted by* $\mathbb{E}[\tilde{D}_i] = \mu, \mathbb{E}[\tilde{D_i}^2] = \Sigma$. *Once we reformulate (4.2) into* $\sup_{\mathbb{P}_{\tilde{D}} \in S_{\tilde{D}}} \mathbb{P}_{\tilde{D}}\{\tilde{D}_i \leq w_i^T y_i\} \leq \epsilon,\ \forall i \in \Phi$, *(4.2) is equivalent to*

$$\sqrt{\Big(\frac{1-\epsilon_i}{\epsilon_i}\Big) I_i^T \Sigma I_i} \leq w_i^T y_i - \mu^T I_i. \tag{4.4}$$

Proof. Consider the following variant of the Chebyshev Inequality for random variable X that has mean μ and variance δ^2, we have $\mathbb{P}[X \geq (1+\delta)\mu] \leq \frac{\delta^2}{\delta^2 + \mu^2 \delta^2}$ for any $0 < \delta < 1$. According to [79, 80], there exists a distribution in $S_{\tilde{D}}$ to make the inequality tight. Therefore, by setting $\delta = -1 + \frac{w_i^T y_i}{I_i^T \mathbb{E}[\tilde{D}]}$ and rearranging terms, we have (4.4). □

Regardless of the estimation for the EV demand uncertainty pattern characterized by any specific probability distribution functions (PDFs), the utilization of the

CC method with ambiguity set could provide a general closed-form using first and second-moment information to guarantee to fulfill the optimization under any unknown distribution of EV charging behavior. Some discussion about the accepted form of candidate PDFs encapsulating uncertainty information can be referred to [81], in which the CC method associated with unimodal distributions and mis-specified modes is also studied.

Remark 1. *In contrast to many other works using Gaussian distribution to approximate the real probability distribution of EV charging demand, the CC method could get rid of such assumptions with the utilization of ambiguity set for fitting realistic dataset, as presented in the numerical study. It is the advantage of data-driven methods over the analytical physical modeling, which often involves charging behavior modeling with arrival time or departure time estimation.*

In this way, the non-analytical formulation (4.3) can be transferred to (4.4), which is a second-order cone constraint that satisfies all the convex characteristics. This reformulated constraints will be incorporated in the following optimization problem, together with various deterministic constraints.

Remark 2. *In the approach of building ambiguity set for the CC method, (4.3) and (4.4) mainly use first-moment and second-moment information of uncertainty variable. They can be further relaxed and combined with a more accurate estimation using well-defined α-unimodality information. For the sake of simplification, we neglect such accuracy as discussed in [81].*

4.1.2 Modeling of Energy Router and Its Mobility Characteristics

We introduce another optimization variable $z_{ij,t}$ to represent the number of ERs at branch $\{ij\} \in \Psi$, where i and j are the 'from' and 'to' buses respectively. Obviously, all of the $z_{ij,t}$ elements form a n-by-n sparse matrix. Importantly, the time-variant

matrix $z_{ij,t}$ links the fast-changing power flow due to EV demand variation and other renewable generations with the coarse time granularity of EVCS planning. The daily power flow pattern under the planning year should satisfy the physical limits, at least with the assistance of ERs. In this model, we assume ER as a power electronics device with a unit reactive power injection $Q_{0,ij}$ at branch $\{ij\} \in \Psi$. Consequently, the reactive power injection at bus i is given as follows by splitting the reactive power at both ends of the branch:

$$Q_{i,t}^{er} = \frac{1}{2} \sum_{\substack{j=1 \\ j \neq i}}^{n} z_{ij,t} Q_{0,ij}, \ \{ij\} \in \Phi. \tag{4.5}$$

Besides the per-unit cost of ER devices, a high amount of ER cost stems from its mobility. Specifically, we include the transport cost, installation cost, and uninstallation cost of ERs in mobility. Define the operation $M(M > 0)$ and $M(M < 0)$ as keeping all the positive and negative elements in M respectively, and let ER mobility matrix $z_{ij,\Delta t} \triangleq z_{ij,t} - z_{ij,t-1}$:

$$\begin{aligned} C_{mob,t}^{er} = F &+ \frac{1}{2} \gamma_{ins} \sum (z_{ij,\Delta t}(z_{ij,\Delta t} < 0)) \\ &+ \frac{1}{2} \gamma_{unins} \sum (z_{ij,\Delta t}(z_{ij,\Delta t} > 0)), \end{aligned} \tag{4.6}$$

where F is the transporting cost of the ERs. It is insignificant since some ER products are simply delivered through trailers [4]. Actually, the optimal cost of ER allocation belongs to the classical optimum distribution problems on goods transportation, which is beyond the scope of this paper. However, due to its relatively small cost comparing to other infrastructures (see the numerical results for more details), this term is assumed to be constant, denoted by F. Moreover, the introduction of the ER location matrix $z_{ij,t}$ makes the ER mobility matrix simple and accessible. By taking the difference between the ER location matrix at two consecutive time slots,

the summation of all negative elements in the resulting matrix is the number of the ERs to be installed; while the summation of all positive elements gives us the number of ERs to be uninstalled. Since $z_{ij,\Delta t}$ is symmetrical, the number goes half.

4.1.3 The Overall Cost for Distribution System Operators

To formulate the EV charging station planning problem along with the adoption of energy routers, we consider the EV charging station cost C_{EV}, the distribution system expansion cost C_{SYS}, and the distribution system operation cost $C_{OP,t}$ that includes the cost of energy routers. The overall EVCS planning cost is formulated below:

$$\begin{aligned}
&\min_{x_i, y_i, z_{ij,t}} \quad \sum_{t=1}^{T} (C_{EV} + C_{SYS} + C_{OP,t}) \\
&\quad \text{s.t. } x_i \in \{0,1\}, \ \forall i \in \Phi, \\
&\qquad y_i, z_{ij,t} \in \mathbb{Z}, \ \forall i, j \in \Phi, \\
&\qquad f\Big(V_{i,t}, \theta_{i,t}, P_{i,t} + P_D, Q_{i,t} + Q_{i,t}^{er}\Big) = 0, \ \forall i \in \Phi, \\
&\qquad (4.4) - (4.6),
\end{aligned} \tag{4.7}$$

where

$$C_{EV} = \sum_{i \in \Phi} (c_{1,i} x_i + c_{2,i} y_i), \tag{4.8}$$

$$\begin{aligned}
C_{SYS} = \sum_{\substack{i,j \in \Phi \\ i \neq j}} c_3 l_{ij} \max(|(V_i - V_j)^2 / Z_{ij}^{rated} - \lambda_S Q_{i,t}^{er} \\
- S_{rated}|, 0) + c_{4,i} h(\Delta P_i^{sub}),
\end{aligned} \tag{4.9}$$

$$\begin{aligned}
C_{OP,t} &= C_{vr} + C_{fix}^{er} + C_{mob,t}^{er} \\
&= c_5 \sum_{i \in \Phi} (V_{sp} - V_i)^2 + \frac{1}{2} \xi \sum_{i,j \in \Phi} z_{ij,t=0} \\
&+ F + \frac{1}{2} \gamma_{ins} \sum (z_{ij,\Delta t} (z_{ij,\Delta t} < 0)) \\
&+ \frac{1}{2} \gamma_{unins} \sum (z_{ij,\Delta t} (z_{ij,\Delta t} > 0)).
\end{aligned} \tag{4.10}$$

Concretely, the objective function has three decision variables: the availability of a charging station x_i, the number of charging spots y_i, and the ER location matrix $z_{ij,t}$. For the nth year to be planned, an estimate of the mean and variance in that year is required. The constraints here include the function $f(\cdot)$ that represents the physical limits stemming from power flow equations, as well as equations (4.4)-(4.6). Furthermore, the three costs in (4.7) are elaborated as follows:

- The term C_{EV} is the sum of the charging station cost and the cost of adding an individual charging spot.

- The term C_{SYS} has two parts. The first part is the line expansion due to load increase, which is proportional to the line length and the increment of the line's MVA rating. We introduce λ_S to indicate the power contribution factor, by which the energy router can contribute to attenuate the power flow congestion in proportional to its reactive power injection. The second part is associated with the substation expansion, whose detail is provided in [82].

- The term $C_{OP,t}$ involves the voltage regulation and the ER cost. The voltage regulation devices are still considered even though ERs are deployed since it is biased if the common voltage regulation approach is eliminated. For the fixed ER cost, we assume $\sum z_{ij,t}$ preserves two times of the deployed ERs when $t = 0$.

4.2 Numerical Results

4.2.1 Case Study Systems

To validate the proposed method, the model have implemented it in multiple IEEE systems. For the demonstration, the IEEE 30-bus system is employed in this section. In the 30-bus system as shown in Fig. 4.2, there are 41 branches. The sys-

tem territory have been divided into north (mainly processes load) and south areas (with six generators) by a dashed line. The purpose is to investigate the impact of regional heavy EV loads on the EVCS planning. The cost coefficients and optimization parameters are shown in Appendix A.1.

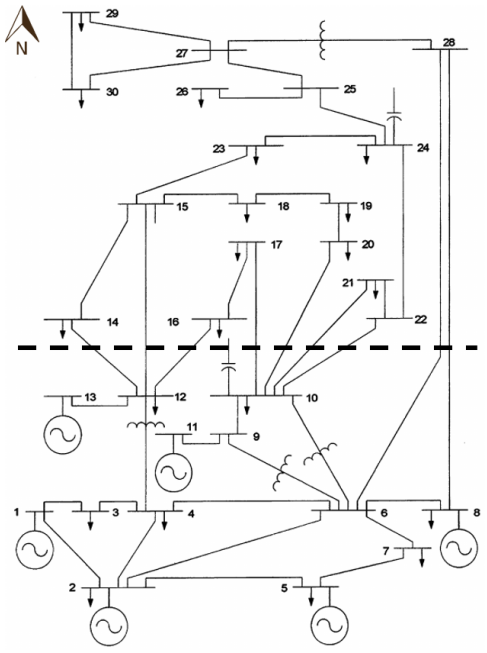

Figure 4.2: IEEE 30-bus System.

4.2.2 The Impact of Regional EV Demand Variation

Three types of demand conditions are considered. It assumes each branch can implement up to 10 ERs.

1. No regional heavy load, uniform bus demand

   No regional heavy load is assumed in this scenario. Specifically, there is no constraint on any particular bus that represents a heavy regional load demand. However, the EV load demand variation during the day is taken into consideration according to the EV load data at Boulder, Colorado, from Jan. 2018 to Feb. 2020 [64]. To simplify the daily variation pattern in the test, the EV

demand is divided into four consecutive time slots during one day, which in turn helps the investigation of the ER placement. The results for this uniform bus demand are presented in Fig. 4.3a and 4.3d. It can be clearly seen that the EVCS placement has no particular pattern since it follows the power flow result to reduce the overall cost. On the other hand, the ER distribution varies as the load change during the day. The load change is based on the realistic data in [64]. Concretely, the used percent is the maximum demands of $[0.5; 0.1; 0.9; 0.8]$ to represent the load condition from 1 am - 6 am, 7 am - 12 pm, 1 pm - 6 pm, and 7 pm - 12 am. Therefore, Fig. 4.3d reflects the ERs' compensation towards a reduced total cost.

2. North heavy load

   In the north region of Fig. 4.2, it is assumed that the EV load demand is heavy since this region has large residential areas. We assume eighty percent of the maximum EV load capacity (250 charging stations) at bus 14-30 has to be satisfied to get rid of the heavy load concern in the north. The optimization results are making sense since the best case for bus 14-30 is to satisfy the demand without any extra investment on EVCS. The only exception is on bus 28, where the preferable charging station number is the maximum, as shown in Fig. 4.3b. If one looks into the location of bus 28, it is connected to one of the six large generators. The load incremental at bus 28 is compensated by the generator, therefore, installing more stations here more beneficial than installing somewhere else.

3. South heavy load

   When the south area requires heavy EV demand, we assume a scenario where bus 2-13 demand heavy load. This represents places like industrial parks where

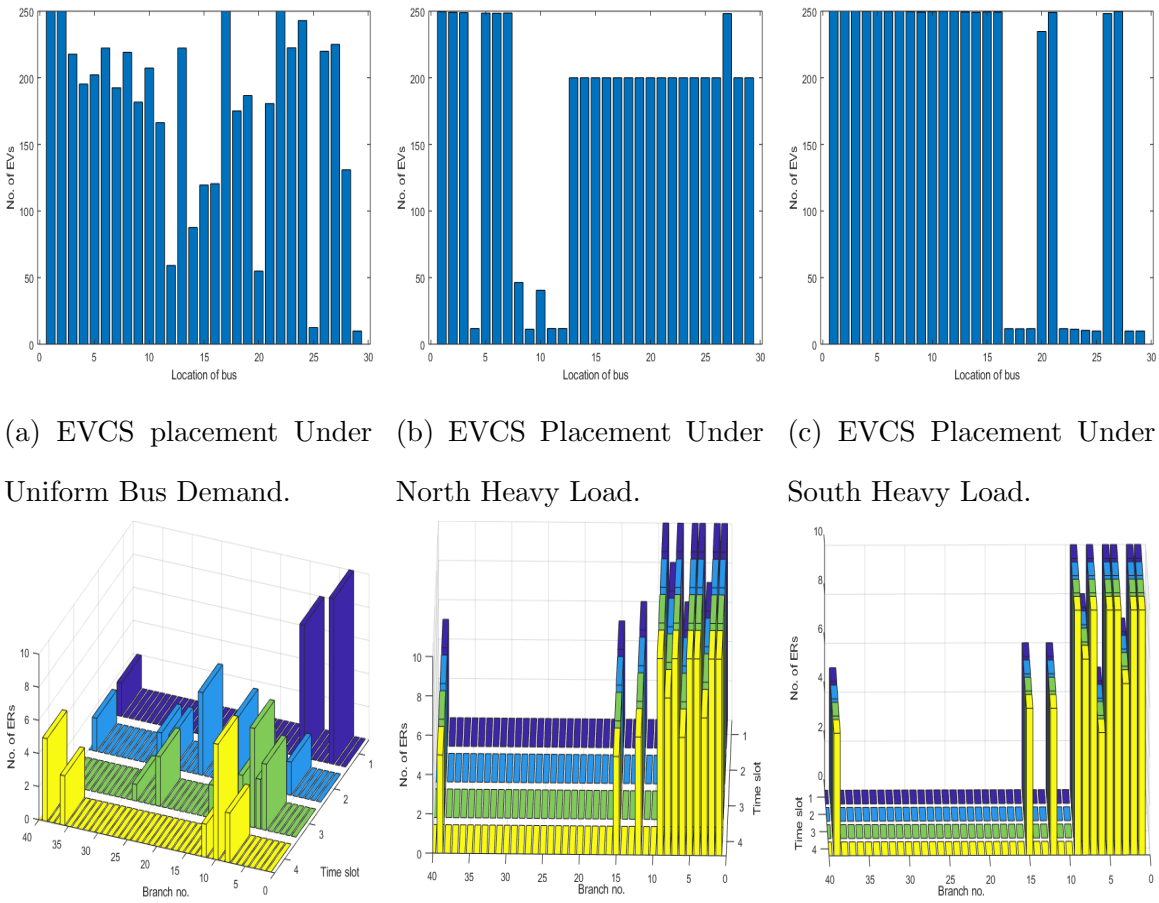

(a) EVCS placement Under Uniform Bus Demand.

(b) EVCS Placement Under North Heavy Load.

(c) EVCS Placement Under South Heavy Load.

(d) ER Distribution Under Uniform Bus Demand.

(e) ER Distribution Under North Heavy Load.

(f) ER Distribution Under South Heavy Load.

Figure 4.3: The Impact of Regional EV Demand Variation on EVCS Placement and ER Distribution. The Capacity Limits for EV Spots and ER at Each Bus are Assumed to be 250 (Charging Spots per Bus) and 10 (ERs per Branch) Respectively. For the ERs' Relocation Resolution, Four Time Slots are Assumed During the Day.

EV possession rate is high. Similar to the north heavy case, bus 2-13 requires at least eighty percent of the maximum EV load capacity to satisfy its EV demand. However, the results in Fig. 4.3c exhibit a higher EVCS installation rate. The reason is covered in the previous paragraph similar to bus 28. The

heavily loaded buses, in this case, are all connected to large generators. If more charging stations are installed in the north region buses, the voltage profile is affected, which results in more cost on system upgrade and operation. ER distribution in Fig. 4.3f is similar to that of Fig. 4.3e. However, the difference exists due to the distinct power flows. For example, the ER number is 2 at the last branch under the south heavy load while it is 5 under the other case.

4.2.3 The Impact of ER on EVCS Planning

Investing in ERs seems extra cost for system operation, however, it saves money when integrating a significant amount of EVs. In Table 4.1, it compares the cost with and without the utilization of ERs. The testing scenarios can refer to the parameters in Section 1. Through comparison, it is noticed that ER cost is high, reaching $\$261,110$. Although no cost on ERs in the case without ER, extra costs have to be spent on a system upgrade, voltage regulation, and, especially, the system operation. A close-up investigation is conducted under three load scenarios in the previous section. As shown in Table 4.2, the optimization cost reduces more than 48% comparing if ERs are installed and their costs are considered in various scenarios.

Table 4.1: Cost Comparison Under Uniform Bus Demand.

Cost	C_{ev}	C_{sys}	C_{vr}	C_{er}	C_{op}	C_{total}
With ERs ($\times 10^5\$$)	1653.0	1759.6	0.1339	2.6111	3.2664	3415.9
Without ERs ($\times 10^5\$$)	1653.0	4941.7	0.0129	0	0.0129	6594.7

To further understand the role that each item in the objective function plays, the

Table 4.2: Cost Comparison with and without ERs.

Total cost	Uniform load	North heavy	South heavy
Without ER [$]	6.5947×10^8	6.9145×10^8	6.5947×10^8
With ER [$]	3.4159×10^8	3.4224×10^8	3.4223×10^8
Saved	48.20%	50.50%	48.11%

cost details are demonstrated in Table 4.3. Interestingly, the voltage regulation cost is lowest in the south heavy case since the reactive power is locally compensated by the generation. Meanwhile, the ER cost is the lowest in the uniform load case since no demand constraint is applied in the system. Thus, the optimal EVCS planning result is to place the charging stations in such a way that reduces the system update and operational cost. Consequently, the operational cost in the first case is also the lowest among the three cases.

Table 4.3: Cost Details Under Different Load Scenarios.

Cost	**Uniform load**	**North heavy**	**South heavy**
C_{ev} [$]	1.6530×10^8	1.6530×10^8	1.6530×10^8
C_{sys} [$]	1.7596×10^8	1.7596×10^8	1.7596×10^8
C_{vr} [$]	1.3388×10^4	1.6791×10^4	7.8630×10^3
C_{er} [$]	2.6111×10^5	9.6486×10^5	9.6459×10^5
C_{op} [$]	3.2664×10^5	9.8165×10^5	9.7245×10^5
C_{total} [$]	3.4159×10^8	3.4224×10^8	3.4223×10^8

4.2.4 *ER Mobility Demonstration and Economical Benefit*

ER's characteristics of mobility lend itself the advantage of being economical. To highlight this advantage, we demonstrate the case where ERs are immobile under uniform bus demand. Although not the same, the EVCS placement results in Fig. 4.4 resemble the left two sub-figures in Fig. 4.3. Nevertheless, the results of ER placement experience the loss of flexibility. Economically, the immobility of the ERs costs 72.9% more on purchasing extra ERs to reach a similar total cost (only 0.19% difference) comparing to the one with mobility capability.

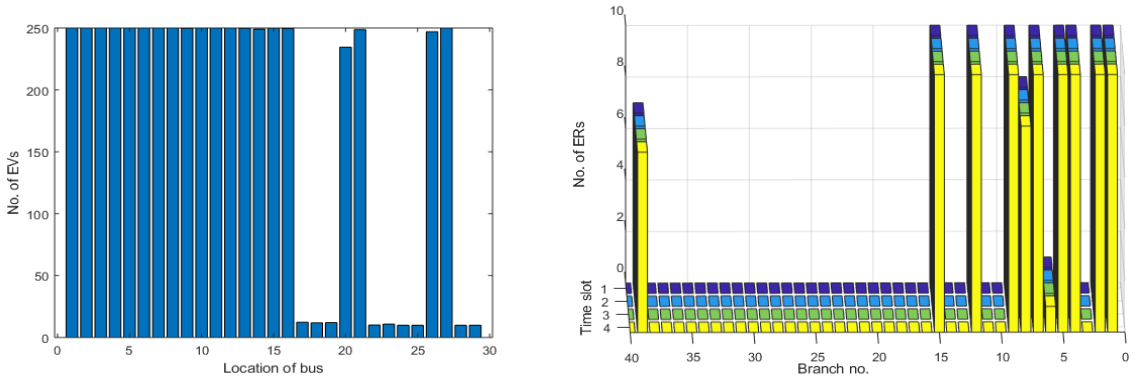

(a) EVCS Placement With Immobile ERs. (b) ER placement with immobile ERs.

Figure 4.4: ER Deployment with and without Mobility. Both Placements are Under the Uniform Demand Scenario. The ER Limits are Assumed to be 10 (ERs per Branch).

4.2.5 *Sensitivity Analysis Under Different EV Estimation Errors*

Sensitivity analysis is conducted to evaluate the impact of parameters in the CC approach on the EVCS planning and ER distribution. Specifically, we change the errors of EV demand estimation mean and variance to observe their impact on planning. On one hand, Table 4.4 and Fig. 4.5 illustrate the cost breakdown, the EVCS

planning, and the ER distribution under various mean errors. On the other hand, Table 4.5 and Fig. 4.6 illustrate the counterparts under various variance errors. It can be seen that the EVCS planning result is not sensitive to the mean EV demand estimation error. However, when the EV demand's variance changes, a large variance deviates a lot from a small variance, which alters the EVCS planning results greatly.

Table 4.4: The Impact of Mean EV Demand Estimation Error on Cost.

μ	**0.001**	**0.005**	**0.05**	**0.1**
C_{ev} ($\times 10^8$\$)	1.65	1.65	1.64	1.64
C_{sys} ($\times 10^8$\$)	1.76	1.76	1.76	1.76
C_{vr} ($\times 10^3$\$)	7.98	7.94	26.9	26.9
C_{er} ($\times 10^5$\$)	9.65	9.65	9.74	9.74
C_{op} ($\times 10^5$\$)	9.73	9.73	10.1	10.1
C_{total} ($\times 10^8$\$)	3.42	3.42	3.41	3.41

Table 4.5: The Impact of the Variance of EV Demand Estimation Error on Each Cost.

μ	**0.01**	**0.05**	**0.4**	**0.6**	**0.8**	**1.0**
C_{ev} ($\times 10^8$\$)	1.65	1.64	1.65	1.65	1.65	1.65
C_{sys} ($\times 10^8$\$)	1.76	1.76	1.76	1.76	1.76	1.76
C_{vr} ($\times 10^3$\$)	160	26.9	8.25	8.62	9.07	9.69
C_{er} ($\times 10^5$\$)	9.65	9.74	9.65	9.65	9.65	9.65
C_{op} ($\times 10^5$\$)	9.84	10.1	9.74	9.73	9.74	9.74
C_{total} ($\times 10^8$\$)	3.42	3.41	3.42	3.42	3.42	3.42

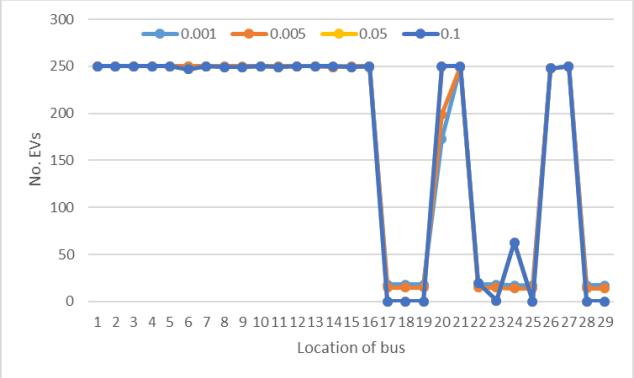

Figure 4.5: The Impact of Mean EV Demand Estimation Error on EVCS Planning. The EV Demand Estimation Variance Error is Assumed to be 15%.

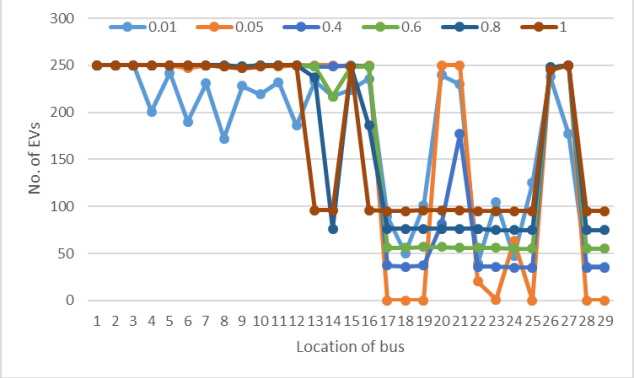

Figure 4.6: The Impact of EV Demand Estimation Variance Error on EVCS Planning. The EV Demand Estimation Mean Error is Assumed to be 10%.

4.3 Conclusion

This chapter formulates the EVCS planning problem by integrating the CC EV demand estimation approach. This approach overcomes the time granularity mismatch issue between the long-term EVCS planning and short-term daily EV demand variation. Meanwhile, ERs are modeled and implemented to observe their impact on EVCS planning. It is concluded that the FACTS-device-based power flower controllers can enhance the EV charging station integration into the electrical grid with

economical benefits. Concretely, we observe that the uniform placement of EVCSs creates the least amount of system operational costs. If regional heavy EV demand cannot be circumvented, it is preferable to install more fast-charging stations near the generators. Moreover, the mobility capability of the ER devices can greatly reduce the associated investment through recycling. Furthermore, through the comparison between the sensitivity of charging demand mean and variance errors, it is noticed that the EVCS planning is more sensitive to a high standard deviation error than the mean error. This sheds light on future research toward an optimal EV charging management, which can eventually and profoundly decrease the EVCS infrastructure investment.

Chapter 5

SUMMARY AND CONCLUSIONS

5.1 Thesis Summary

Electricity has been assisting humanity by providing more comfort. It started with turning on a spark to light and today it is possible to build an electric flight that carries an individual.

"Electric power is everywhere present, in unlimited qualities. This new power for the driving of the world's machinery will be derived from the energy which operates in the universe, without the need for coal, gas, oil, or any other fuel" – Nikola Tesla [83].

The more items operate on electricity, the bigger need for generating and transmitting it will happen. Transmission lines are the most efficient method to deliver power, which requires to be updated so it can meet the new demand. Increasing the line capacity is not a simple task because of the tower's height, and their locations that can be unfriendly such as mountains or underwater. Also, the upgrade is costly, which can be the main reason for delaying projects connected to the same circuit. Transmission line capacity obstacle can be solved with a shorter time, and cheaper price by applying the ER. ER will assist in providing more freedom to control the power flow on the transmission line, which gives additional capacity and more stability.

Through the work of the thesis, ER is tested in six case studies to find how it will impact on the transmission line and maintain secured power flow. The demand that affects the transmission line is studied in terms of EVCSs. Three time series

analysis methods are applied to predict the future load of the EVCSs. The behavior of the load is also considered to find when are the peak times, which will be perfect for scheduling mobile ER placement to avoid the overload. Because EVCS planning also depends on the power flow, an optimal planning EVCS model considering the ER is formulated.

ER mathematical principles are studied to understand how it will assist the line's stability. The ER controls the power flow by injecting the reactance of the line that can be in either inductive or capacitive mode. When LUA transmission line reactance value is injected, the overload has been solved in three different locations. A realistic ER model has been attached to the same three locations to verify the results, which was provided by Smart Wires. The two methods guarantee ER assistance to secure the power flow.

EVCSs data set of Boulder, CO, and Palo Alto has been analyzed to find their load behavior of the electrical grid. EVCS location is found for each zip code, and the one with the largest recorded transactions is selected. Then, for each year and month, the sum of kWh usage during every hour is founded to understand the load variation during the day. The mean and standard-deviation of the data sets are demonstrated. Since Palo Alto had more records covering the years 2011 to 2017, three TSA methods are applied to predict it's future. Polynomial curve fitting matched the data in a good shape, but it requires additional variables to fit the details so it can predict the future. So, polynomial curve fitting assisted in observation the EVCS characteristics, but not forecasting it. Thus, ARMA is applied, but it also found bad prediction because it depends on exponential smoothing and it didn't use the data set trend or seasonality. Although ARMA is more popular in predicting the future, exponential smoothing had better findings. Exponential smoothing using the multiplicative seasonality and additive trend predicted the future with better fitting to the testing data.

Finally, the thesis finds an optimal planning EVCS method that formulates an ER model and estimated the demand based on Boulder data set mean and variance behaviors. The ER and its mobility using the mobility matrix is found by a unit reactive power injection. For the charging demand mean values are considered by the formulated CC stochastic integer program for planning EVCS. The objective function is designed to minimize the charging station, distribution system operation, and distribution system expansion costs. The model is tested for three case studies, which are a south heavy load, north heavy load, and uniform load. The three of them use the EVCS demand from an estimation depending on the founded mean values of Boulder with the day separated into four periods.

5.2 Conclusion

The work in this thesis focus on power system, especially for the transmission line and EVCS. The three case studies on LUA transmission line solved the overload in the system when an outage occurs in another location connected to the same circuit. The first case study has the overload happening on a switch and the ER was attached to it. However, injecting the reactance of a switch didn't assist in solving the problem because the switch has lower reactance value, which means less impact on the received power. So, the ER is placed on the neighbors, which successfully solves the problem for more than 10 years. ER placement on for the other two case studies also assisted in maintaining the current in the line limits. The ER proved its ability to control the power flow of the transmission line, which assists the utilities in securing their system.

For EVCS data set analysis it finds that EV number is growing, the peak load consumption is occurring on specified hours, and the charging duration for an EV is decreasing. Boulder and Palo Alto peak hours are found in the morning times. The

charging duration has been decreasing annually, which proves that fast-charging is being used in the EVCS. From the polynomial curve fitting for Palo Alto data, the load behavior is observed by specifying the slope shape. Exponential smoothing has good prediction behavior, but for a small short time because for long durations, it starts to repeat it's forecasting over and over due to the seasonality influence.

For formulating EVCS planning with ER and its mobile an optimal solution is found that considers the EVCS mean value as the demand. The load is tested as uniform, south heavy, and north heavy. The ER placement for each load changed to fit the demand. Even though the ER adds additional cost to the system, but the total cost almost cuts in half for all case studies due to the reactive power injection.

5.3 Recommendations for Future Work

While ER impacts transmission system and EVCS planning additional work can also be studied in the future.

1. A techno-economic analysis model for the deferral project can be developed by considering the costs of line and ER. Then, formulate an optimal ER placement model to reach maximum profit. The optimal method will assist in purchasing the least number of ER while ensuring the stability of the system. The model presented in the thesis tested each line and switch manually, which can increase the chance of error when considering the whole transmission system.

2. ER Impact on harmonics and oscillation can be utilized for LUA grid especially in the areas close to the solar and wind power plants.

3. D-FACTS has similar behavior as the ER, but for the distribution system, which can be considered to avoid the overload on the distribution lines.

4. Applying exponential smoothing method on Palo Alto data set to forecast all

24 hours using different seasonality and trend values. If the data is forecasted, EVCS planning can apply the future demand to find an optimal placement.

REFERENCES

[1] K. . Kuypers, R. E. Morrison, and S. B. Tennakoon, "Power quality implications associated with a series facts controller," in *Ninth International Conference on Harmonics and Quality of Power. Proceedings (Cat. No.00EX441)*, vol. 1, Oct 2000, pp. 176–181 vol.1.

[2] J. J. Thomas, J. Hernandez, and S. Grijalva, "Power flow router sensititvities for post-contingency corrective control," in *2013 IEEE Energy Conversion Congress and Exposition*, Sep. 2013, pp. 2590–2596.

[3] (2017) Leading power factor and lagging power factor. [Online]. Available: https://www.electrical4u.net/electrical-basic/leading-lagging-power-factor/

[4] Smart Wires Inc., "Smartvalve 5-1800i," 2019. [Online]. Available: https://www.smartwires.com/smartvalve/?dc=thanks51800i#tab-id-3

[5] Smart Wires Inc, "Deploying smart wires at the tennessee valley authority," 2014. [Online]. Available: http://www.smartwires.com/wp-content/uploads/2015/01/Smart-Wires-Tennessee-Valley-Authority-Report_FINAL.pdf

[6] S. Wires, "Smartvalve." [Online]. Available: https://www.smartwires.com/dev-design#tab-id-1

[7] E. E. Institute, "Electric vehicle sales:facts & figures," 2019. [Online]. Available: https://www.eei.org/issuesandpolicy/electrictransportation/Documents/FINAL_EV_Sales_Update_April2019.pdf

[8] T. S. Writer, "Nikola tesla vs. thomas edison: Who was the better inventor?" 2014. [Online]. Available: https://rmi.org/news/pulling-back-veil-ev-charging-station-costs/

[9] M. Sivak and B. Schoettle. (2018, Jan) relative costs of driving electric and gasoline vehicles in the individual u.s. states. [Online]. Available: http://www.umich.edu/ umtriswt/fuel-economy.html

[10] K. Padiyar, *FACTS Controllers in Power Transmission and Distribution.* Anshan LTD, 2009.

[11] L. Gyugyi, C. D. Schauder, and K. K. Sen, "Static synchronous series compensator: a solid-state approach to the series compensation of transmission lines," *IEEE Transactions on Power Delivery*, vol. 12, no. 1, pp. 406–417, Jan 1997.

[12] A. K. Jadhav and V. A. Kulkarni, "Improvement in power system stability using sssc based damping controller," in *2018 International Conference on Smart Electric Drives and Power System (ICSEDPS)*, June 2018, pp. 162–166.

[13] M. R. Shaik and A. S. Reddy, "Optimal placement and sizing of facts device to overcome contingencies in power systems," in *2016 International Conference on Signal Processing, Communication, Power and Embedded System (SCOPES)*, Oct 2016, pp. 838–842.

[14] H. Johal and D. Divan, "Design considerations for series-connected distributed facts converters," *IEEE Transactions on Industry Applications*, vol. 43, no. 6, pp. 1609–1618, Nov 2007.

[15] S. M. Sadeghzadeh, M. Ehsan, N. H. Said, and R. Feuillet, "Improvement of transient stability limit in power system transmission lines using fuzzy control of facts devices," *IEEE Transactions on Power Systems*, vol. 13, no. 3, pp. 917–922, Aug 1998.

[16] S. Ahmed, Z. Shen, P. Mattavelli, D. Boroyevich, and K. J. Karimi, "Small-signal model of voltage source inverter (vsi) and voltage source converter (vsc) considering the deadtime effect and space vector modulation types," *IEEE Transactions on Power Electronics*, vol. 32, no. 6, pp. 4145–4156, June 2017.

[17] M. S. El-Moursi and A. M. Sharaf, "Novel controllers for the 48-pulse vsc statcom and sssc for voltage regulation and reactive power compensation," *IEEE Transactions on Power Systems*, vol. 20, no. 4, pp. 1985–1997, Nov 2005.

[18] J. Miao, N. Zhang, and c. Kang, "Generalized steady-state model for energy router with applications in power flow calculation," *IEEE Power and Energy Society General Meeting (PESGM), Boston, MA*, 2018.

[19] K. Johnson, G. Venkataramanan, and M. Manjrekar, "A hybrid solid state phase shifter for continuous phase shift control in transmission lines," *Canadian Conference on Electrical and Computer Engineering*, 1996.

[20] P. State and M. T. Dept. (2014) Power flow on transmission lines. [Online]. Available: https://www.pjm.com/-/media/training/nerc-certifications/gen-exam-materials/bet/20160104-basics-of-elec-power-flow-on-ac.ashx?la=en

[21] K. K. Sen and A. J. F. Keri, "Comparison of field results and digital simulation results of voltage-sourced converter-based facts controllers," *IEEE Transactions on Power Delivery*, vol. 18, no. 1, pp. 300–306, Jan 2003.

[22] M. Mahdavian, M. Janghorbani, I. Eshaghpour, E. Ganji, and A. Movahedi, "Impacts of the sssc on damping power system oscillations," in *2017 14th International Conference on Electrical Engineering/Electronics, Computer, Telecommunications and Information Technology (ECTI-CON)*, June 2017, pp. 54–57.

[23] B. Ioan, B. Horia, and O. P. T. Susana, "Determination of the power generated by a wind turbine in constant wind and variable wind," in *2015 9th International Symposium on Advanced Topics in Electrical Engineering (ATEE)*, May 2015, pp. 769–773.

[24] M. Al-Sarray and R. A. McCann, "Control of an sssc for oscillation damping of power systems with wind turbine generators," in *2017 IEEE Power Energy Society Innovative Smart Grid Technologies Conference (ISGT)*, April 2017, pp. 1–5.

[25] S. Gandhar, J. Ohri, and M. Singh, "Application of sssc for compensation assessment of interconnected power system," in *2014 IEEE 6th India International Conference on Power Electronics (IICPE)*, Dec 2014, pp. 1–5.

[26] Z. Moravej, M. Pazoki, and M. Khederzadeh, "Impact of upfc on power swing characteristic and distance relay behavior," *IEEE Transactions on Power Delivery*, vol. 29, no. 1, pp. 261–268, Feb 2014.

[27] L. Dong, M. L. Crow, Z. Yang, C. Shen, L. Zhang, and S. Atcitty, "A reconfigurable facts system for university laboratories," *IEEE Transactions on Power Systems*, vol. 19, no. 1, pp. 120–128, Feb 2004.

[28] U. Gabrijel and R. Mihalic, "Direct methods for transient stability assessment in power systems comprising controllable series devices," *IEEE Transactions on Power Systems*, vol. 17, no. 4, pp. 1116–1122, Nov 2002.

[29] R. Mihalic and U. Gabrijel, "A structure-preserving energy function for a static series synchronous compensator," *IEEE Transactions on Power Systems*, vol. 19, no. 3, pp. 1501–1507, Aug 2004.

[30] B. Lu and B. Ooi, "Nonlinear control of voltage-source converter systems," *IEEE Transactions on Power Electronics*, vol. 22, no. 4, pp. 1186–1195, July 2007.

[31] B. S. Hender, "Future of the battery-electric car," *Electronics and Power*, vol. 10, no. 8, pp. 250–254, 1964.

[32] G. F. Sever and R. A. Fliess, "Operating costs of horse and electric delivery wagons in new york city," *Transactions of the American Institute of Electrical Engineers*, vol. XVI, pp. 485–507, 1899.

[33] R. MATULKA, "The history of the electric car," 2014. [Online]. Available: https://www.energy.gov/articles/history-electric-car

[34] E. A. Sperry, "Electric automobiles," *Transactions of the American Institute of Electrical Engineers*, vol. XVI, pp. 509–525, 1899.

[35] H. E. Dance, "The electric battery vehicle," *Journal of the Institution of Electrical Engineers*, vol. 61, no. 323, pp. 1100–1108, 1923.

[36] G. A. McNeal, "The electric battery vehicle," *Students' Quarterly Journal*, vol. 5, no. 18, pp. 82–87, 1934.

[37] W. D. Sheers, "Electrical equipment of battery road vehicles," *Proceedings of the IEE - Part II: Power Engineering*, vol. 99, no. 71, pp. 457–464, 1952.

[38] S. S. Mackeown and V. Wouk, "Generation of electric charges by moving rubber-tired vehicles," *Transactions of the American Institute of Electrical Engineers*, vol. 62, no. 5, pp. 207–210, 1943.

[39] B. Berman and G. H. Gelb, "Propulsion systems for electric cars," *IEEE Transactions on Vehicular Technology*, vol. 23, no. 3, pp. 61–72, 1974.

[40] J. N. Park, "A chopper converter for electric vehicle propulsion battery charging and propulsion motor field excitation," in *1980 IEEE Power Electronics Specialists Conference*, 1980, pp. 203–210.

[41] R. Guise, "Computer controlled electric vehicle," *Electronic Systems News*, vol. 1982, no. 2, pp. 16–18, 1982.

[42] E. H. Wakefield, "An ac drive electric vehicle," *IEEE Transactions on Industry Applications*, vol. IA-10, no. 5, pp. 544–552, 1974.

[43] J. T. Salihi, "The electric car - fact and fancy," *IEEE Spectrum*, vol. 9, no. 6, pp. 44–48, 1972.

[44] K. Rudman, "Eei celebrates 1 million electric vehicles on u.s. roads." [Online]. Available: https://www.eei.org/resourcesandmedia/energytalk/Pages/Issue-In-Depth-11-1-2018.html#99

[45] A. Hove and D. Sandalow, "Electric vehicle charging in china and the united states," 2019. [Online]. Available: https://energypolicy.columbia.edu/research/report/electric-vehicle-charging-china-and-united-states

[46] S. Deb, K. Tammi, K. Kalita, and P. Mahanta, "Review of recent trends in charging infrastructure planning for electric vehicles," *IEEE Access*, vol. 7, no. 6, p. e306, 2018.

[47] DOE, "Reducing pollution with electric vehicles," 2020. [Online]. Available: https://www.energy.gov/eere/electricvehicles/reducing-pollution-electric-vehicles

[48] Tesla, "Charge on the road," 2020. [Online]. Available: https://www.tesla.com/supercharger

[49] Nissan, "More range. more power. more leaf." 2020. [Online]. Available: https://www.nissanusa.com/vehicles/electric-cars/leaf/features/range-charging-battery.html

[50] Chevrolet, "Chevrolet bolt ev - 2020," 2020. [Online]. Available: https://media.chevrolet.com/media/us/en/chevrolet/vehicles/bolt-ev/2020.tab1.html

[51] Audi, "e-trone battery," 2020. [Online]. Available: https://www.audiusa.com/models/audi-e-tron/battery

[52] N. Zhou, J. Wang, Q. Wang, and N. Wei, "Measurement-based harmonic modeling of an electric vehicle charging station using a three-phase uncontrolled rectifier," *IEEE Transactions on Smart Grid*, vol. 6, no. 3, pp. 1332–1340, May 2015.

[53] U. D. of Energy (office of Energy Efficiency and R. Energy. Vehicle charging. [Online]. Available: https://www.energy.gov/eere/electricvehicles/vehicle-charging

[54] E. wong. (2018) Electric vehicle charging station usage (fy 2011 - fy 2017). [Online]. Available: https://data.cityofpaloalto.org/dataviews/241685/ELECT-VEHIC-CHARG-STATI-USAGE/

[55] S. Sun, Q. Yang, and W. Yan, "Hierarchical optimal planning approach for plug-in electric vehicle fast charging stations based on temporal-soc charging demand characterisation," *IET Generation, Transmission Distribution*, vol. 12, no. 20, pp. 4388–4395, 2018.

[56] X. Huang, J. Chen, H. Yang, Y. Cao, W. Guan, and B. Huang, "Economic planning approach for electric vehicle charging stations integrating traffic and power grid constraints," *IET Generation, Transmission Distribution*, vol. 12, no. 17, pp. 3925–3934, 2018.

[57] M. M. Islam, H. Shareef, and A. Mohamed, "Optimal location and sizing of fast charging stations for electric vehicles by incorporating traffic and power networks," *IET Intelligent Transport Systems*, vol. 12, no. 8, pp. 947–957, 2018.

[58] G. Wang, Z. Xu, F. Wen, and K. P. Wong, "Traffic-constrained multiobjective planning of electric-vehicle charging stations," *IEEE Transactions on Power Delivery*, vol. 28, no. 4, pp. 2363–2372, Oct 2013.

[59] H. Zenk and A. S. Akpinar, "Pi, pid and fuzzy logic controlled sssc connected to a power transmission line, voltage control performance comparison," in *4th International Conference on Power Engineering, Energy and Electrical Drives*, 2013, pp. 1493–1497.

[60] K. Rachananjali, N. Pavani, S. Suman, and D. V. S. B. Chaitanya, "Damping of subsynchronous resonance using sssc with hysteresis current control," in *2014 International Conference on Green Computing Communication and Electrical Engineering (ICGCCEE)*, 2014, pp. 1–5.

[61] J. Li, D. Xu, J. Zhang, J. Xiao, and H. Wang, "The comparison of arma, exponential smoothing and seasonal index model for predicting incidence of newcastle disease," in *2010 World Automation Congress*, 2010, pp. 145–148.

[62] C. Zheng and L. Li, "The improvement of the forecasting model of short-term traffic flow based on wavelet and arma," in *2010 8th International Conference on Supply Chain Management and Information*, 2010, pp. 1–4.

[63] C. Sriram, D. R. Kumar, and G. S. Raju, "Blocking the distance relay operation in third zone during power swing using polynomial curve fitting method," in *2014 International Conference on Smart Electric Grid (ISEG)*, 2014, pp. 1–7.

[64] L. Markram, "Electric vehicle charging stations: Energy consumption & savings," Available at https://bouldercolorado.gov/open-data/electric-vehicle-charging-stations/ (2020).

[65] J. White and E. Tobin. (2020) Exclusive: Tesla's secret batteries aim to rework the math for electric cars and the grid. [Online]. Available: https://www.reuters.com/article/us-autos-tesla-batteries-exclusive/exclusive-teslas-secret-batteries-aim-to-rework-the-math-for-electric-cars-and-the-grid-idUSKBN22Q1WC

[66] T. S. community, "Polynomial module (numpy.polynomial.polynomial)," 2014. [Online]. Available: https://docs.scipy.org/doc/numpy-1.17.0/index.html

[67] J. Kiusalaas, *Numerical Methods in Engineering with Python*. Cambridge, 2005.

[68] Petris, Giovanni, Petrone, Sonia, Campagnoli, and Patrizia, *Dynamic Linear Models with R*. Springer Science & Business Media, 2009.

[69] Stephanie, "Arma model," 2014. [Online]. Available: https://www.statisticshowto.com/arma-model/

[70] WordPress. (2019) Introduction to exponential smoothing for time series forecasting using python. [Online]. Available: https://uncoolai.com/exponential-smoothingfortimeseriesforecasting/

[71] G. A. R. Hyndman. (2016) Forecasting: Principles and practice. [Online]. Available: https://otexts.com/fpp2/ses.html

[72] N. Vandeput. (2018) Exponential smoothing. [Online]. Available: https://supchains.com/article/exponential-smoothing-python/

[73] S. Deb, K. Tammi, K. Kalita, and P. Mahanta, "Charging station placement for electric vehicles: A case study of guwahati city, india," *IEEE Access*, vol. 7, pp. 100 270–100 282, 2019.

[74] D. Gong, M. Tang, B. Buchmeister, and H. Zhang, "Solving location problem for electric vehicle charging stations—a sharing charging model," *IEEE Access*, vol. 7, pp. 138 391–138 402, 2019.

[75] H. Liu, M. Yang, M. Zhou, and G. Tian, "An integrated multi-criteria decision making approach to location planning of electric vehicle charging stations," *IEEE Transactions on Intelligent Transportation Systems*, vol. 20, no. 1, pp. 362–373, Jan 2019.

[76] I. S. Bayram, A. Tajer, M. Abdallah, and K. Qaraqe, "Capacity planning frameworks for electric vehicle charging stations with multiclass customers," *IEEE Transactions on Smart Grid*, vol. 6, no. 4, pp. 1934–1943, July 2015.

[77] F. Kreikebaum, A. Wang, and S. Broad, "Integration of series facts into interconnect-scale production cost and long-term planning tools," in *CIGRE 2016*, Aug 2016, pp. 1–10.

[78] Y. Zhang, R. Jiang, and S. Shen, "Ambiguous chance-constrained binary programs under mean-covariance information," *SIAM Journal on Optimization*, vol. 28, no. 4, pp. 2922–2944, 2018.

[79] D. Bertsimas and I. Popescu, "Optimal inequalities in probability theory: A convex optimization approach," *SIAM Journal on Optimization*, vol. 15, no. 3, pp. 780–804, 2005.

[80] M. R. Wagner, "Stochastic 0–1 linear programming under limited distributional information," *Operations Research Letters*, vol. 36, no. 2, pp. 150–156, 2008.

[81] B. Li, R. Jiang, and J. L. Mathieu, "Distributionally robust chance-constrained optimal power flow assuming unimodal distributions with misspecified modes," *IEEE Transactions on Control of Network Systems*, vol. 6, no. 3, pp. 1223–1234, 2019.

[82] Q. Cui, Y. Weng, and C.-W. Tan, "Electric vehicle charging station placement method for urban areas," *IEEE Transactions on Smart Grid*, vol. 10, no. 6, pp. 6552–6565, 2019.

[83] M. Mitra, "Nikola tesla's free electricity electronic circuit," *Journal of Electronics and Communication*, vol. 20, no. 1, p. 6, Mar 2018.

[84] A. Dimitrovski, Z. Li, and B. Ozpineci, "Magnetic amplifier-based power-flow controller," *IEEE Transactions on Power Delivery*, vol. 30, no. 4, pp. 1708–1714, 2015.

APPENDIX A

EVCS

A.1 Parameters and Settings

The fixed costs for each EV charging station is assumed to be $c_{1,i} = 163,000\,(\$)$. The land use costs are $407\,\$/\mathrm{m}^2$ and adding one extra charging spot requires $20\,\mathrm{m}^2$ land. The per-unit purchase cost for one charging spot is $23,500\,\$$. Thus we have $c_{2,i} = 407 \times 20 + 23,500 = 31,640\,(\$)$. The distribution line cost is assumed to be $c_{3,i}$ =120 ($/(kVA $\cdot$ km)) and the substation expansion cost is assumed to be $c_{4,i}$ =788 ($/kVA). The rated charging power for each charging spot is 44 kW. The voltage regulation coefficient c_5 is assumed to be $50,000$ ($), given the base power of 100 MVA. The readers can find the references for these coefficients in [82]. As for the ER price, it is assumed to be \$10/kVA, according to a similar device in [84]. For simplification, we assume the serviceability coefficient w_i to be with the order of one. Moreover, we set $\lambda_S = 1$, $\gamma_{ins} = \$550$, and $\gamma_{unins} = \$500$ per ER.